From Department of Molecular Medicine and Surgery
Karolinska Institutet, Stockholm, Sweden

# Combining Mass Spectrometric Tissue Imaging with Conventional Histology

## Focus on Alzheimer's Disease

Santiago Solé Domènech


Stockholm 2012

About the cover: The image displays a sagittal section of the Tg2576 mouse hippocampus stained with glial acidic fibrillary protein (GFAP, green), ionized calcium binding adaptor molecule 1 (Iba1, red), pentamer formyl thiophene acetic acid (p-FTAA, yellow) and BOBO-1 cell nuclei marker (blue). In the area, p-FTAA stains an extracellular senile plaque surrounded by immunoreactive astrocytes (GFAP) and microglia (Iba1).



Published by Karolinska Institutet. Printed by Larserics Digital Print AB



ISBN 978-91-7457-639-9

*Als meus pares*

# ABSTRACT

Historically, most scientific discoveries have been accompanied by previous technological innovation. Representative examples are the introduction of gene sequencing technologies, which allowed for the mapping of the human genome, or the constant improvement in the microscopy field that lead to the introduction of modern multiphoton imaging techniques, allowing for live imaging of body organs in animal specimens. In this regard, the molecular imaging of analytes in tissue has traditionally been a challenging field. For instance, mass spectrometric techniques did not initially allow for the imaging of compounds in a given sample. Technological improvement lead to the introduction of instruments that could transform the spectra acquired from samples into images of the distribution of surface analytes. In the present thesis work, we approach the study of biological samples using Time-of-Flight Secondary Ion Mass Spectrometry (ToF-SIMS), a surface imaging technique specially suited for the imaging of lipids and lipid precursors in biological tissue. Our project started with the optimization of ToF-SIMS protocols for the study of mouse brain and fat adipose tissues, which allowed us to learn ways to systematically process biological material in a reliable and reproducible manner. Next, we focused our efforts on the application of ToF-SIMS to the study of a well established biological problem: Alzheimer's disease. We developed a methodology combining ToF-SIMS with fluorescence imaging techniques in order to visualize lipids, lipid precursors and cell populations in brain regions undergoing senile plaque deposition. This multiplexed imaging approach enabled us to simultaneously observe lipid and glial cell distributions in regions undergoing senile plaque deposition with great lateral (<500 nm) resolution, and revealed micrometer-sized cholesterol accumulations in hippocampal regions occupied with senile plaques likely to mirror an AD-related pathological event. The systematic study of brain tissue sections from mouse models of Alzheimer's disease followed; we investigated the cholesterol profile of brain regions occupied by senile plaques and compared it to that of wild-type, control brain. Regions undergoing plaque deposition displayed, often, severe cholesterol granulation, whereas regions devoid of plaques displayed a homogeneous sterol profile. Furthermore, investigation of glial profiles revealed increased astrocytic immunoreactivity in regions associated to cholesterol granulation, which was consistent with the already known role played by astrocytes during central nervous system injury. Besides cholesterol, other lipid compounds were studied, such as sulfatides and fatty acids, revealing specific surface distributions associated to distinct tissue structures. Given the growing attention paid to the involvement of lipids and lipid precursors in health and disease, tools that allow for the study of such compounds might play a vital role in the understanding of disease pathogenesis. The implementation of technological improvements that allowed for the study of biological samples, with reduced analyte fragmentation and increased efficiencies, lead to the modern "ToF-SIMS imaging" concept presented in this thesis work. The current sensitivity and resolution are sufficient for cellular imaging of many lipids of likely pathophysiological importance.

# LIST OF PUBLICATIONS

I. *Bélazi D, **Solé-Domènech S,** Johansson B, Schalling M, Sjövall P.
**Chemical Analysis of Osmium Tetroxide Staining in Adipose Tissue Using Imaging ToF-SIMS**.
*Histochemistry and Cell Biology*. 2009;132(1): 105-115

II. ***Solé-Domènech S,** Johansson B, Schalling M, Malm J, Sjövall P.
**Analysis of Opioid and Amyloid Peptides Using Time-of-Flight Secondary Ion Mass Spectrometry.**
*Analytical Chemistry*. 2010;82(5): 1964-1974. Epub 2010 Feb 1

III. ***Solé-Domènech S,** Sjövall P, Vukojević V, Fernando R, Codita A, Salve S, Bogdanović N, Mohammed H.A, Hammarström P, Nilsson P, LaFerla F, Giménez-Llort L, Schalling M, Terenius L, Johansson B.
**Simultaneous Localization of Cholesterol, Amyloid and Glia in Brain Tissue Using Combined Time-of-Flight Secondary Ion Mass Spectrometry (ToF-SIMS) Imaging and Fluorescence Techniques.**
*Submitted* 2012.

IV. ***Solé-Domènech S,** Sjövall P, Vukojević V, Fernando R, Codita A, Salve S, Hammarström P, Nilsson P, Winblad B, LaFerla F, Giménez-Llort L, Terenius L, Schalling M, Johansson B.
**Hippocampal Regions Occupied by Senile Plaques Exhibit Cholesterol Granulation in the 3xTg-AD Mouse Model of Alzheimer's Disease.**
*Manuscript.*

*Corresponding author

# CONTENTS

# LIST OF ABBREVIATIONS

| | | | |
|---|---|---|---|
| 24OHCh | 24(S)-hydroxycholesterol | 24OHChSE | Cholesterol 24-hydroxylase |
| ACAT | Acyl-coenzyme A cholesterol acyltransferase | CSF | Cerebrospinal fluid |
| AD | Alzheimer's disease | Aβ | Amyloid-beta |
| Ch | Cholesterol | ECh | Esterified cholesterol |
| CID | Collision-Induced Dissociation | TIM | Total ion image |
| CNS | Central nervous system | ABC | ATP-binding cassette transporter |
| GalC | Galactocerebroside | MTs | Microtubules |
| GFAP | glial fibrillary acidic protein | ST | Sulfatides |
| HDL | High density lipoprotein | VLDL | Very low density lipoprotein |
| HMG-CoA | 3-hydroxy-3-methylglutaryl-coenzyme A | LCAT | Lecithin cholesterol acyltransferase |
| KO | Knockout | Iba1 | Ionized calcium binding adaptor molecule 1 |
| LRP | Lipoprotein receptor-related protein | LDLR | Low density lipoprotein receptor |
| LXR | Liver X receptor | SREBPs | Sterol Regulatory Element Binding Protein |
| MALDI | Matrix-Assisted Laser Desorption Ionization | DESI | Desorption Electrospray Ionization |
| MCI | Mild cognitive impairment | MSI | Mass Spectrometry Imaging |
| MLD | Metachromatic leukodystrophy | CGT | UDP-galactose: ceramide galactosyltransferase |
| NFT | N-terminal fragment | BBB | Blood-brain barrier |
| NPC1 | Niemann-Pick type C protein1 | SR-B1 | Scavenger receptor class 1 |
| $OsO_4$ | Osmium tetroxide | DAG | Diacylglyceride |
| PC | Phosphatidylcholine | pc | Phosphocholine head group |
| PI | Phosphatidylinositol | BACE | β-secretase |
| RT | Room temperature | p-FTAA | *Pentamer Formyl Thiophene Acetic Acid* |
| TAG | Triacylglyceride | MAG | Monoacylglyceride |
| Tg | Transgenic | WT | Wild-type |
| ToF | Time-of-Flight | 7DHC | 7-dehydrocholesterol |
| ToF-SIMS | Time-of-Flight Secondary Ion Mass Spectrometry | SIMS | Secondary Ion Mass Spectrometry |
| UCh | Unesterified cholesterol | CFT | C-terminal fragment |

# INTRODUCTION

This thesis work will mainly focus on the study of the lipid-related structures cholesterol (Ch) and sulfatides (ST), in the context of Alzheimer's disease (AD), using imaging techniques. Therefore, the roles played by these two compounds in the central nervous system (CNS) and during AD pathogenesis will be extensively discussed herein. The involvement of other lipid structures such as phospholipids (Pettegrew et al., 2001; Farooqui et al., 2004; Pai et al., 2006), fatty acids (Zamaria, 2004; Hooijmans and Kiliaan, 2007; Wang et al., 2008), gangliosides (Molander-Melin et al., 2005; Ariga et al., 2008), prostaglandins (Bazan et al., 2002; Zagol-Ikapitte et al., 2005; Hoshino et al., 2007), sphingolipids (Mutoh et al., 2006; Katsel et al., 2007) and others (Dietschy and Turley, 2004; Hartmann et al., 2006; Hirsch-Reinshagen et al., 2009) in AD is out of the scope of the present work and has been extensively discussed elsewhere.

## CHOLESTEROL IN THE CENTRAL NERVOUS SYSTEM

### Distribution

The sterols, of which Ch and its derivatives are the most widely studied in mammalian systems, constitute an important component of membrane lipids, along with the glycerophospholipids and sphingomyelins (Bach and Wachtel, 2003). In the CNS, Ch is mainly present as a free, non-esterified molecule (UCh), whereas the fraction of esterified cholesterol (ECh), stored in lipid droplets in neurons and glia, is comparatively much smaller. UCh plays an essential role in controlling the electrical properties of many cellular membranes, including the plasma membrane, as well as determining their fluidity and permeability characteristics, which has implications on the development and maintenance of neuronal plasticity (Ledesma and Dotti, 2006). Due to the brain's unique anatomy and the relative isolation from the rest of the body, many properties of Ch metabolism in the CNS are unique compared to other organs. One of the most striking differences is the distribution of Ch in brain and spinal cord; besides being present in the plasma membrane of neurons and glial cells, Ch is mainly stored in the form of myelin sheaths, which are synthesized mainly by oligodendrocytes and further wrapped and dehydrated around numerous adjacent neurons to form compact sheets (Dietschy and Turley, 2004; Dietschy, 2009). Myelin is mainly composed of Ch, phospholipids and glycolipids, as is the case for most plasma membranes. However, the lipid content in myelin is much higher as compared to cellular plasma membranes. Myelin forms thick layers that insulate the hydrophobic membranes of the axons and reduce their capacitance; the need for such nerve insulation may be explained in the grounds of evolution of larger organisms and the subsequent need of increasing the speed of electrical conduction along neurons. As a result, axons acquire higher capacity for transmission of electrical signals (Dietschy, 2009). Hence, CNS Ch is divided into two main pools consisting of i) the Ch in the plasma membranes of glial cells and neurons and ii) the Ch present in the specialized membranes of myelin, whereas in the other organs of the body Ch is mostly found in

the plasma membrane of cells, with the exception of fat adipose tissue. The CNS contains almost a 25% of the UCh present in the body, even though the organ accounts only for 2% of the body mass.

## Transport and supply

In vertebrates, lipids are almost entirely transported by spherical particles containing apolipoproteins, phospholipids, fatty acids and Ch called lipoproteins (Christopher K. Mathews, 1990). During lipid mobilization, Ch is rapidly esterified and transported condensed within the lipoprotein core, of hydrophobic nature, whereas the outer layer of the particle is of hydrophilic nature, containing the phospholipids head group and UCh. The apolipoprotein is embedded into the structure, acting as a ligand that facilitates the recognition of the lipid particle by lipid receptors expressed at the cell surface. ApoE is a ligand for receptors of the low density lipoprotein receptor superfamily such as the low density lipoprotein receptor (LDLr), the low density lipoprotein receptor-related protein (LRP), the very low density lipoprotein receptor (VLDLr) and the apoE2 receptor, all of them expressed in the plasma membrane of CNS neurons (Herz and Beffert, 2000). The density of lipoproteins is inversely related to the capacity of the particles to transport Ch (and lipids). High density particles are very rich in apolipoprotein content and less rich in lipids, whereas low density lipoproteins carry higher amounts of lipids and Ch and have a lower content in apolipoproteins (Christopher K. Mathews, 1990).

It has been proposed that, after differentiation of astrocytes, neurons reduce their endogenous production of Ch and rely mainly on Ch delivery from astrocytes via lipoprotein-like particles that contain astroglia-derived apoE (Argmann et al., 2005). Astrocytes have been shown to synthesize Ch and apoE under the influence of ATP-binding cassette transporters (ABC), which facilitate the efflux of Ch to apoE and apoA-I-bearing lipoproteins (Wahrle et al., 2004; Karten et al., 2005; Abildayeva et al., 2006), being the predominant source of apoE in the brain. Microglia are also capable of synthesizing apoE, however, to a much lesser extent (Martins et al., 2008).

Astrocytes secrete Ch, phospholipids and apoE in the form of small, high density lipoprotein (HDL) particles into the pericellular fluid (Gong et al., 2002; Dietschy, 2009). These are taken up by neurons and other glial cells at especially high rates during development, regeneration after injury, or during the formation of new synaptic contacts. These lipoproteins are recognized by their specific membrane receptors and subsequently internalized via endocytosis (coated pit pathway). Once internalized, the lipoprotein-receptor unit undergoes hydrolysis by a neutral cholesteryl-ester hydrolase (Acton et al., 1996). Ch is transported from the lysosomal to the metabolically active pool in a process mediated by functional Niemann-Pick type C protein 1 (NPC1) transport system (Dietschy and Turley, 2001; Xie et al., 2006). Figure 1-1 presents a speculative scheme on the transport and uptake pathways of Ch in the CNS.

The CNS is provided with Ch by *de novo* synthesis but mainly by recycling of existing sterol reservoirs (Shobab et al., 2005). Oligodendrocytes (Dietschy, 2009) and astrocytes (Pfrieger, 2003) account for the major part of Ch synthesis carried out in the CNS. Nevertheless, despite the fact that *in vivo* measurements of net Ch movement into the brain have not succeeded, there may be a small transfer of Ch from circulating plasma across the blood-brain barrier (BBB) as suggested by the presence of LDLRs and other lipoprotein transporters such as scavenger receptor class 1 (SR-B1) and ABC-A1 transporters in brain endothelial cells (Dehouck et al., 1997; Dietschy, 2009).

### Uptake and recycling by glial cells

Astrocytes and microglia are supporting cells that undertake several different functions in the CNS. Astrocytes supply nutrients to the nervous tissue, maintain the extracellular ion balance and play an important role in the repair and scarring process of the brain and spinal cord following traumatic injuries (Kandel, 1991). In contrast, microglia are the main immune cells of the brain (Nimmerjahn et al., 2005). Under nonpathological conditions, microglia are highly ramified cells. When activated by injury or insult to the brain, microglia proliferate, undergo morphological changes, and secrete chemokines and cytokines (Lucin and Wyss-Coray, 2009).

In the event of neuronal loss and synaptic degeneration, astrocytes gather around the affected areas and recycle Ch and lipid fragments resulting from plasma and myelin membrane damage (Shobab et al., 2005). ApoE synthesis dramatically increases in glial cells recruited around the lesioned region, probably in order to facilitate lipid uptake (Poirier et al., 1991; Hayashi et al., 2004). Astrocytes not only recycle lipid and Ch debris from lesioned regions; they are capable of transporting large amounts of lipids to regions undergoing reinnervation (Poirier et al., 1993). In contrast, despite their capacity for synthesizing apoE, it is not clear whether microglia are able to secrete or internalize Ch in significant amounts (Gilardi et al., 2009).

### Clearance through the blood-brain barrier

The Ch turnover in brain is remarkably slower than the turnover in all other organs. From 0.02% (human) up to 0.4% (mouse) of the Ch stored in the CNS is replaced each day. Accordingly, the absolute flux of Ch is approximately 0.9% as fast as the turnover of sterol in the whole body in these species. A fraction of the Ch levels in the plasma membrane of neurons and glial cells is constantly being replaced (e.g. 7-9% in mouse brain and 0,7% in human, daily) (Dietschy and Turley, 2001; Dietschy, 2009).

In order to maintain Ch levels at steady state, it is necessary to maintain a balance between the newly incorporated and excreted sterol pools. Clearance is accomplished partly via conversion of Ch into 24(S)-hydroxycholesterol (24OHCh) and further excretion through the BBB (Björkhem and Meaney, 2004). Cholesterol 24-hydroxylase (24OHChSE) is the enzyme responsible for the selective hydroxylation of Ch and is uniquely expressed in the brain (Lund et al., 1999). Due to the addition

of an oxygen atom into the structure, 24OHCh is a far more polar molecule than Ch and, as a result, it can easily go across the BBB and possibly the neuronal plasma membrane without any further transport mechanisms.

Animal studies have shown that the amount of Ch excreted from the CNS is of about 1,4 mg/day, 0,9 mg/day being excreted via formation of 24OHCh (Dietschy, 2009). In humans, the brain releases approximately 6 mg of 24SOHC into the periphery each day, which is subsequently uptaken by the liver (Björkhem et al., 1999).

Furthermore, 24OHCh acts as a signaling molecule that induces the apoE-mediated Ch efflux from astrocytes but not from neurons. Therefore, large amounts of 24OHCh may induce *de novo* Ch synthesis by astrocytes, as means of maintaining the sterol steady state. Due to the selective upregulation of ABC-G4 transporters caused by 24OHCh, it is possible that ABC-G4 mediates its efflux (Abildayeva et al., 2006). In addition, 24OHCh increases the apoA-I mediated Ch efflux from neuronal cells, which may be indicative of an additional clearance pathway (Abildayeva et al., 2006).

Besides the 24OHCh excretion pathway, other clearance mechanisms may account for the excretion of at least 0.5mg Ch/day. The mechanism, although not yet completely understood, seems to regulate the excretion of Ch via a coupled ABC-apoE transport system. ABC-A1 transporters may excrete Ch, which is uptaken by apoE-containing lipoproteins to formation of immature, poorly lipidated particles. In further maturation steps, Ch may be released from ABC-G1 transporters leading to a mature fully loaded lipoprotein. Finally, these particles may be presumably mobilized directly across the BBB for excretion to the circulating plasma (Dietschy, 2009).

## Regulatory elements of cholesterol synthesis

*Liver X Receptors*

Liver X Receptors **(**LXRs) have been shown to play a central role in the regulation of Ch metabolism (Joseph et al., 2002). Two isoforms have been identified in the CNS, namely LXRα and LXRβ, the oxysterols being their natural ligands and activators (Whitney et al., 2002; Russell et al., 2009). *In vitro* studies showed that 24OHCh, which is thought to mediate its action through LXRs (Abildayeva et al., 2006), induces expression of ABC-A1, ABC-G1 and apoE in astrocytic cells, primary rat and murine astrocytes, and elevates apoE-mediated Ch efflux (Abildayeva et al., 2006). Indeed, ABC-A1, ABC-G1 and ABC-G4 have been identified as LXRs target genes in the brain (Tontonoz and Mangelsdorf, 2003; Yu et al., 2003). In mouse brain, deletion of LXRα and LXRβ function leads to diminished expression of a number of LXR target genes (Wang et al., 2002) while administration of LXR agonists enhances the expression of genes controlling the synthesis of ABC-A1, ABC-G1 and apoD (Repa et al., 2007) although not clear for apoE (Whitney et al., 2002). Alterations in LXRα/β function may lead to a variety of CNS defects upon aging such as lipid accumulation, astrocyte proliferation, and disorganized myelin sheets, as shown in LXRα/β null mice (Wang et al., 2002).

*Sterol Regulatory Element Binding Protein (SREBPs)*

The Sterol Regulatory Element Binding Proteins (SREBPs) are transcription factors that bind to sterol regulatory factors. A number of isoforms have been described, the SREBP-2 isoform being involved in the regulation of genes implicated in Ch metabolism preferentially. In the Golgi apparatus, proteolytic cleavage of the ~120 kDa SREBP precursor protein bound to the Ch sensing protein *scap* (forming SREBP-*scap* complex) releases a transcriptionally active N-terminal fragment (NTF) and allows it to move to the nucleus through the cytoplasm. Once in the nucleus, the active domain binds to specific DNA sequences (the sterol regulatory elements or SREs) leading to a transient increase in the transcription of the target genes responsible for the expression of enzymes involved in the synthesis of Ch (Gasic, 1994; Wang et al., 1994). These nuclear fragments normally drive the expression of many of the enzymes required for cholesterogenesis, including 3-hydroxy-3-methylglutaryl-coenzyme A (HMG-CoA) reductase (Dietschy, 2009).

*In vitro* studies shown a transient down-regulation of SREBP-, LDLR and HMG-CoA reductase mRNA levels in astrocytoma but not neuroblastoma cell lines upon incubation with 24OHCh (Abildayeva et al., 2006). It is long since known that oxysterols reduce the activity of HMG-CoA reductase and are more potent inhibitors of Ch synthesis than Ch itself (Kandutsch and Chen, 1974). However, the mechanisms by which Ch and oxysterols reduce Ch synthesis differ (Adams et al., 2004). 24OHCh seems to downregulate the mechanisms responsible for Ch synthesis (namely SREBPs, LDLR and HMG-CoA reductase) while upregulating the synthesis of proteins responsible for Ch efflux and transport between astrocytes and neurons (namely ABC-A1, G1 and G4 as well as apoE and apoA-I transporters).

## SULFATIDES

### Function, synthesis and distribution

Glycosphingolipids are important components of the outer leaflet of plasma membranes; their structures contain carbohydrate moieties believed to be involved in important cellular mechanisms such as intercellular recognition, transmembrane signal transduction and regulation of cell development and differentiation (Curatolo, 1987; Hakomori, 1990). The glycosphingolipids galactocerebrosides (GalC) and their derived sulfated form, sulfatides, are major lipid constituents of the myelin sheaths surrounding axonal processes (Marcus and Popko, 2002) and play an important role in maintaining the proper insulating conditions of the membrane.

GalC and ST bear carbohydrate groups that associate through divalent cation linkages, which are believed to provide and stabilize the proper curvature of the myelin membrane bilayer (Curatolo, 1987). Furthermore, not only do these glycolipids play a role in membrane stability, but they are also believed to participate in the early differentiation and myelination process occurring post-natally, suggesting that they are necessary for the proper development and maintenance of myelin (Ranscht et al.,

1982). Furthermore, sulfated glycolipids play essential roles in the plasma membrane of cells; ST species contain a negative charge moiety, which facilitates the non-covalent binding to any positively charged amino acid side chain at accessible external sites of a protein. This type of interaction results in low-affinity binding which will be strengthened if the protein has additional binding site domains. Concentration of ST molecules in membrane microdomains may constitute an array of negative charges that, after initial recognition via specific receptors, may form close contacts between cells, membranes or macromolecules (Vos et al., 1994). Therefore, ST may be involved in cell adhesion, close contact between biomembranes, cell fusion and endocytosis, among other functions.

Given the important functions attributed to GalC and ST, special interest has been paid to characterizing their biosynthesis. GalC are synthesized by UDP-galactose: ceramide galactosyltransferase (CGT), a synthase that catalyzes the transfer of galactose to ceramide (Coetzee et al., 1996). The enzyme is mainly expressed by oligodendrocytes and myelinated regions of the nervous system. In contrast, ST is synthesized by the sulfation of the galactose residue in GalC through the enzymatic activity of the enzyme cerebroside sulfotransferase (Vos et al., 1994). ST species are mainly synthesized by oligodendrocytes, which also synthesize and maintain myelin sheaths in the CNS. A number of ST structures have been identified, which vary in the length and number of unsaturations of the fatty-acid chain constituting the ceramide moiety. Due to the length of the acyl chains contained in the ceramide moiety, the total length of a ST molecule usually spans more than half the width of a regular bilayer. Hence, ST molecules are packed within the bilayers (Vos et al., 1994).

## Abnormalities associated with alterations in galactocerebrosides content

Galactolipids are molecular determinants of myelin development. Mice lacking CGT, which is necessary for the production of GalC and subsequent synthesis of ST, form an altered type of myelin sheaths containing glucocerebroside, which although not identified in normal myelin, is gathered in altered myelin perhaps in order to compensate for the lack of GalC. Although these animals display an apparently normal myelin sheath structure, they exhibit severe trembling, mild ataxia, age-dependent hindlimb paralysis and extensive vacuolation of the ventral region of the spinal cord, consistent with a reduced isolating capacity of the myelin sheath (Bosio et al., 1996; Coetzee et al., 1996). Furthermore, these mice display hypomyelinated axonal processes and there is a significant increase in the number of unmyelinated axons in the CNS (Marcus et al., 2000).

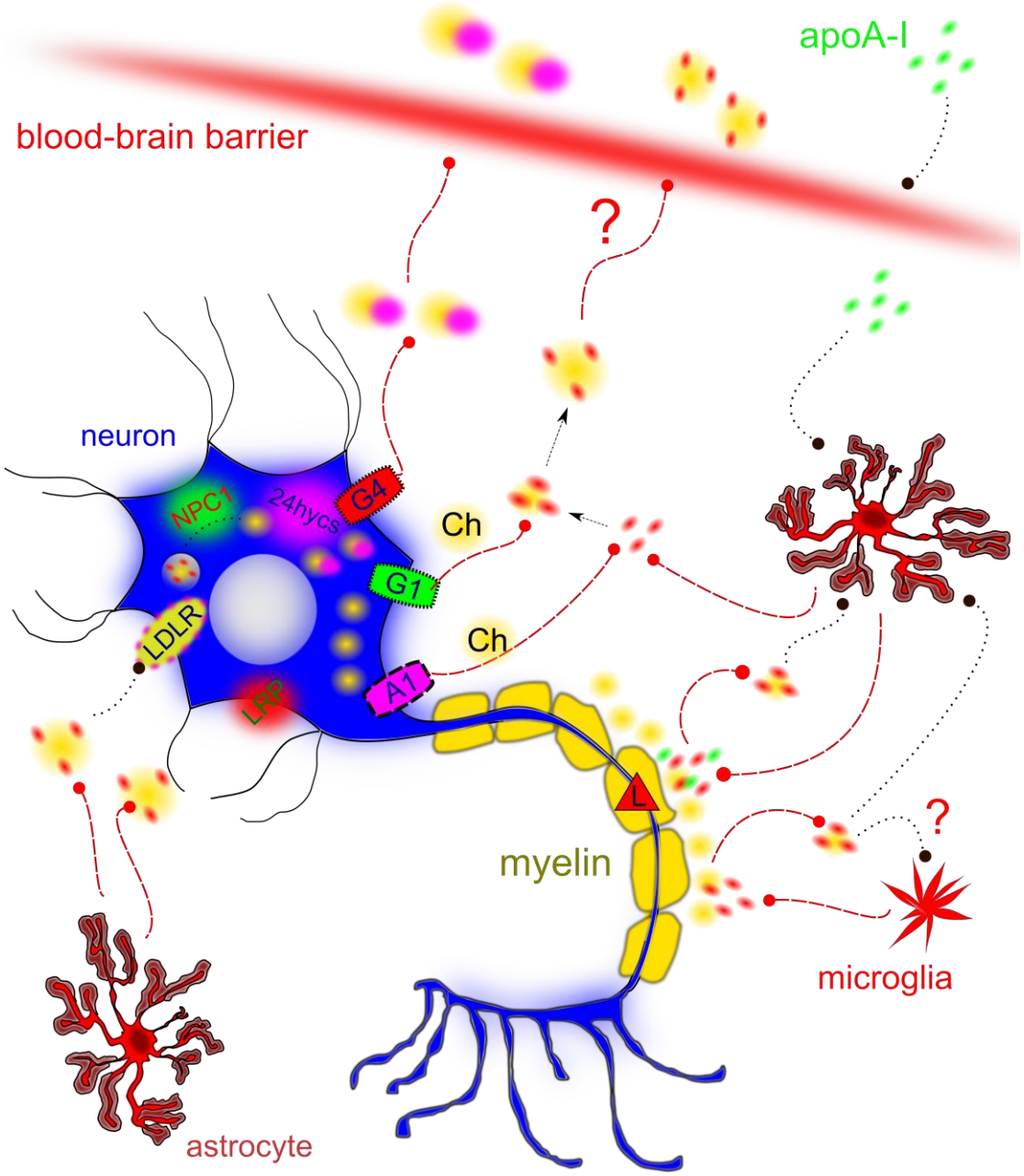


**Figure 1-1**. Speculative mechanism for the transport and recycling of Ch in the CNS. **Lower left/upper left:** Astrocytes synthesize apoE and secrete apoE-containing lipoproteins loaded with Ch and lipids, which are then recognized and internalized by specific membrane receptors (LDLR and LRP, among others) via endocytosis (coated pit pathway). The internalized lipoprotein is then hydrolyzed and Ch is transferred to the metabolically active pool by the action of NPC1. Ch excretion from the neuron is mediated by i) the addition of an OH group by the action of 24ChOHSE to produce 24ChOH, which is far more polar than Ch and capable of traversing the plasma membrane by itself or by the mediation of ABC-G4, and by ii) excretion via ABC-A1 and ABC-G1 transporters to form premature apoE-bearing lipoproteins, which will subsequently mature and become fully loaded particles. The mechanism of excretion of these apoE-loaded particles is not yet understood, but may involve selective crossing of the BBB. **Lower right/upper right:** in the event of synaptic or neuronal damage (indicated by *L* in a red triangle), lipid debris from degenerating myelin are captured by apoE-containing particles, which are secreted by astrocytes and microglia, and reuptaken by these glial cells once loaded (although the role of microglia in the reuptake of lipid debris is not yet clarified). Loaded astrocytes may then transport the reuptaken lipid storages for further recycling and reuse in other metabolic processes. Apo A-I may assist apoE in the reuptake of lipid debris by entering the CNS across the BBB or being perhaps synthesized by local glia.

Metachromatic leukodystrophy (MLD), also called Arylsulfatase A deficiency, is a lysosomal storage disease characterized by the accumulation of ST in the brain, which is caused by a dramatic reduction in the activity of the enzyme Arylsulfatase A (Poeppel et al., 2005). ST builds up in the CNS, leading to demyelination and resulting in neuromotor co-ordination deficits and regression. A recent study has suggested lysosulfatide, a ST species lacking the acyl group, as a central player in the pathogenesis of the disease (Blomqvist et al., 2011). MLD-associated symptomatology includes muscle wasting, weakness and rigidity, developmental delays, progressive loss of vision leading to blindness, convulsions, impaired swallowing, paralysis, and dementia. The late infantile form is the most common form of MLD, accounting for 50 to 60% of all cases, whereas the adult form commonly begins after the age of 16 as a psychiatric disorder or progressive dementia. Adult-onset MLD progression is slower than the late infantile and juvenile forms, with a protracted course of a decade or more. Several treatment options are being investigated and include gene therapy, enzyme replacement therapy, substrate reduction therapy, and potentially enzyme enhancement therapy. However, at the present moment, there is neither cure nor standard treatment for MLD.

Abnormal sulfatide metabolism and homeostasis have been found in association with multiple other diseases, such as cardiovascular diseases (Hu et al., 2007) and colorectal adenocarcinoma (Morichika et al., 1996).

## ALZHEIMER'S DISEASE: THE LIPID CONNECTION

### Background information on Alzheimer's disease

Alzheimer's disease is the most common form of dementia, affecting up to 15 million individuals worldwide. By 2050, approximately the 25% of people living in the Western hemisphere will be over 65 years of age, and one third of them are likely to develop AD (Puglielli et al., 2003). AD is characterised by loss of neurons and synapses in the cerebral cortex and certain subcortical regions. This loss results in gross atrophy of the affected regions, including degeneration in the temporal and parietal lobes, and parts of the frontal cortex and cingulate gyrus (Wenk, 2003). Research in the field has been dramatically increasing in recent years, due to the global aging of the population and the increasing health costs. Efforts are gradually being focused on finding alternative theories to the amyloid-beta (Aβ) cascade hypothesis and treatments not involving the removal of Aβ plaques. Increasing evidence supports the involvement of Ch in the pathogenesis of the disease (Puglielli et al., 2003; Sambamurti et al., 2004; Hirsch-Reinshagen et al., 2009). However, the role of lipids during AD progression, especially at early stages, has yet not been understood. The following sections present an extensive discussion of some of the pathogenic mechanisms underlying AD as well as the implication of Ch and ST in the pathogenesis of the disease.

## The amyloidogenic cascade

The amyloid precursor protein (APP) is an integral membrane protein with a single membrane-spanning domain that presents different isoforms ranging from 695 to 770 amino acids, the $APP_{695}$ being the most abundant isoform in the brain. The role of APP has not been yet completely understood, but it is mainly synthesized by neurons and may contribute to maintain neuronal plasticity and normal synaptic activity. APP is the substrate of three basic enzymatic pathways involving α-, β- and γ-secretases; Cleavage of APP by α-secretase produces (s)APPα at the cell surface and leaves an 83 amino acid carboxy-terminal fragment (CFT) (C83). The amyloidogenic processing of APP involves then sequential cleavages by β-secretase (also called β-site APP cleavage enzyme, or BACE) and γ-secretase at the N and C terminal sides of the Aβ domain, respectively. Concretely, cleavage of APP at the BACE site will leave a 99-amino-acid CFT which can be subsequently internalized and processed by γ-secretase to produce $Aβ_{1-40/42}$ in endocytic compartments (Mattson, 2004). γ-secretase is a multicomplex enzyme composed of four subunits (presenilin, nicastrin, APH-1 and PEN-2); mutations in the presenilin subunits lead to alteration in enzyme activity and are associated with familial forms of AD (Haass and De Strooper, 1999). It is to note that APP is only one of several proteins uptaken and processed by γ-secretase, with Notch-1 being another well-studied γ-secretase substrate (Hardy, 1997). $Aβ_{1-40}$ and $Aβ_{1-42}$ are the main Aβ peptides synthesized during the amyloidogenic processing of APP; $Aβ_{1-42}$ includes two extra hydrophobic residues (isoleucine and alanine) in the sequence, as compared to the more abundantly generated $Aβ_{1-40}$ peptide. Interestingly, the Aβ 42/40 ratio is increased in familial cases as well as in sporadic AD patients. Figure 1-2 displays a schematic representation of the amyloidogenic processing of APP described above.

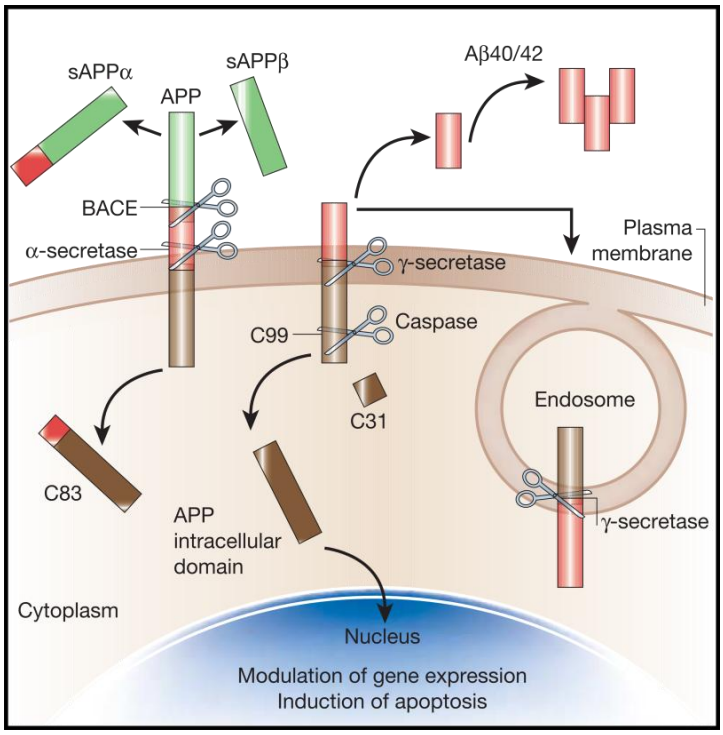


**Figure 1-2.** Schematic representation on the amyloidogenic processing of the APP protein in the plasma membrane system of neurons. The transmembrane APP protein is cleaved by α and β secretases to produce the extracellular NTFs (s)APP α and (s)APP β. Alternative cleavage by γ-secretase releases the an 83 amino acid CTF (C83). After β-secretase cleavage, further processing of the remaining transmembrane domain by the γ-secretase complex releases $Aβ_{1-40}$ and $Aβ_{1-42}$ to the extracellular milieu. The remaining 99 amino-acid CTF (C99) is either released and mobilized to the nucleus or cleaved by caspases to release a 31 amino-acid CTF (C31). The amyloidogenic processing of APP can partially occur in cellular compartments, such as endosomes, leading to intracellular release of Aβ species and CTFs. Figure adapted from Mattson et *al* (2005) with permission of Nature Publishing Group.

Aβ is a naturally occurring peptide in brain and cerebrospinal fluid of healthy humans through life (Haass et al., 1992; Walsh et al., 2000). Aβ *per se* does not cause neurodegeneration; neuronal injury seems to require the prolonged self-association of Aβ units (Pike et al., 1991). Apparently, long term Aβ overproduction leads to peptide aggregation, fibrillation and subsequent formation of extracellular insoluble Aβ deposits. Affected regions display two types of plaques; mature neuritic plaques and diffuse deposits. Neuritic plaques contain skeins of insoluble amyloid fibrils, intermixed with an array of non-fibrillar forms of the peptide. These deposits contain both $A\beta_{1-40,}$ $A\beta_{1-42}$ and a number of N-terminal truncated peptides (Iwatsubo et al., 1994) and are surrounded by dystrophic neurites and immunoreactive astrocytes and microglia (Selkoe, 2011). In contrast, diffuse deposits are mostly non fibrillar, granular structures lacking the surrounding dystrophic neurites and immunoreactive glia. These structures are mostly composed of the highly amyloidogenic $A\beta_{1-42}$ (Iwatsubo et al., 1994) and are likely to transform into fibril-containing classic senile plaques upon maturation (Selkoe, 1994). As these diffuse forms begin to acquire fibrils, local gliosis occur, followed by spine loss and dystrophic neurites (Haass and Selkoe, 2007). Extracellular deposits have been associated with increased oxidative stress and deregulation of $Ca_2^+$ homeostasis (Mattson, 2004). However, AD progression and dementia correlate poorly with brain plaque load (Dickson, 1997) and the role of extracellular deposits as an active cause of dementia is under discussion. Indeed, older humans have substantial amounts of diffuse Aβ deposits in their limbic cortices and still remain healthy (Haass and Selkoe, 2007).

Aβ in AD brain, however does not only exist as extracellular deposits; Aβ forms a large number of complex mixtures that excert a wide spectrum of deleterious effects, and include aggregated, fibrillar and the so-called oligomeric Aβ units. Oligomeric Aβ species comprise a wide range of structures arising from the assembly of Aβ peptide monomer subunits. Although the precise molecular identity of these structures is not yet completely understood, it seems that they are not fibrillary in nature (Walsh and Selkoe, 2007). Oligomers tend to polymerize and form aggregates; in fact, the formation of stable low molecular weight oligomers is a relatively unfavoured process (Walsh et al., 1997; Walsh and Selkoe, 2007). Evidence suggests that intraneuronal accumulation of oligomeric $A\beta_{1-42}$ species precedes plaque deposition and may contribute to the AD-related cascade of neurodegenerative events (Gimenez-Llort et al., 2007). Soluble low-n oligomeric species are potent synaptotoxins; intracellular accumulation of oligomeric species, either via membrane-mediated internalization or intracellular compartmented production, has been associated with synaptic dysfunction and neurodegeneration (Haass and Selkoe, 2007); inhibition of hippocampal long term potentiation (Walsh et al., 2002); inhibition of the cellular proteasome (Tseng et al., 2008) and alteration of the intracellular signaling mechanisms, calcium regulation and organelle function (Mattson, 2004; Tseng et al., 2004). It seems that intraneuronal Aβ excretion is mediated by the ability of synaptic activity to clear Aβ from somas and synapses (Tampellini et al., 2011). Cultured neurons from a mouse model of AD displayed reduced $A\beta_{1-42}$ excretion upon time as compared to wild-type (WT) control, and early intraneuronal $A\beta_{1-42}$ accumulation and

fibrillization has been observed within cell bodies, neurites, and synapses in a mouse model of AD, prior to plaque formation (Capetillo-Zarate et al., 2011). Hence, plaque deposition may be the result of a mechanism aiming at excreting the toxic oligomeric Aβ units from neuronal somas and synapses rather than an actual critical disease hallmark. Figure 1-3 displays a speculative scheme on the interrelation between oligomeric Aβ and senile plaques in AD.

Formation of tau aggregates is another typical protein-associated lesion in AD. Tau is a microtubule-associated protein, particularly abundant in the axons of neurons. The primary function of tau is to stabilize microtubules (MTs) for an optimal axonal transport. During AD progression, the binding of tau to the MTs is perturbed, probably due to deregulation of tau kinases and/or phosphatases, mutations of the tau gene, and covalent modification of tau causing and/or promoting misfolding (such as phosphorylation) (Ballatore et al., 2007). Tau detachment from MTs leads to increased cytosolic protein levels, which in turn facilitates protein misfolding and subsequent formation of aggregated forms of the protein, such as neurofibrillary tangles (NFTs) that accumulate in the cytoplasm of degenerating neurons. Evidence suggests that hyperphosphorylated tau is the main component of the NFTs (Busciglio et al., 1995), but the cause of such aberrant tau hyperphosphorylation is currently not yet understood. NFTs sequester normal MT-associated tau, leading to massive MT disruption and impaired axonal transport, which in turn causes synaptic dysfunction and neurodegeneration (Ballatore et al., 2007).

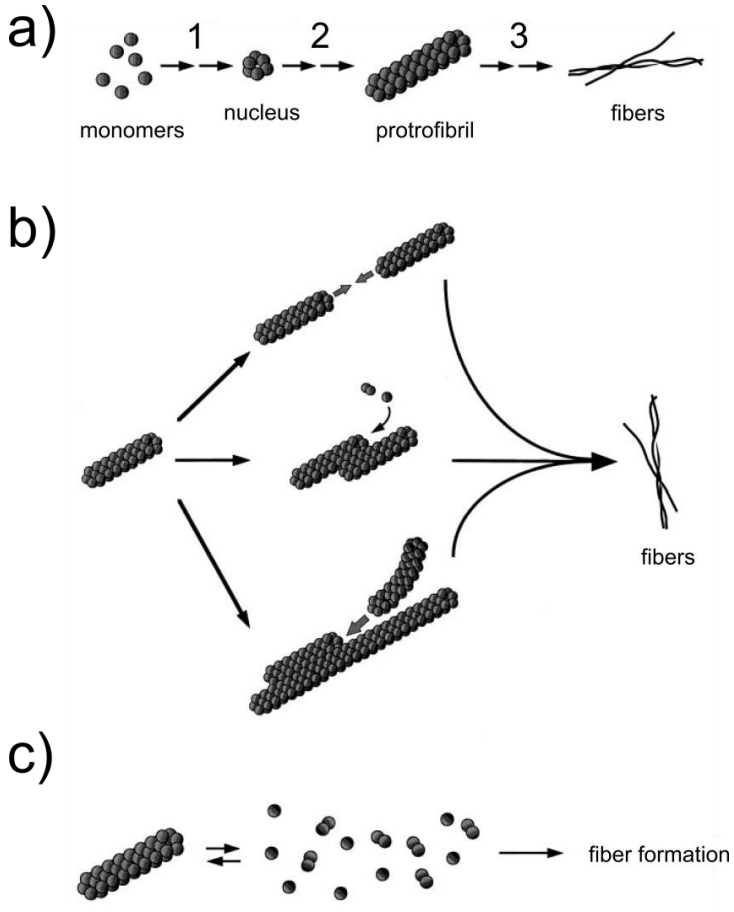


**Figure 1-3.** Speculative model on Aβ fibrillogenesis. **(a):** fibrillogenesis seems to start with the production of seeding nucleus constituted by the addition of monomeric Aβ species (1). Further addition of monomeric species to these nucleated units gives rise to protrofibrillar structures (2) which in turn may lead to production of mature Aβ fibers (3). **(b):** protrofibrillar structures may aggregate to form dimers, which in turn may act as nucleating units and incorporate single monomers or protrofibrillar species, giving rise to formation of fibrillar structures. **(c):** alternatively, protrofibrils alone may be incapable of forming fibers but may serve as bioavailable sources of monomeric Aβ species, which in turn may act as precursors in fibrillogenic pathways. Note that the different Aβ species are not drawn in scale. Reproduced from Walsch et *al* (1997) with permission of the American Society for Biochemistry and Molecular Biology.

Even though Aβ seems to precede tau pathology in the context of AD progression, the connection between oligomeric, fibrillary and deposited forms of Aβ with hyperphosphorylated tau and NFT formation is unclear. In fact, the two pathologies can occur independently in humans; NFT composed of aggregated hyperphosphorylated tau are similar to other tau-associated deposits described in several neurodegenerative diseases, such as frontotemporal dementia, in which neither Aβ deposits nor neuritic plaques can be found (Selkoe, 2011). Similarly, diffuse Aβ deposits can be seen in aged healthy cortex in absence of tangles. Nevertheless, Aβ fibrils have been shown to promote tau hyperphosphorylation and further MT detachment by increasing kinase activity in a mechanism mediated by nicotinic receptors (Wang et al., 2003). The culmination of the amyloidogenic cascade involves widespread synaptic and neuronal dysfunction followed by cell death, leading to progressive dementia associated with extensive Aβ and tau pathology.

## Cholesterol and Alzheimer's disease

*Epidemiological studies*

A number of epidemiological studies suggest that high Ch levels are associated with increased risk for AD. Indeed, AD patients show increased levels of total serum and LDL Ch together with reduced levels of apoA/ HDL in plasma (Kuo et al., 1998), as compared to age-matched controls. Epidemiological evidence suggests that reduction of Ch levels by administration of Ch synthesis inhibitors reduces AD prevalence (Vance et al., 2005). Statins are drugs that inhibit Ch synthesis and are widely used for treatment of hypercholesterolemia, and are currently being actively considered for treatment of AD. However, the data on the effectiveness of statin treatment in AD is somewhat contradictory; two retrospective epidemiological studies have shown that the use of statins in the treatment of hypercholesterolemia reduced the risk of AD by 40 to 70% (Jick et al., 2000; Wolozin et al., 2000), whereas two other similar investigations failed to show a beneficial effect of statins for treatment of AD (2002; Shepherd et al., 2002). It is to note that, since the latter studies focused primarily on cardiovascular disease, the potential beneficial effects of statins in the treatment of AD need to be further evaluated (Casserly and Topol, 2004; Wolozin, 2004). Additional studies are required to determine whether statins delay the onset of dementia and/or decrease the risk of developing AD as well as the biological mechanisms behind such effects. So far, statins have been shown to enhanced Ch efflux, upregulate of ABC-A1 and ABC-G1 expression and impair Ch synthesis in macrophages (Argmann et al., 2005) In addition, statins reduced plasma levels of 24OHCh in AD patients without lowering apoE levels (Vega et al., 2003).

ApoE4 isoform has been identified as a major risk factor for AD in several independent epidemiological studies (Tanzi and Bertram, 2001), suggesting a link between Ch homeostasis and AD. As previously discussed, apoE is a major component of lipoproteins responsible for transporting of Ch in the CNS. Three different apoE alleles have been so far identified in humans, namely apoE2, E3 and

E4. These alleles produce protein isoforms that differ in certain amino acids at specific positions (Puglielli et al., 2003). It has been hypothesized that apoE may affect the pathogenesis of AD by isoform-specific effects on lipid trafficking between astrocytes and neurons (Michikawa et al., 2000). Individuals carrying the apoE4 isoform have shown a poor prognosis for recovery of neurological function after head trauma (Masliah et al., 1995; Jordan et al., 1997), suggesting that apoE may play an important role in Ch recycling and redistribution upon CNS injury.

*Underlying molecular mechanisms*

During recent years, a number of investigations showed increased Aβ deposition (Sambamurti et al., 2004), increased immunoreactivity (Sparks et al., 1995) and tau hyperphosphorylation (Rahman et al., 2005) in different animal models of AD fed with high Ch diets. However, the molecular mechanisms underlying the Ch-AD connection remain enigmatic. Studies in cell lines have shown that Ch can actively regulate APP processing and Aβ generation. Ch-enriched microdomains in the plasma membrane of neurons display an increased amyloidogenic processing of APP (Ehehalt et al., 2003). Concretely, the neuronal membrane system seems to distribute APP into two differentiated pools, namely i)APP associated with Ch-rich lipid rafts clusters which seems to undergo BACE cleavage, and ii) APP outside lipid rafts, which undergoes α-secretase cleavage. Hence, increased Ch levels in the plasma membrane of neurons (and even glia) may trigger the amyloidogenic processing of APP by increasing the fraction of protein colocalized with BACE.

Furthermore, it has been shown that intracellular Ch distribution modulates APP processing and Aβ generation. Cellular Ch is stored either as UCh in the plasma membranes or as ECh in lipid droplets; the action of acyl-coenzyme A cholesterol acyltransferase (ACAT) controls the equilibrium between these two forms of cellular Ch and maintains Ch homeostasis. It has been suggested that this dynamic equilibrium ultimately regulates the generation of Aβ (Puglielli et al., 2001). That is, an increase in ECh is sufficient to up-regulate Aβ generation and increase the production of β-APP CFTs. Consistently, ACAT inhibitors reduced both ECh and Aβ synthesis, while increasing UCh levels (Puglielli et al., 2001). ACAT inhibitors have been suggested as suitable drugs in the treatment of AD; an increase in the cytosolic levels of UCh, however, may potentially induce cytotoxic events.

In fact, the function of several important enzymes controlling Ch homeostasis may be altered in AD. For instance, the levels of lecithin cholesterol acyltransferase (LCAT), an enzyme found in plasma, are significantly reduced in AD patients (Knebl et al., 1994). The enzyme plays a central role in the reverse Ch transport, which eliminates Ch from peripheral cells. LCAT converts UCh into ECh, which is then transferred to lipoprotein particles and mobilized. Reduced LCAT activity leads to increased Ch plasma levels, increased LDL-associated Ch (leading to Ch accumulation in tissues) and reduced HDL-Ch (responsible for transporting Ch to the liver for further excretion) (Puglielli et al., 2003).

The transport of Ch and other lipids may directly or indirectly control the Ch-induced Aβ production. The role of apoE in maintaining brain Ch homeostasis may contribute to the increased risk for AD associated with apoE4. For instance, apoE may alter brain Ch homeostasis by modifying lipoprotein-particle formation; apoE4 tends to associate with VLDL particles, which contain more Ch, whereas apoE3 binds to HDL particles. Indeed, subjects homozygous for apoE4 allele show higher levels of Ch in plasma (Ehnholm et al., 1986) and 24OHCh in cerebrospinal fluid (CSF) (Papassotiropoulos et al., 2002). However, apoE4 has shown reduced Ch transport capacity as compared with the other alleles (Elliott et al., 2010). Besides, several studies have shown that apoE can bind to Aβ (Näslund et al., 1995) and facilitate its aggregation in an isoform-dependent manner E2>E3>E4 (LaDu et al., 1994). apoE may mediate Aβ toxicity by internalization through LDLRs, in a process mediated by LRPs (LaDu et al., 1994; Chung et al., 1999) which are mainly expressed in neurons and activated astrocytes (Bu et al., 1994) whereas LDLRs are expressed mainly in glia (Pitas et al., 1987). LRP1 conditional knockout (KO) mice display increased cerebral apoE levels and a 40% decrease in brain Ch levels, consistent with the function of LRP1 as a mediator of apoE uptake in the CNS (Liu et al., 2007).

## Sulfatides and Alzheimer's disease

The analysis of ST has been traditionally challenging, mainly due to important technical limitations. Han and collaborators created an approach called *shotgun lipidomics* (Han and Gross, 2005) consisting in the use of electrospray ionization mass spectrometry in the study of complex mixtures of ST and lipids, allowing for qualitative and quantitative determination of the levels of number of ST species in tissue. Han and collaborators, using their *shotgun lipidomics* approach, and others investigators, have studied the content and distribution of ST in human and animal tissues affected by AD pathology.

A dramatic decrease in ST levels has been observed in post mortem brain tissue from AD patients (Svennerholm and Gottfries, 1994; Han et al., 2002), patients with incipient dementia and patients with mild cognitive dementia (MCI) (Han et al., 2003b; Irizarry, 2003) whereas the levels and activity of the enzymes involved in the synthesis of the glycosphingolipid remained apparently unaltered (Cheng et al., 2003). ST depletion seems to occur specifically in brain tissue affected by AD, as study of brain samples from patients suffering from other neurodegenerative processes did not reveal significant variations in ST levels (Cheng et al., 2003).

Studies in mouse models of AD suggested that ST depletion is mediated by apoE. $APP_{swe}$ transgenic (Tg) mice displayed a decrease in ST levels that was age and region dependent; ST levels were significantly decreased in cortical structures, but only slightly decreased in cerebellum, already at 9 months of age. Surprisingly, the levels of other glycosphingolipids (such as GalC) were not altered as compared to WT (Cheng et al., 2008). Furthermore, $APP_{swe}$ animals KO for apoE displayed unaltered ST levels as compared to age-matched $APP_{swe}$ normally expressing apoE.

Furthermore, it has been shown that ST associates preferentially to apoE-containing HDL particles, and that apoE presents a ST transport capacity in an E4>E3>E2 fashion (Han et al., 2003a). Based on these observations, Han and collaborators suggested a mechanism in which nascent apoE-bearing particles, released from astrocytes, approach myelinated regions of the neurons and capture ST in a *kiss-and-run* mechanism. The loaded lipoprotein is then either internalized by the neurons through an LDLr superfamily membrane receptor (for further degradation) or excreted through the BBB. Given the fact that apoE4 exhibits increased ST binding affinity, brain structures in apoE4 carriers may undergo accelerated ST loss and myelin alteration, thus increasing the risk of developing dementia (in an AD context). However, it is difficult to conceive a selective apoE-mediated sequestration of myelin ST, as apoE-bearing lipoproteins display very high binding affinity for Ch and no concomitant decrease in Ch levels has been observed in mouse or human brain regions affected by ST depletion. Furthermore, the excretion of ST-loaded lipoproteins through the BBB must necessarily involve crossing the barrier; as discussed previously, such mechanism may exist, but has not yet been clarified.

The fact that ST depletion has been observed in cortical structures but not in cerebellum of $APP_{swe}$ animals suggests that ST may be associated with Aβ, as cortical regions display much more Aβ load than cerebellum. Consistently, the onset of decreased ST matched to that of the underlying Aβ pathology in these animals. Furthermore, poorly myelinated regions seem to be more prone to undergo ST depletion, as MCI patients displayed a 90% decrease in the levels of grey matter ST, compared to only 50% in white matter structures (Han et al., 2002). It has been shown, also by Han and collaborators, that ST species present in vesicles bind to Aβ and mediate its clearance via an endocytotic pathway. Concretely, ST administered to H4-APPwt cells, which secrete large amounts of Aβ into the cell media, reduced Aβ production in a dose-dependent manner (selectively for $Aβ_{1-42}$) whereas other anionic lipids did not alter media Aβ levels significantly (Zeng and Han, 2008). The role presumably played by ST in the clearance of Aβ species is consistent with the selective vulnerability of cortical regions to Aβ pathology; the decrease in cortical levels of ST may reduce Aβ clearance rate in these regions, boosting the amyloidogenic cascade and leading to increased Aβ levels and subsequent senile plaque deposition.

## LIPID IMAGING TECHNIQUES

Given the tight association between lipids and neuropathology, it is necessary to develop tools allowing for the detailed molecular imaging of lipids and lipid precursors in human and animal brain tissue samples. Fluorescence techniques such as selective lipid stains are capable of imaging the distribution of lipids using confocal microscopy with great lateral and axial resolution. Furthermore, mass spectrometric imaging techniques offer the possibility to simultaneously image a wide range of analytes in a particular sample. The different techniques differ in terms of specificity, sensitivity and resolution, each technique being appropriate for each particular analytical problem. The following section will discuss lipid imaging methods with special attention being paid to Time-of-Flight Secondary Ion Mass Spectrometry (ToF-SIMS) imaging.

### Cholesterol imaging by fluorescent techniques

A number of commercially available fluorescent assays offer the possibility to image Ch in cells and biological tissue samples. Filipin was developed in the late 1950s as an antibiotic compound with potent antifungal activity (Whitfield et al., 1955). In cellular biology, Filipin is used as an inhibitor of the raft/caveolae endocytosis pathway on mammalian cells, but most importantly, the dye binds to cellular Ch and related sterols with high affinity. The currently available Filipin dye is a mixture of four different complexes (namely Filipin I, II, III and IV) and is especially suited for binding and imaging of cellular UCh. However, the dye undergoes rapid photobleaching, and exhibits modest fluorescence under UV excitation, thus hampering imaging using confocal microscopy and limiting its application in cell biology and tissue imaging.

Cholesterol can also be imaged using a colorimetric method based on the selective oxidation of Ch by Ch-oxidase, which produces $H_2O_2$ that, in turn, oxidizes 10-acetyl-3.7 dihydroxyphenoxazine (Amplex Red) into the highly fluorescent compound resorufin, in the presence of horseradish peroxidase (HRP). The compound can then be imaged using fluorescence microscopy. However, a recent study suggests that Amplex Red may exhibit significant autofluorescence depending on the oxidative status of the biological sample being imaged. For instance, senile plaques treated with the colorimetric assay have been shown to emit fluorescence even in the absence of Ch-oxidase (Lebouvier et al., 2009), which could be partially due to the Ch-oxidase-like activity presented by senile plaques (Puglielli et al., 2005).

A new Ch binding agent, BCθ, has been shown to bind to UCh in cells and biological tissue with high affinity. BCθ originates from a toxin produced by *Clostridium perfringens.* For imaging purposes, the toxin has been biotinylated, allowing for subsequent imaging of BCθ bound to Ch-enriched domains using avidin-conjugated fluorescent indicators. The assay presents robust fluorescent properties and can be optimally imaged using fluorescence microscopy in a manner superior to that of Filipin (Reid et al., 2004).

## TIME-OF-FLIGHT SECONDARY ION MASS SPECTROMETRY

The following section includes a brief historical perspective on the application of SIMS and ToF-SIMS to the analysis of biological samples. The reader is asked to refer to the last section, entitled *Background information on secondary ion mass spectrometry (SIMS)* in order to understand the physical and chemical principles underlying the methodology.

*Broad perspective on the analysis of biological samples using ToF-SIMS*

The first steps in the analysis of biological preparations were given by Benninghoven in the late 70s. At that time, prior to the introduction of cluster ion sources and Time-of-Flight (ToF) detectors, the analysis of biological substances was primarily performed using monoatomic primary ions (Benninghoven et al., 1976) In 1978, Benninghoven et al. used an $Ar^+$ ion source to study more than 40 biologically relevant compounds, including amino acids, peptides, drugs, vitamins, and pharmaceuticals (Benninghoven and Sichtermann, 1978). Emission of highly specific secondary ions was observed from these compounds, such as molecular ions and smaller characteristic fragment ions.

At the beginning of the 80s, Chait and Standing reported significant improvements in the mass resolution and transmission efficiency of SIMS by implementing the ToF analyzers for SIMS analysis of biological compounds (Chait and Standing, 1981). In 1986, Jabs et al. used ToF-SIMS, also equipped with $Ar^+$ primary ions, to investigate structural differences among apolipoprotein isoforms. In their work, spectral analysis allowed for structural differentiation of two apolipoprotein mutants (Jabs et al., 1986). Some more work dealing with the structural determination of apolipoproteins followed (Voneckardstein et al., 1989; Voneckardstein et al., 1990). At that stage, some of the currently known advantages of ToF-SIMS were revealed, such as the high accuracy of molecular weight determination (±1 Da) within a mass range up to 3000 Da, the small amount of sample required for the analyses and the associated easy handling and preparation of samples.

Besides the introduction of ToF analyzers, the implementation of the currently used cluster ion sources facilitated a significant improvement in the analysis of not only peptide and protein preparations but also of biological tissue material, providing enhanced secondary ion yields and detection efficiencies for large characteristic secondary ions (Kollmer, 2004). Studies on biological peptides and tissues benefited from such technical improvements; Touboul et al. reported the analysis of several biological peptides as well as of mouse brain tissue sections using polyatomic $Au_3^+$ ions (Touboul et al., 2004), achieving high sensitivity and high lateral resolution with low primary ion doses and without any tissue pretreatment or matrix deposition. Furthermore, Sjövall et al. reported the detailed study of Ch, ST, phosphatidylinositols (PI) and phosphatidylcholines (PC) in mouse brain structures, also using $Au_3^+$ primary ions (Sjövall et al., 2004). In their work, principal component

analysis of spectra recorded at different regions of the tissue allowed for identification of common spectral fingerprints, and revealed large variations in the lipid composition among several brain structures.

Important work involving biological tissue followed; Touboul et al. studied the lipid profile of tissue affected by Duchenne muscular dystrophy, allowing for discrimination between tissue regions affected by different degrees of pathogenic progression (Touboul et al., 2005), and Brulet et al. studied colon tissue sections of a mouse model of cystic fibrosis, showing a significant increase in vitamin E and C16:0 fatty acid in the epithelial border of the colon, together with localization of specific lipid compounds in several other tissue structures (Brulet et al., 2010). Furthermore, Seedorf et al. used ToF-SIMS to diagnose Smith-Lemli-Opitz syndrome, an autosomal recessive metabolic and developmental congenital disorder that causes the inability to synthesize Ch due to a low occurrence of the 7-dehydrocholesterol (7DHC) reductase enzyme, leading to accumulation of the Ch precursor in tissues (Seedorf et al., 1995). Only minute amounts of blood, analyzed with ToF-SIMS, were necessary to perform the diagnosis, revealing increased 7DHC levels in patients, as compared to controls. It is to note that the work involving ToF-SIMS imaging of lipids in biological tissue is considerably extensive, and has been reviewed in detail elsewhere (Brunelle et al., 2005; Passarelli and Winograd, 2011).

In parallel, the study of cells and cell membranes using ToF-SIMS received considerable attention; Ostrowski et al. used ToF-SIMS to study the lipid content of cellular membranes involved in fusion processes, revealing differences in high and low-curvature lipids in regions involved in the fusion process (Ostrowski et al., 2004). Furthermore, Ostrowski et al. used ToF-SIMS to comparatively quantify the difference in Ch levels in the plasma membranes of two cells, which allowed for discrimination of two macrophage populations treated to contain different cellular levels of Ch (Ostrowski et al., 2007). Although similar work followed, the use of ToF-SIMS in cell biology is limited, partly due to analytical problems related to sample preparation and data interpretation (Walker, 2008). Nevertheless, important efforts are being focused on optimizing sample preparation and analysis conditions (Malm et al., 2009).

At the current stage, the use of ToF-SIMS in the study of biological and medical paradigms is still under development, and mainly descriptive work has been reported. Given the increasing evidence supporting the involvement of lipids in several neurodegenerative diseases such as Niemann-Pick or AD, techniques allowing for imaging and quantification of lipids and lipid precursors in biological tissues are gaining growing attention. ToF-SIMS and other mass spectrometry imaging (MSI) techniques, capable of providing detailed insight of the content and distribution of lipids in tissues, might be of great use in the study of lipid-related disorders.

*Background information on Secondary Ion Mass Spectrometry (SIMS)*

Secondary ion mass spectrometry (SIMS) is a surface analysis technique that provides detailed information on the atomic and molecular composition of the uppermost monolayer of a solid (Benninghoven, 1975, 1994). In SIMS, the ionization process involves the use of primary ions that, upon impacting the sample surface, cause ejection of secondary (analyte) ions, which are further mobilized and processed by a detector to generate mass spectra from the scanned areas. Each secondary ion, belonging to a specific analyte or compound in the sample surface, will display a distinct peak in the spectrum, with variable intensity depending on its mass and chemical characteristics. Figure 1-4 displays a schematic representation of the ionization process underlying SIMS.

The primary ion beam originates from a source or *metal gun* that emits primary ions. Initial SIMS spectrometers were equipped with ionization sources that emitted monoatomic primary ions, such as $Ar^+$ or $Cs^+$. However, the use of monoatomic primary ions in the study of biological samples is limited, as they provide low secondary ion efficiencies and cause extensive analyte fragmentation. The introduction of polyatomic cluster ions, such as $Au_3^+$, $Bi_3^+$ or $C_{60}^+$ reduced analyte fragmentation and improved the secondary ion yields of larger molecules such as lipids. Generally, the efficiency of a particular primary ion is improved with the mass of the monoatomic primary ion, and a further increase is obtained by the use of polyatomic primary ions (Kollmer, 2004).

ToF-SIMS allows for imaging of the scanned areas. During analysis, the primary ion beam is *swept* over the analysis area, causing desorption of analyte secondary ions, which are then collected and analyzed to generate separate mass spectra. The recorded data is then used to produce ion images from the areas scanned, showing the signal intensity distribution over the analysis area of selected secondary ion peaks representing specific compounds. That is; after data acquisition, ToF-SIMS software allows for generation of images by selecting and integrating a particular peak representing a specific secondary ion (i.e. cholesterol or sulfatides).

The *lateral resolution* in ToF-SIMS and other MSI techniques is determined by the focus diameter of the ionization beam. In ToF-SIMS, the reduced diameter of the primary ion beam allows for acquisition of images with great lateral resolution; the instrument operates either optimized for high mass resolution (*bunched mode*, mass resolution $m/\Delta m \approx 5000$, lateral resolution 3-5 μm) or for high image resolution (*burst alignment mode*, mass resolution $m/\Delta m \approx 300$, lateral resolution <500 nm). Remarkably, in some cases the instrument has been capable of imaging with lateral resolutions down to ~100nm provided that certain experimental conditions were given (Touboul et al., 2011). Our studies dealing with the distribution of Ch and other lipid structures in mouse and human brain tissue provided images acquired with great lateral resolution (<500 nm); cell nuclei displayed by $CN^-$ and $CNO^-$ ion patterns were resolved at ~15-25 $\mu$m, whereas the smallest detected Ch deposit was resolved at ~2 $\mu$m.

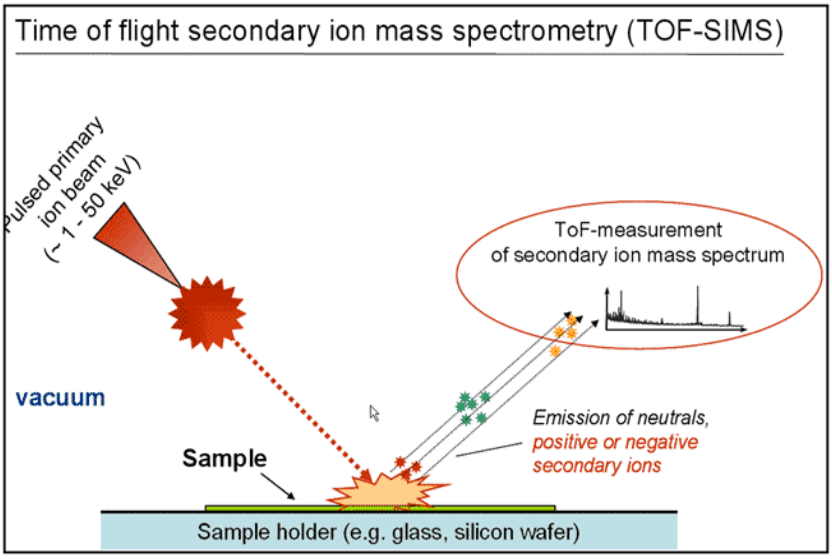


**Figure 1-4.** Generation of secondary ions in ToF-SIMS

The implementation of ToF detectors, cluster ion sources and other technological improvements that allowed for the study of biological samples with reduced analyte fragmentation and increased efficiencies lead to the modern "ToF-SIMS imaging" concept presented in this thesis work. The current sensitivity and resolution are sufficient for cellular imaging of many lipids of likely pathophysiological importance.

## Other mass spectrometry imaging techniques relevant to biological tissue imaging

Imaging of biological tissue samples has been broadly approached by the mass spectrometry community. A number of different instruments have been used in the analysis of biological tissue, with variable results. In MSI, the ionization source is an energetic photon or particle beam that impacts the sample, causing analyte ionization. Charged analyte particles are then mobilized and processed into the instrument's detector, to generate mass spectra form the scanned regions. As previously discussed, an important feature in MSI is the size of the ionization beam, which determines the lateral resolution of the acquired images. Concretely, the size of the ionization beam determines the dimensions of the image pixel corresponding to each point scanned, for which a mass spectrum has been acquired. Furthermore, a factor likely to restrict the information that is acquired from the sample is the fragmentation caused by a particular ionization source, which determines the molecular weight of the analyte fragments being produced and detected by the instrument. Mass spectrometers equipped with ionization sources that induce high analyte fragmentation will produce and detect low molecular weight ion fragments. In contrast, instruments inducing softer analyte ionization will produce larger analyte fragments, allowing for the study of larger compounds such as macromolecules and proteins.

| | DESI | MALDI | TOF-SIMS |
|---|---|---|---|
| Ultimate spatial resolution | 100–200 mm | 5–50 mm | 400 nm–2 mm |
| Sample preparation | No preparation, analysis at atmospheric pressure | Dehydrated, homogeneous matrix coating | Dehydrated, not fixed, no matrix |
| Mass range | m/z 1000 | m/z > 200 | m/z 1500 |
| Accessible compounds | Lipids, natural products | Lipids, peptides, proteins, drugs, metabolites,... | Lipids, drugs, metabolites, elements,... |
| Mass analyzer | Q-TOF, FT (Orbitrap# ) | TOF/TOF, Q-TOF, FT (Orbitrap# ), ion mobility coupled to Q-TOF, QqQ | TOF |

**Table 1-1**. Comparison between DESI, MALDI and ToF-SIMS imaging mass spectrometers in the context of biological tissue/sample imaging. Adapted from Touboul et *al* (2011) with permission of Elsevier.

Two of the most broadly used MSI techniques are Desorption Electrospray Ionization (DESI) and Matrix-Assisted Laser Desorption Ionization (MALDI). DESI can be operated at atmospheric pressure, and uses a pneumatically assisted electrospray source to desorb analytes from the sample surface. DESI is very sensitive for low molecular weight compounds such as lipids and peptides. However, its current lateral resolution is limited to 100 mm. MALDI is the most popular MSI method; the instrument is equipped with a low UV laser beam as ionization source, and the sample is treated with a matrix (of variable composition) that absorbs UV light, leading to ablation of the upper layer (1 µm) of the matrix material for subsequent ionization and fragmentation of analyte molecules. The method allows for imaging of lipids as well as of large ions such as from proteins, with a lateral resolution of ~50 µm. In these techniques, as compared to ToF-SIMS, the lateral resolution is restricted by the large diameter of the focal ionization beam.

In order to contextualize ToF-SIMS, a brief comparison of these mass spectrometers, commonly applied to the analysis of biological samples, has been summarized in Table 1-1. Mass spectrometers commonly applied to the analysis of biological samples have recently been reviewed in detail by Touboul et al. (Touboul et al., 2011).

# AIMS

The general aim of this thesis was to apply ToF-SIMS to the study of biological samples. A first, basic optimization of ToF-SIMS protocols relevant to the study of tissue sections was followed by application of the developed methodology to the study of tissue affected by Alzheimer's disease pathology.

I. Investigate the effect of common histological stains and analysis conditions to the distribution of lipids and other analytes at the surface of biological tissue sections using ToF-SIMS.

II. Study of opioid and amyloid–related fingerprints present in ToF-SIMS spectra obtained from the analysis of synthetic peptide preparations.

III. Develop a methodology combining ToF-SIMS and fluorescence techniques allowing for the simultaneous spatial study in biological tissue of lipids and cell populations relevant to Alzheimer's disease, and further determine the spectral and visual fingerprints associated with extracellular amyloid-beta deposits.

IV. Further use of the imaging methodology developed to study the interaction between extracellular amyloid-beta deposits, cholesterol and glial cells in biological tissue affected by Alzheimer's disease pathology.

# MATERIALS AND METHODS

## BIOLOGICAL TISSUE SAMPLES

### Mouse tissue

Experiments were performed in accordance with the relevant guidelines from the Swedish National Board for Laboratory Animals, the Spanish legislation on "Protection of Animals Used for Experimental and Other Scientific Purposes" and the European Communities Council Directive (86/609/EEC Council). Mice were kept under standard laboratory conditions of food and water *ad libitum*, 22 + 2 ºC, a 12 h light: dark cycle and relative humidity of 40-60%. Tg2576 and 3xTg-AD animals were 24 and 18 month old (± 2 weeks) when sacrificed, respectively. 3xTg-AD mice were euthanized using $CO_2$ whereas Tg2576 mice were sacrificed by cervical dislocation. The brains were quickly dissected and immediately frozen on dry ice, followed by storage at -80°C.

Adipose tissue was obtained from 129xC57BL6 hybrid mice. Animals were briefly anesthetized with $CO_2$ and decapitated. The gluteal fat pads were collected, immediately frozen on dry ice and stored at -80°C. All animals had been previously behaviorally tested. Behavioral data is, however, beyond the scope of the current report, and will not be presented herein.

*3xTg-AD model*

Female 3xTg-AD mice were provided by Dr. Lydia Giménez-Llort (UAB, Spain) from her Spanish colony of homozygous mice after *Material Transfer Agreement* with Dr. Frank LaFerla (University of California Irvine, California, USA). The 3xTg-AD mouse model (Oddo et al., 2003) bears three human mutant genes; *presenilin-1* (PS1) with the M146V mutation, the human *APP* gene with the Swedish mutation, and *tau* with the P301L mutation, the latter two expressed under the control of the Thy 1.2 regulatory element. The animals display progressive age-related memory impairment already evident at 6 months of age that correlates with intraneuronal Aβ pathology (Gimenez-Llort et al., 2007). Intracellular Aβ becomes evident at 3-4 months in neocortex, and by 6 months in CA1 subfield of hippocampus. At 12 months of age, the animals show widespread Aβ deposition in cortical regions and hippocampus. Tangle formation becomes evident first affecting the CA1 subfield at 12 month of age and later spreading to cortical regions, followed by tau reactive dystrophic neurites surrounding globular structures in 18 month old animals (Oddo et al., 2003). Age-matched wild-type control 129xC57BL6 hybrid mice were also provided by Dr. Giménez-Llort.

*Tg2576 model*

Female Tg2576 mice were purchased from Taconic (Cologne, Germany). The Tg2576 mouse model (Hsiao et al., 1996) expresses the human $APP_{695}$ isoform with the Swedish double mutation K670N-M671L under control of the hamster PrP promoter. Tg2576 animals show impaired learning and memory abilities already at 7 month of age, accompanied by dramatic increase in Aβ production. Diffuse focal deposits are already present in cortical and limbic structures at 10-12 month of age, together with dystrophic neuritis (Balducci and Forloni, 2011). Age-matched wild-type control B6SJLF1 mice were also purchased from Taconic.

## Human brain tissue

Human brain samples, provided by Huddinge Biobank (Karolinska Institutet Huddinge, Sweden), were handled and stored according to the regional Swedish Ethical Review Board guidelines. Temporal lobe blocks were obtained from a female patient (age 65, postmortem time 23h) diagnosed with AD Braak stage IV (Braak and Braak, 1991) after post-mortem brain study. The tissue presented severe brain atrophy and moderate congophilic angiopathy. Temporal lobe blocks from a non-demented female patient (age 79, postmortem time 17h), also subjected to post-mortem inspection, did not present any signs of AD-related pathology and were included in the study as control tissue. Cryosections were prepared and stored as described above.

## Synthetic peptide preparations

Eight different peptides were analyzed with ToF-SIMS; six endogenous opioids and two separate fragments of Aβ, listed together with their molecular weights and amino acid sequences in Table 2-1. The peptides were provided in pure crystal form by Bachem (Bubendorf, Switzerland). Each peptide sample was introduced into a sterilized Eppendorf tube and dissolved in Milli-Q water without further purification at concentrations given in Table 2-1. The resulting solutions were vortexed several minutes to ensure complete dissolution of the peptide. A 5-10 $\mu$L drop of the peptide solution was deposited onto the surface of a silicon wafer substrate and allowed to dry at RT, leaving a peptide deposit coating the surface. The wafers were previously cleaned by washing sequentially in heptane, acetone, and ethanol. After preparation, the samples were introduced into the vacuum chamber of the ToF-SIMS instrument for analysis of the pure peptide deposits.

| Peptide name | Sequence (one-letter code) | n. of residues | Mass (Da) | Purity (%) | Conc. (mg/mL) |
|---|---|---|---|---|---|
| Leucine-enkephalin | YGGFL | 5 | 555.27 | 98.1 | 1.0 |
| Dynorphin A 1-6 | YGGFLR | 6 | 711.37 | 99.2 | 3.3 |
| Methionine-enkephalin-lysine-lysine | YGGFMKK | 7 | 829.42 | 96.0 | 1.0 |
| Amyloid beta 29-40 | GAIIGLMVGGVV | 12 | 1084.63 | 95.9 | 2.0 |
| Dynorphin A 1-9 | YGGFLRRIR | 9 | 1136.66 | 98.9 | 2.0 |
| Dynorphin A 1-10 | YGGFLRRIRP | 10 | 1233.71 | 99.0 | 1.0 |
| Amyloid beta 1-11 | DAEFRHDSGYE | 11 | 1324.53 | 98.0 | 2.0 |
| Dynorphin B | YGGFLRRQFKVVT | 13 | 1569.88 | 97.0 | 1.0 |

**Table 2-1.** List of peptides analyzed with ToF-SIMS (paper II)

## TOF-SIMS ANALYSIS

### ToF-SIMS instrumentation

The ToF-SIMS analysis of peptide preparations and biological tissue sections was carried out using a ToF-SIMS IV instrument (ION-TOF GmbH, Münster, Germany) equipped with a reflectron-type time-of-flight mass spectrometer. Tissue sections were analyzed using 25 keV $Bi_3^+$ primary ions, whereas peptide preparations were analyzed using both 25keV $Bi_3^+$ and 25keV $Au_3^+$ primary ions. The data was acquired using low-energy electron flooding for charge compensation and with the instrument optimized for high mass resolution (bunched mode, mass resolution $m/\Delta m \approx 5000$, lateral resolution 3-5 $\mu$m) or for high image resolution (burst alignment mode, mass resolution $m/\Delta m \approx 300$, lateral resolution 200 nm). Here, $\Delta m$ is the FWHM of a peak in the mass spectrum at mass $m$ and the lateral distribution is determined by the focus diameter of the primary ion beam. The pulsed primary ion current was 0.1 pA in the bunched mode and 0.04 pA in the burst alignment mode when using 25 keV $Bi_3^+$ primary ions, whereas 0.03/0.04 pA intensity was reached when using $Au_3^+$ primary ions in the bunched mode. The accumulated ion dose was always kept below $1x10^{12}$ ions/cm$^2$. During analysis, the primary ion beam was scanned over the analysis area, collecting separate mass spectra of the emitted secondary ions from 128x128, 256x256 or 512x512 raster points (pixels). The recorded data were used to produce total area mass spectra and/or ion images showing the signal intensity distribution over the analysis area of selected secondary ion peaks representing specific compounds. Images generated in the analysis of biological tissue samples were normalized to the maximum signal intensity in a single pixel.

### Spectral analysis

The increased useful mass range from use of cluster primary ions allows for the analysis of biosubstances of higher molecular mass, but masses are thus often calculated from flight times by extrapolation. However, interpolation is inherently more accurate than extrapolation. This is in agreement with our experience from ToF-SIMS analysis of biomedical samples. Therefore, calibration of the recorded spectra was carried out including the molecular ions as well as some ions at the low mass ranges –$CH_3$, $C_2H_2$, $C_3H_2$, $C_4H_2$ for the positive and C, $C_2$, $C_3$, $C_4H$ for the negative ion spectra– in order to cover a wide range of masses and allowing the assignment of peaks by interpolation. In the peptides study, reliable signals from $(M + H)^+$ and $(M - H)^-$ molecular ions were observed and included in the calibration procedure. Assignments were slightly less ambiguous after including the molecular ions in the calibration. In the analysis of biological tissue, spectra were calibrated including ions in the low mass range and ions related to Ch, namely the peak at 369 u corresponding to the de-hydroxylated fragment of Ch, $[Ch\text{-}OH]^+$, and the peak at 385 u corresponding to the deprotonated Ch molecule, $[Ch\text{-}H]^+$. However, it should be noted that this procedure can only be applied when a safe assignment of the molecular peak can be

made, such as in the present case. Spectra were analyzed using the standard IonSpec software (ION-TOF, Münster, Germany).

## Imaging of biological tissue

*Preparation of tissue sections*

In ToF-SIMS, the mass spectrometry analysis from a particular region of a biological tissue sample is very sensitive to small modifications of the chemical structures in the sample. The application of chemical fixatives to the tissues may substantially alter the chemical composition and the lateral distribution of the probed analyte ions (Bélazi et al., 2009). Therefore, only fresh frozen non-fixed brain tissue was analyzed in this work. In order to avoid sample contamination, all surfaces and instruments used during cryosectioning of tissues were washed in ethanol and acetone, air dried and pre-cooled at -20°C. Furthermore, the use of mounting glue to hold the tissue blocks during cryosectioning caused contamination of the tissue sections, which could be recognized in the ToF-SIMS spectra and lead to artifacted images. In order to avoid the contamination of tissues, mouse brains were hold to the cryostate's chuck using water, which would freeze and hold the brain during sectioning.

*Analysis at -80°C*

Sample temperature is another important factor in ToF-SIMS analysis that may affect the distribution of lipids in tissue sections. It has been shown that tissues analyzed at temperatures above 0°C display altered lipid signals, as compared to samples recorded at low temperatures, probably due to diffusion of analytes from within interior layers of the tissue (Sjövall et al., 2006). In order to prevent analyte diffusion, cryosections were transported and kept at -80°C or below during the entire sample preparation and ToF-SIMS analysis procedure. In order to allow for cold analysis, the surface of the glass slides holding the particular brain section had to be cut in 1x1 cm square areas using a standard glass cutter, and put onto the ToF-SIMS mobile stage holder, previously refrigerated in liquid nitrogen. The ToF-SIMS analysis was carried out at -80°C by refrigerating the instrument with liquid nitrogen.

*Localization and imaging of selected areas*

In order to locate relevant areas for ToF-SIMS analysis, tissue sections adjacent to those planned for ToF-SIMS analysis were stained with *Pentamer Formyl Thiophene Acetic Acid (*p-FTAA) amyloidotropic fluorescent dye and BOBO-1 nuclei marker (described below) and imaged using confocal laser scanning microscopy (CLSM). These CLSM images were then used as navigation-guiding templates during the ToF-SIMS measurements. The recorded data was then used to produce ion images from the areas scanned, showing the signal intensity distribution over the analysis area of selected secondary ion peaks representing specific compounds, as described above.

## FLUORESCENCE TECHNIQUES

### p-FTAA staining of senile plaques

Mouse brain sections analyzed with ToF-SIMS were thereafter incubated with p-FTAA, an amyloidotropic fluorescent dye (Åslund et al., 2009). Sections were fixed in absolute ethanol for 10 min and rehydrated in water followed by PBS. Working solution of p-FTAA (1.5 mM) was diluted 1:500 in PBS and added to the brain sections, which were then incubated for 30 min at room temperature (RT) and washed with PBS. The sections were mounted with Dako mounting solution for fluorescence (Dako, Glostrup, Denmark) and kept at 4°C until imaged.

### Combined Iba1/GFAP/p-FTAA immunostaining of tissue sections

Mouse brain sections analyzed with ToF-SIMS (or adjacent sections) were immunostained with antibodies against glial fibrillary acidic protein (GFAP) and ionized calcium binding adaptor molecule 1 (Iba1) as well as for Aβ (using p-FTAA) and nucleic acid (using BOBO-1 cell nuclei marker). Sections were air-dried and post-fixed in 4% PFA for 1 hour at RT. Treatment in 0,3% $H_2O_2$ followed (10 min RT) to block endogenous peroxidase activity. Sections were then treated with blocking solution (5% normal goat serum, 2% bovine serum albumin and 0,3% Triton-X100 in PBS) at RT for 2h and thereafter incubated with rabbit polyclonal anti-Iba1 IgG antibody (1:200, Wako, Osaka, Japan) in diluted blocking solution at 4°C for 13 days. Iba1 was detected with an Alexa 633 goat anti-rabbit IgG secondary antibody (1:800, Invitrogen Life Technologies, Stockholm, Sweden) in diluted blocking solution at RT for 1h. An additional 10 min post-fixation step in 4% PFA was performed afterwards, in order to reinforce the primary-secondary antibody binding. Next, sections were incubated in rat monoclonal anti-GFAP antibody (1:400, Invitrogen Life technologies, Stockholm, Sweden) at 4°C for 20h. GFAP was detected with an Alexa 546 goat anti-rat IgG secondary antibody (1:800, Invitrogen Life Technologies, Stockholm, Sweden) at RT for 1h. After treatment with primary and secondary antibodies, sections were incubated in p-FTAA working solution diluted 1:500 in PBS at RT for 30 min. Incubation in BOBO-1 solution followed (1:1000, Invitrogen Life Technologies, Stockholm, Sweden) in PBS at RT for 30 min. Sections were finally mounted in Dako mounting solution for fluorescence (Dako, Glostrup, Denmark) and kept at 4°C until imaged.

### Fluorescence microscopy

High resolution images from the immunostained brain sections were acquired using a ConfoCor3 system (Carl Zeiss, Jena, Germany), consisting of an inverted microscope (Axiovert 200 M) coupled to a VIS-laser module comprising the tunable Ar/ArKr (458, 477, 488 and 514 nm), HeNe 543 nm and HeNe 633 nm lasers and a scanning module LSM 510 META. The instrument was specially modified to enable fluorescence

detection in the imaging mode using silicon avalanche photodiodes (SPCM-AQR-1X; PerkinElmer, USA).

*p-FTAA imaging and quantification*

p-FTAA quantification was accomplished by recording the fluorescence from the Aβ deposits with an epifluorescence microscope Leica DM6000 B (Leica, Wetzlar, Germany) equipped with a SpectraCube (optical head) module (Applied Spectral Imaging, Migdal Ha-Emek, Israel), with the 405/20 and 535/50 longpass filters. Spectra were quantified using the standard software (SpectraView). Furthermore, high resolution p-FTAA imaging was accomplished using the ConfoCor 3 system described above. In brief, the green component of the emitted p-FTAA fluorescence was collected using the band pass filters BP 505-530 and BP 530-575, whereas the red component was collected using the long pass filter LP 580. Plan-Apochromat 5x/0.16 and C-Apochromat 40x/1.2 W objectives were used throughout. Images were recorded at 512x512 pixel resolution and processed using the standard software (LSM Image Browser).

*Confocal microscopy of immunostained sections*

Imaging of sections immunostained with GFAP and Iba1 (together with p-FTAA and BOBO-1 staining) was accomplished using the ConfoCor 3 system described above. A multi-track configuration was used for fluorescence imaging, acquiring the signal for one fluorophore at a time. BOBO-1 fluorescence was excited using the 458 nm line of Ar/ArKr laser, and the emitted light was collected through a band pass filter BP 470-495 nm (pseudo-colored blue); p-FTAA fluorescence was excited using the 488 nm line of the Ar/ArKr laser, and the emitted light was collected through a band pass filter BP 505-530 nm (pseudo-colored green) and a long pass filter LP 580 nm (pseudo-colored red); GFAP was visualized through the Alexa 546-bound anti-GFAP antibody, Alexa 546 fluorescence was excited using the HeNe 543 nm laser and the emitted light was collected through a band pass filter BP 560-610 nm (pseudo-colored green); Iba1 was visualized through the Alexa 633-bound anti-Iba1 antibody, Alexa 633 fluorescence was excited using the HeNe 633 nm laser and the emitted light was collected through a band pass filter BP 655-710 nm (pseudo-colored red). Plan-Apochromat 5x/0.16 and C-Apochromat 40x/1.2 W objectives were used throughout. Images were recorded at 512x512 pixel resolution and processed using the standard software (LSM Image Browser). Fluorescence images from large brain areas were composed by aligning a number of 318x318 $\mu m^2$ images (acquired with the 40x objective) using the open source vector graphics editor Inkscape (available at www.inkscape.org). High resolution ToF-SIMS images and fluorescence images (acquired for the adjacent immunostained sections) were overlaid using Inkscape, and matched areas were localized. GFAP and Iba1 fluorescent immunostainings were quantified in these matched areas, using ImageJ (available at imagej.nih.gov).

### Scanning-electron microscopy (SEM)

The Tg2576 brain section studied with ToF-SIMS and CLSM was thereafter analyzed using SEM in order to investigate the morphological structure of previously imaged senile plaques. Immediately before SEM analysis, the tissue section was rinsed in PBS, in order to demount it from the fluorescent mounting media, and air dried. SEM analysis was carried out on the uncoated tissue sample in a Zeiss Supra 40VP FEG microscope (1 keV electron energy, 5 mm working distance) using an Everhardt-Thornley secondary electron detector.

# RESULTS AND DISCUSSION

The following section briefly summarizes and discusses the major findings obtained in papers I-IV, in the perspective of the thesis as a whole. The reader is asked to refer to the individual articles for the actual results including additional data as well as detailed images and statistics.

## TEMPERATURE VARIATIONS, TISSUE STAINING AND LIPID REDISTRIBUTION

We have analyzed several types of biological tissue using ToF-SIMS. During our experiments, the distribution of most substances on the cut tissue surface analytes has shown a dependence on certain analysis conditions, temperature and tissue treatment being the most important ones.

### Temperature *(unpublished)*

ToF-SIMS analysis of biological tissue sections provides the distribution of numerous surface analytes. As will be discussed in the following sections, most analyses aimed at investigating the distribution of Ch in brain tissue of animal models of AD. During ToF-SIMS measurements, we observed important variations in the surface distribution of Ch that were associated with temperature variations.

Figure 4-1 displays the ToF-SIMS analysis and subsequent CLSM imaging of a region occupied by senile plaques in the subiculum of a 3xTg-AD mouse brain section. Figure 4-1a displays the BOBO-1 cell nuclei marker staining (pseudo-colored red) and p-FTAA amyloidotropic fluorescent dye staining (pseudo-colored yellow). The white and green squares delineated in the image were previously analyzed with ToF-SIMS, generating TIM surface images (Figs. 4-1b and 4-1d) and Ch (Fig. 4-1c and 1e) images of the areas scanned. Despite being acquired at the same region, the distribution of Ch displayed in Fig. 4-1c presents a homogeneous profile whereas the Ch pattern displayed in Fig 4-1e is much more heterogeneous. It was known before that temperature affects ToF-SIMS measurements; the changes in analyte distribution, however, were considerable in the experiments for this thesis.

Variations in the surface distribution of Ch are probably due to the fact that lipids and other analytes may diffuse from inner layers of the tissue sections (Sjövall et al., 2006) and reach the surface through micro orifices generated during the freezing and/or cryosectioning processes, which account for most artifacts generated during preparation and handling steps. Figure 4-2 displays the signal variations displayed by some ions measured from freeze-dried mouse brain tissue as a function of sample temperature.

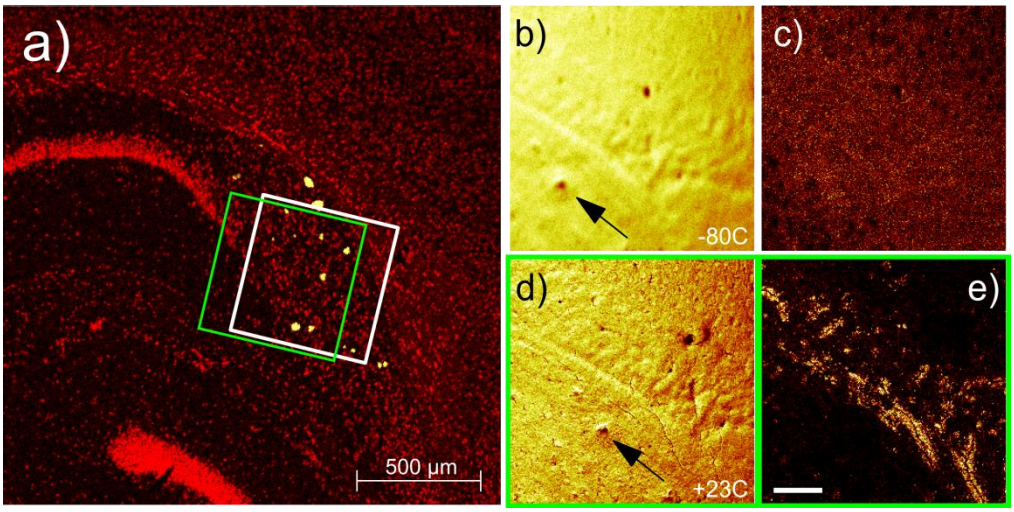


**Figure 4-1.** The distribution of Ch at the tissue surface undergoes redistribution upon temperature variations. **(a):** CLSM image from a 3xTg-AD mouse brain section displays the p-FTAA staining of senile plaques (yellow) and BOBO-1 staining of cell nuclei (red). The regions delineated with white and green squares include stratum oriens and subiculum of hippocampus and were analyzed with ToF-SIMS at -80°C and +23°C, respectively. **(b-c):** ToF-SIMS images acquired in the region delineated with a white square in (a) display the (b) TIM and the (c) Ch distributions in the area recorded at -80°C. Note that Ch presents a homogeneous profile over the entire region analyzed. The black arrow in (b) highlights a senile plaque. **(d-e):** ToF-SIMS images acquired in the region delineated with a green square in (a), display the (d) TIM and (e) Ch distributions of the area analyzed at +23°C. Note that the Ch has been redistributed in (e), as compared to (c). White scale bar (e): 100 $\mu$m.

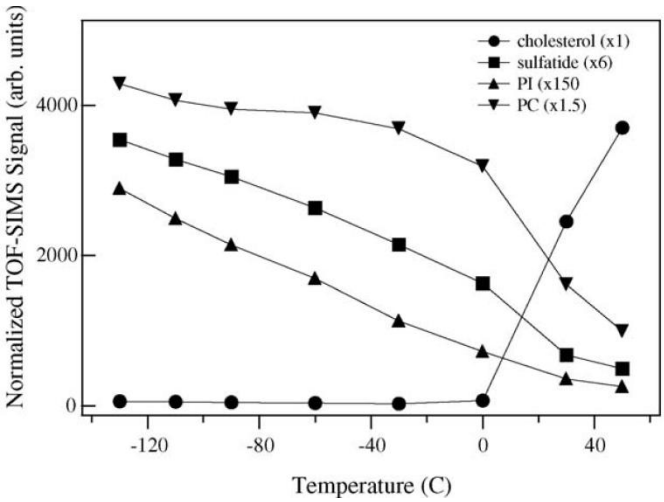


**Figure 4-2.** Normalized signal intensities of selected ions in ToF-SIMS spectra from freeze-dried mouse brain sections. Signal intensities of Ch, ST, phosphatidylinositol (PI) and phosphatidylcholine (PC) ions are measured in a Ch-rich area (anterior commissure) as a function of sample temperature upon heating from -130°C to 50°C. Note that Ch signal dramatically increases when measuring at temperatures above 0°C, whereas all other analytes display a progressive signal decrease with decreasing temperature. Reproduced from Sjövall et al. (2006) with permission of Elsevier.

The literature on ToF-SIMS analysis of Ch in biological tissue is extensive (Touboul et al., 2004; Brunelle et al., 2005; Touboul et al., 2005; Debois et al., 2009; Brulet et al., 2010). However, in these works, tissues have seldom been analyzed at low temperature. As shown here, the distribution of Ch may undergo considerable redistribution as a function of sample temperature. Therefore, handling and analysis

of biological tissues at low temperatures should be taken into consideration in future ToF-SIMS work. In the present thesis, an extensive work dealing with ToF-SIMS analysis of brain tissue sections is presented. Since previous studies and pilot experiments indicated large temperature effects, and in order to reduce lipid diffusion, biological tissue was maintained at -20°C during cryosectioning and tissue sections were stored at -20°C. Furthermore, most ToF-SIMS measurements on mouse and human brain tissue were carried out at -80°C, as described in the experimental section.

### Staining of tissue sections with osmium tetroxide *(paper I)*

The study of biological tissue using light or electron microscopy usually requires fixation and staining in order to preserve the material during the processing. Different fixatives cause different chemical modifications and alter the physical status of the tissues. Osmium tetroxide ($OsO_4$) is extensively used to stain and fix tissues for electron microscopy (Studer et al., 2008) and to monitor the distribution of unsaturated lipids in electron and optical microscopy of cells and tissues. The gradual tissue blackening upon incubation with $OsO_4$, especially during the dehydration step through ethanol, is a commonly observed phenomenon. The $OsO_4$ binding to unsaturated fatty acid double bonds alone does not give rise to a color switch in the stained tissue; the characteristic orange/brown/black "osmium blacks" color is instead generated by the products from the osmium ester reduction, forming a high accumulation of osmium in the stained tissue region.

We investigated the localization of osmium oxide and specific lipids in mouse adipose tissue by using ToF-SIMS. Osmium species, saturated and unsaturated fatty acids and protein-related ions were independently monitored. Before osmium incubation, saturated and unsaturated fatty acid, diacylglyceride (DAG) and triacylglyceride (TAG) ions were mainly colocalized in specific structures, most likely corresponding to TAG deposits in the adipose tissue. Figure 4-3 presents ToF-SIMS spectra recorded prior to $OsO_4$ staining (Fig 4-3a), after $OsO_4$ staining (Fig 4-3b) and after $OsO_4$ staining and subsequent ethanol rinsing (Fig. 4-3c). DAG and monoacylglyceride (MAG) associated peaks are strong before staining and display increased intensity after staining and ethanol rinsing, whereas peaks associated with proteins (pc) display decreased intensity after staining and rinsing steps. Figure 4-4 presents the distribution of saturated and unsaturated fatty acids as well as osmium oxide before (Figs. 4-4a to 4-4c) and after $OsO_4$ staining (Figs. 4-4d to 4-4i) and subsequent ethanol rinsing (4-4j to 4-4o). After osmium staining, two forms of osmium oxide (type I and type II) were observed in the ToF-SIMS spectra and on the tissue surface that were associated with different spatial distributions and different Os/O ratios. Type I osmium oxide presented an inhomogeneous distribution without topographic features and was monitored by the $OsO_3$ ion (Fig. 4-4i). In contrast, type II osmium oxide (not shown in the figure) displayed a particle-like distribution with topographic features and was monitored by ion clusters of the form $OsO_3(OsO)_n$ suggesting a less oxygen rich oxide than the type I osmium oxide.

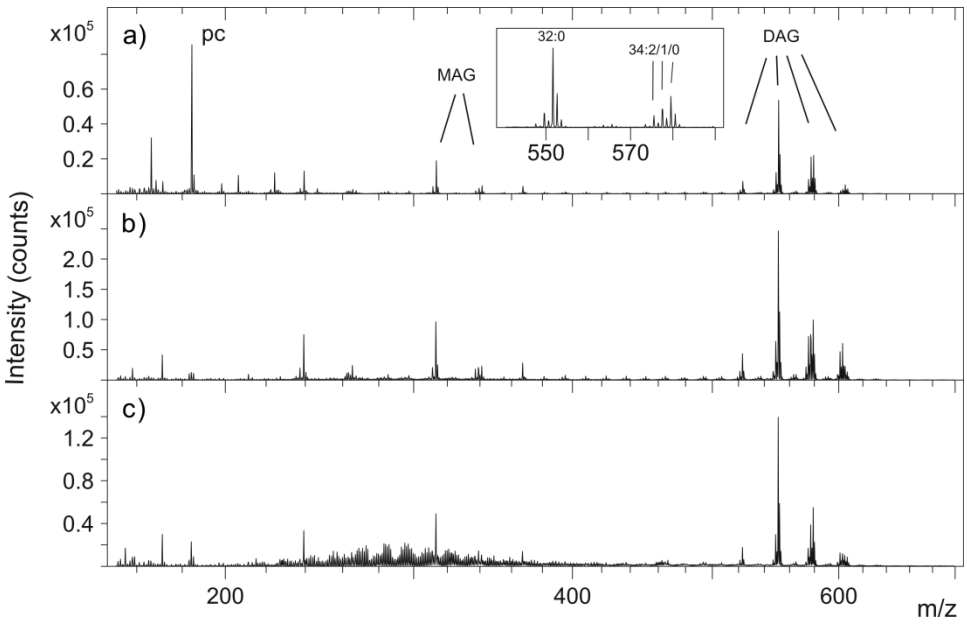


**Figure 4-3**. ToF-SIMS spectra from analysis of mouse adipose tissue. **(a):** spectrum recorded prior to OsO4 staining displays strong signal from monoacylglyceride (MAG), dyacylclyceride (DAG) and phosphocholine (pc) ions representing the head group of phosphatidylcholine or sphingomyelin. **(b-c):** spectrum recorded in a similar region of the tissue after (b) $OsO_4$ staining and after (c) staining and subsequent ethanol rinsing display increased MAG and DAG signal but reduced pc signal as compared to (a). The inset shows an expanded region of the spectrum highlighting the different DAG-related peaks. Reproduced from Bélazi et al. (2009) with permission of Springer Link.

Unsaturated C18 fatty acids (C18:1 and C18:2), and DAGs containing these fatty acids were found to be colocalized with type I osmium oxide (Figs. 4-4h and 4-4i), while the saturated C18 fatty acid and C16 (saturated and unsaturated) fatty acids, and DAGs containing these fatty acids, displayed complementary localizations as compared to the type I oxide (Fig. 4-4d to 4-4f, 4-4g). Furthermore, fragment peaks assigned to proteins and phospholipids showed a strong decrease in signal intensity after $OsO_4$ incubation, indicating that a considerable fraction of the proteins and phospholipids were removed from the tissue surface during the $OsO_4$ incubation (Fig. 4-3b/c). However, the remaining proteins and phospholipids were strongly colocalized with type II osmium oxide.

Interestingly, after ethanol dehydration of the stained tissue, both type I and type II osmium oxides as well as the unsaturated C18 fatty acids presented a homogeneous distribution in the regions scanned (Fig. 4-4m to 4-4o) , whereas the saturated C18 and the C16 (saturated and unsaturated) fatty acids chains displayed a comparatively inhomogeneous distribution (Figs. 4-4j to 4-4l).

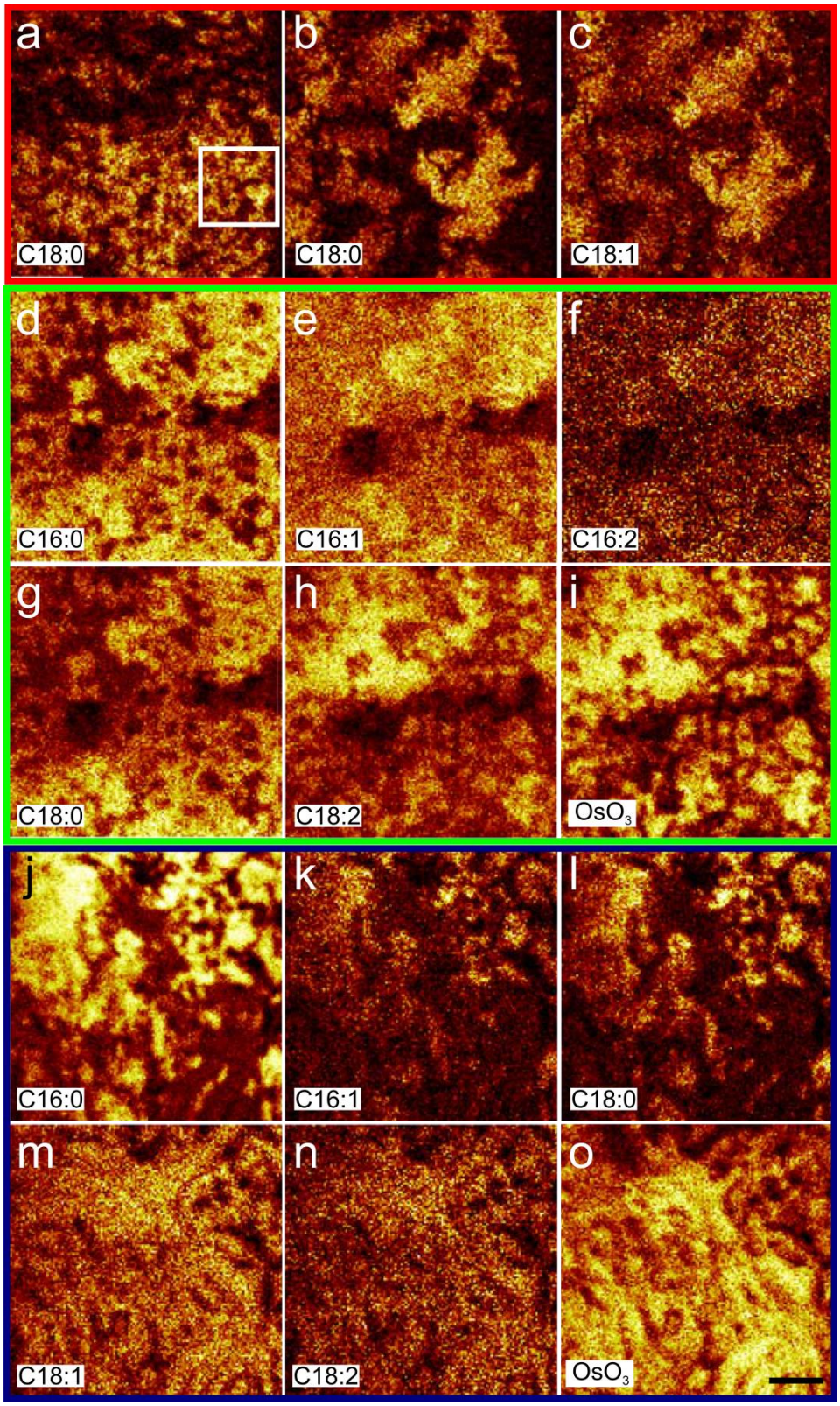


**Figure 4-4.** ToF-SIMS analysis of mouse adipose tissue stained with $OsO_4$ and subsequently rinsed with ethanol. **(a-c):** ToF-SIMS analysis of a tissue region prior to $OsO_4$ staining provided the (a) distribution of C18:0; the (b) inset of the area delineated with a square in (a), which presents very similar spatial distribution compared to the (c) distribution of C18:1 in the same region. **(d-i):** ToF-SIMS analysis of a similar region after $OsO_4$ staining displays the (d) C16:0, (e) C16:1, (f) C16:2, (g) C18:0, (h) C18:2 and (i) $OsO_3$ ion distributions of the region. Note that $OsO_3$ and C18:2 distributions colocalize spatially whereas C18:0 and all other C16 fatty acid chain ions display a complementary localization. **(j-o):** ToF-SIMS analysis of a region, similar to those previously imaged, after $OsO_4$ staining and subsequent ethanol rinsing provided the (j) C16:0, (k) C16:1, (l) C18:0, (m) C18:1, (n) C18:2 and (o) $OsO_3$ distributions in the area analyzed. Note that $OsO_3$ and unsaturated C18 distributions colocalize spatially and display a more homogeneous profile as compared to (h) and (i). Adapted from Bélazi et al. (2009) with permission of Springer Link. Scale bar: 100 $\mu$m.

The observed colocalization between type I osmium oxide and unsaturated C18 fatty acids is consistent with the established view that $OsO_4$ binds to unsaturated lipids. However, our results also indicate that the osmium oxide binding is considerably stronger to unsaturated C18 fatty acids chains as compared to the binding to unsaturated C16 fatty acids, which was an unexpected finding. Furthermore, ToF-SIMS images revealed a strong complementary localization between saturated and unsaturated C18 fatty acids after $OsO_4$ incubation, whereas such complementarity was not observed prior to staining. This suggests that the $OsO_4$ incubation may give rise to some redistribution of lipids in the tissue, at least at the >10 $\mu$m length scale. However, the macroscopic distribution of osmium oxide found in the tissue after $OsO_4$ staining is still likely to reflect the original distribution of unsaturated (C18) fatty acids and their associated glycerides. Nevertheless, the fact that a large fraction of the proteins and phospholipids originally in the tissue were extracted during the $OsO_4$ incubation step together with the increased homogeneity presented by osmium oxide and the unsaturated C18 fatty acid chains after ethanol rinsing of the stained tissue suggests that important chemical and physical modifications are possible, and emphasizes the importance of analyzing non-fixed, chemically preserved biological tissue as means of maintaining tissue integrity and surface analyte distribution.

## TOF-SIMS ANALYSIS OF AMYLOID-RELATED STRUCTURES *(paper II-III)*

Given the detailed information provided by ToF-SIMS in terms of spectral quantification and lateral distribution of analytes in biological samples, we focused our efforts on the study of biological tissue affected by AD. A first step, however, dealt with the analysis of amyloid-related structures in the form of synthetic preparations (peptides), followed by a second stage involving the study of biological tissue affected by AD. The evaluation of the spectra obtained from ToF-SIMS analysis of opioid and amyloid peptides revealed a molecular fragmentation pattern that adjusted to that of Collision-Induced Dissociation (CID), which is the way to intentionally drive molecular fragmentation in most mass spectrometers equipped with collision-based ionization sources. Figure 4-5 shows the ToF-SIMS spectrum obtained from fragmentation of the opioid peptide leucine-enkephalin. A number of CID-related fragment peaks were observed in the spectrum, namely i) single amino acid fragments (immonium ions); ii) multiple amino acid fragments and iii) molecular ions. Immonium ions (m/z 0-200) are formed after internal cleavage of the peptide bonds at the N and C terminal sites, and provide information about the amino acid composition of the peptide. In contrast, multiple amino acid fragments (m/z 150-500) arising from cleavage of the peptide backbone skeleton provide information about the peptide sequence. Molecular ions arise from the protonation (or deprotonation) of the molecular peptide species and provide the molecular mass of the peptide structure. Most opioid peptides presented specific spectral fragment fingerprints and their sequences and composition could be obtained from the information provided by ToF-SIMS spectra.

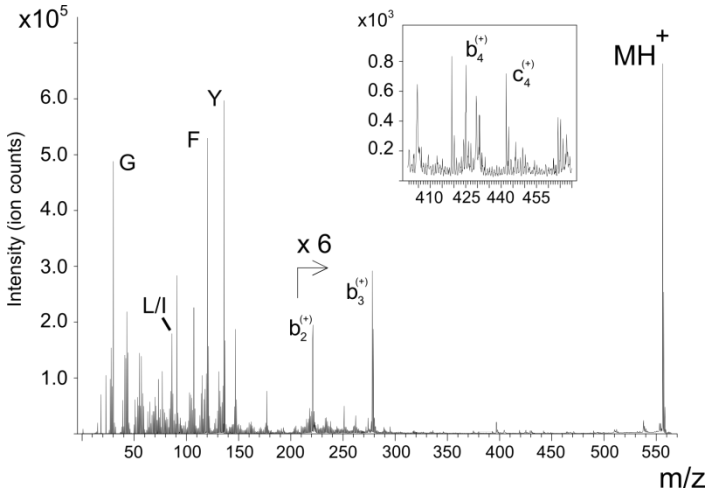


**Figure 4-5**. ToF-SIMS spectrum obtained from analysis of the opioid peptide leucine-enkephalin (YGGFL). Immonium ion peaks are labeled with the single amino acid coded letter in the low mass region; multiple amino acid fragment peaks are labeled with the corresponding sequence-coding letter in the middle mass region, and the peptide molecular ion (protonated form) is labeled as $MH^+$. The inset shows an expanded region of the spectrum highlighting peaks from different multiple amino acid fragments. Reproduced from Solé-Domènech et al. (2010) with permission of the American Chemical Society.

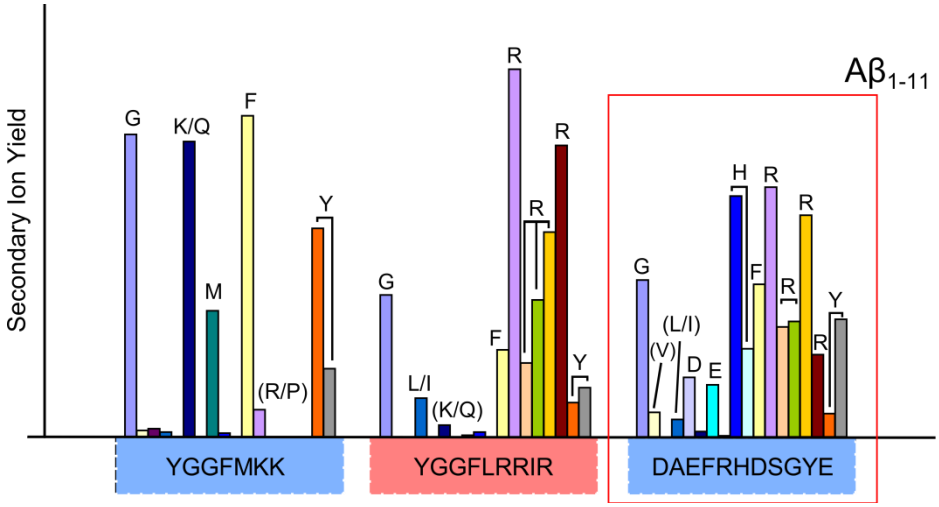


**Figure 4-6**. Immonium ion profiles obtained from opioid and amyloid peptide preparations provided information regarding peptide composition. Amino acids are indicated with the single-letter code on top of each bar. Adapted from Solé-Domènech et al. (2010) with permission of the American Chemical Society.

Figure 4-6 displays representative immonium ion profiles from opioid and amyloid peptides upon ToF-SIMS molecular fragmentation. Amyloid peptide substructures Aβ1-11 and Aβ29-40 (not shown) displayed specific spectral immonium and molecular ion fingerprints, whereas Aβ1-40 and Aβ1-42 peptides displayed weak but identifiable molecular ion peaks in the ToF-SIMS spectra (unpublished data).

After evaluation of synthetic amyloid preparations, we approached the study of biological tissue affected by AD. Regions occupied by senile plaques in brain tissue sections presenting neuropathology were identified as described in the experimental section and scanned with the ToF-SIMS instrument. Total ion images (TIMs) generated from Aβ regions (by adding, in one single image, the distribution of all secondary ions detected within a range of 1-2000 Da, as described in the experimental section) provided topographical information about the sample surface (Lee et al., 2011). In the TIMs, Aβ regions presented a number of dark features that appeared to be protrusions from the tissue surface (Fig. 4-7a), with sizes in the range of 20-50 $\mu$m in diameter that were identified as plaques by subsequent p-FTAA Aβ staining (pseudo-colored blue, Fig. 4-7b). The Aβ deposits did not produce any chemically specific signals in the ToF-SIMS spectra, as would have been expected from their deviating composition compared to the surrounding tissue. Instead, as shown in the TIMs, the inner areas of the plaques presented very low ion signal, indicating a significantly decreased yield of all secondary ions.

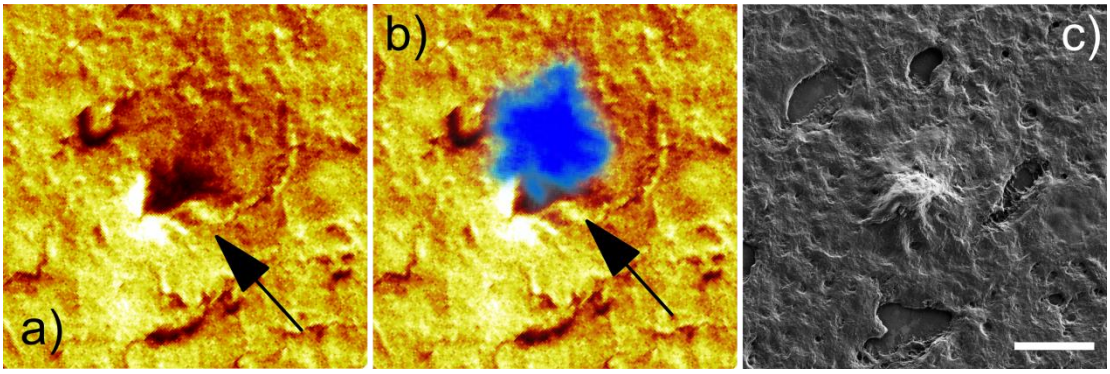


**Figure 4-7.** ToF-SIMS and SEM analysis of a region occupied by a senile plaque. **(a-b):** ToF-SIMS TIM image reveals a (a) surface feature with protrusion-like structure identified as a senile plaque by subsequent (b) p-FTAA staining, overlaid on top of the TIM image. **(c):** SEM analysis of the same region reveals a fibrillary deposit matched with the senile plaque presented in (a,b). Scale bar: 20 $\mu$m.

Signal variations due to topographic features on the surface are a well-known effect in ToF-SIMS and are mainly caused by the limited angular acceptance of the analyzer (Lee et al., 2011). In order to confirm the topographic nature of the plaques, Aβ regions analyzed with ToF-SIMS were subsequently imaged using SEM. Indeed, plaque regions visualized with SEM revealed the presence of fibrillary bodies that matched the surface protrusions observed in the ToF-SIMS TIMs (Fig. 4-7c), thus confirming the topographic protrusion-like nature of Aβ deposits on the tissue surface. Hence, the observed low secondary ion yield may primarily be a topographic effect.

Taken together, ToF-SIMS analysis of Aβ revealed structure-related fingerprints in the spectra obtained from synthetic preparations, whereas the study of extracellular Aβ deposits in brain tissue revealed surface-related Aβ features with no specific spectral fingerprints.

## SIMULTANEOUS SPATIAL IMAGING OF CHOLESTEROL, GLIAL CELLS AND AMYLOID-BETA *(paper IV)*

The diverse units that compose biological structures possess a natural interactive role with each other. Therefore, tools that provide the opportunity to simultaneously study these biological units might provide a more accurate picture of the biological events occurring in health and disease. After having learned ways to detect and analyze regions undergoing plaque deposition, we decided to study the lipid profile of these areas affected by neuropathology. Furthermore, given the fact that glial cells play a key role in the synthesis, transport and recycling of lipids in the central nervous system, we needed to develop a method that would allow for simultaneous spatial study of lipids and glial populations. However, the combination of techniques that allow study of lipid profiles or proteins is challenging. With those caveats in mind, we combined ToF-SIMS imaging of lipids and molecular fragments in mouse and human brain structures affected by AD pathology with confocal fluorescence imaging of glial proteins and deposits of Aβ, in order to study these biological units at the same location of a particular tissue section.

Most immunolabeling protocols require previous fixation of tissues (usually by perfusion) in order to stabilize cell morphology and disable proteolytic enzymes, as well as to prevent the detection of hematologic antigens. The application of chemical fixatives may substantially alter the chemical composition of the tissue sections, thus hampering or even preventing their subsequent analysis using other complementary techniques. In early preliminary experiments, the application of fixatives to the tissues subjected to ToF-SIMS analysis hampered the experiments, causing the so-called matrix effects (Piwowar et al., 2009). In order to prevent for such effect, fresh frozen tissues were used in essentially all subsequent analysis for this thesis.

Furthermore, multiple immunolabeling of fresh frozen non-fixed tissues is not trivial. In the present approach, tissues analyzed with ToF-SIMS were subsequently immunostained with Iba1, GFAP, BOBO1 and p-FTAA in order to visualize immunoreactive astrocytes, immunoreactive microglia, cell nuclei and extracellular Aβ deposits. The fact that tissue sections do not suffer any major damage during ToF-SIMS analysis, as only the uppermost molecular layers (approximately 10 nm) are affected, together with the possibility of analyzing the samples at -80°C, helped in preserving the tissue's structural and chemical integrity. Astrocyte and Aβ labeling with GFAP and p-FTAA did not involve any additional difficulty, despite of having to perform the immunolabeling in fresh frozen tissue. However, Iba1 immunostaining was only successfully performed provided that long post-fixation (up to 2 hours) and incubation (up to 17 day) steps were carried out.

Figure 4-8 displays a representative example of a region occupied by a senile plaque successfully analyzed with the combined methodology. Figures 4-8a and 4-8b present the TIM and Ch distributions whereas Figs. 4-8c and 4-8d display the GFAP (green) and Iba1 (red perinuclear staining) immunostainings together with BOBO-1 (blue) and p-FTAA (yellow) stainings of the region. At the current stage, no direct correlation

between the Ch profile and glial cell distribution was found. Note that Fig. 4-8b displays a granular Ch distribution; interestingly, regions occupied by senile plaques usually presented severe Ch granulation. The evaluation of Ch profiles will be discussed in the following section.

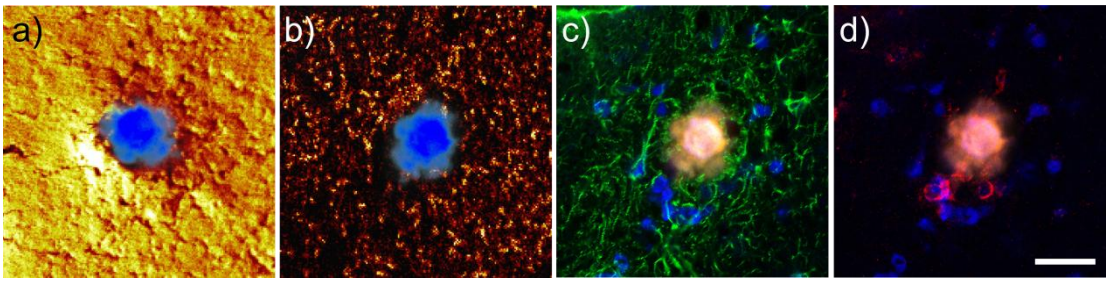


**Figure 4-8**. ToF-SIMS analysis of 3xTg-AD hippocampus combined with GFAP and Iba1 immunostaining of reactive astrocytes and microglia. **(a-b)**: ToF-SIMS analysis of a region occupied by a senile plaque displays the (a) TIM and (b) Ch distribution of the area. The senile plaque was stained with p-FTAA (pseudo-colored blue, overlaid on top of (a) and (b)). Note that Ch presents a granular distribution widespread over the area scanned. **(c):** Confocal fluorescence images of the same region analyzed with ToF-SIMS in (a) and (b) displays the (c) GFAP immunostaining (pseudo-colored green) of reactive astrocytic processes and (d) Iba1 immunostaining of reactive microglia, together with p-FTAA (pseudo-colored yellow) and BOBO-1 (pseudo-colored blue) staining of Aβ and cell nuclei. ToF-SIMS images were acquired with the instrument optimized for maximum spatial resolution. Scale bar: 20 $\mu$m.

Importantly, the combined methodology allowed for simultaneous spatial imaging of Ch, glia and Aβ deposits with great lateral (<400nm) resolution. Imaging of lipids and glial populations at the same spatial localization and with such remarkable resolution might provide a more accurate measure of how these components interact, as compared to studies conducted in adjacent or semi-adjacent sections.

Provided that some precautions are taken, the technique is capable of processing a wide range of biological tissues. Hence, experimental research dealing with the study of lipid composition, lipid turnover and impaired lipid metabolism, not only in brain tissue but in other types of biological samples might benefit from the combined methodology developed. Given the fact that ToF-SIMS allows for analysis at low temperatures, tissue sections may even be subsequently studied with *in-situ* hybridization methods or other techniques specifically oriented to determine gene expression profiles and RNA levels in tissue, thus providing a tool to investigate the relationship between lipid profiles and gene expression.

## REGIONS UNDERGOING SENILE PLAQUE DEPOSITION EXHIBIT CHOLESTEROL GRANULATION *(paper III-IV)*

Having become experienced with the analysis of biological tissue affected by AD pathology using MSI and confocal immunohistochemistry, we proceeded to investigate the brain lipid profile of the 3xTg-AD and Tg2576 mouse models using the combined methodology. The present section deals with the study of Ch profiles in 3xTg-AD and Tg2576 mouse brains, whereas the coming chapters will discuss the study of tissue sections using fluorescence techniques.

Regions undergoing plaque deposition in 3xTg-AD and Tg2576 brains were localized as described in the experimental section, and Ch images were generated from several areas undergoing plaque deposition. Figure 4-9 displays the ToF-SIMS analysis of a region located in the molecular layer of hippocampus, for Tg2576. The region is occupied by senile plaques presenting protrusion-like characteristics (Fig. 4-9a). In the area, the distribution of Ch presents a highly inhomogeneous profile (Fig 4-9b). Generally, hippocampal regions occupied by Aβ displayed abundant Ch deposits with granular distribution, ranging 2-9 $\mu$m in diameter, not only in Tg2576 but also in 3xTg-AD brains. Ch granules did not exclusively colocalize with Aβ but were rather widely spread over the areas analyzed. Some Aβ regions displayed severe Ch granulation whereas others presented a more discrete sterol accumulation pattern, perhaps not associated with a pathological event. Figure 4-9c displays a region similar to the hippocampal area analyzed for Tg2576, but in a matching WT mouse brain. In the area, Ch presents a homogeneous distribution, lacking major accumulations. In fact, most regions devoid of plaques (not only in WT but also in Tg mice) presented reduced or no sterol accumulation; 3xTg-AD brain regions including corpus callosum and stratum oriens of hippocampus as well as some cortical regions displayed a generally homogeneous Ch distribution, whereas only a very limited number of areas presented Ch granulation.

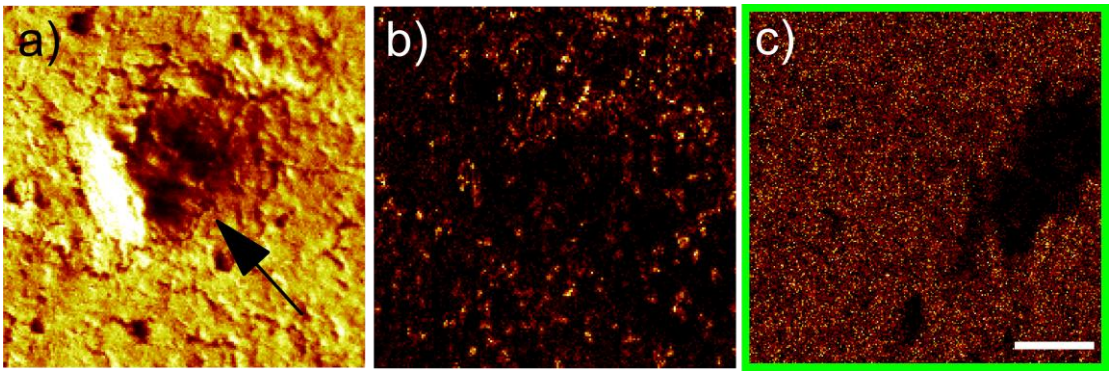


**Figure 4-9**. ToF-SIMS analysis of Tg2576 and WT hippocampus. **(a-b):** ToF-SIMS analysis of an area occupied with a senile plaque in the molecular layer of hippocampus (3xTgAD) displays the (a) TIM and (b) the distribution of Ch in the region. Note that the TIM presents a protrusion-like structure (highlighted by a black arrow) that was identified as a senile plaque by subsequent p-FTAA staining (not shown), whereas the distribution of Ch in (b) presents a granular profile. **(c):** ToF-SIMS analysis of a WT hippocampal area spatially matched to the region analyzed in 3xTgAD. Note that the distribution of Ch is homogeneous. The images were acquired with ToF-SIMS optimized for maximum image resolution. Scale bar: 20 $\mu$m.

Similarly, a preliminary ToF-SIMS study conducted in WT control brains (age-matched to 3xTg-AD) presented a generally homogeneous Ch distribution in areas spatially matched to those regions studied in 3xTg-AD, and only a very limited number of areas in WT presented Ch granulation.

In contrast, a limited number of senile plaques in both 3xTg-AD and Tg2576 hippocampal areas presented local Ch accumulations only, localized at the plaque-tissue junction, as shown in Fig. 4-10. The sterol may diffuse from inner tissue layers and exit to the surface through micro orifices at the plaque-tissue junction, produced during the cryosectioning process. In fact, as seen in the previous section, plaques possess a shape similar to large dense blocks inserted within tissue layers, and their structural and chemical properties differ substantially from those of the surrounding tissue (Knowles and Buehler, 2011). Sectioning may probably cause certain bending or physical stress to the deposits, pulling them inside-out and causing damage to the surrounding tissue, likely to cause damage at the tissue-plaque junction and facilitate the diffusion of small amounts of sterol.

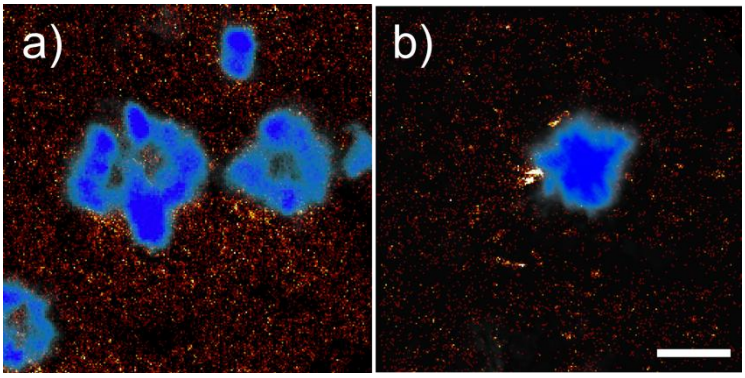


**Fig 4-10**. Representative example of plaques showing local Ch accumulation in their vicinities. **(a):** ToF-SIMS analysis of a 3xTg-AD brain area located in hippocampal subiculum displays multiple discrete Ch deposits in close proximity to the two central Aβ deposits (pseudo-colored blue), stained with p-FTAA and overlaid on top of the Ch image. **(b):** analysis of Tg2576 hippocampus revealed local sterol accumulations also in close proximity to a plaque. The images were acquired with ToF-SIMS optimized for maximum image resolution. Scale bar: 20 $\mu$m.

Interestingly, two regions analyzed in cerebellum and caudate putamen of Tg2576 revealed the presence of Ch accumulations too; compared to Aβ regions, these deposits presented larger sizes (3-19 $\mu$m) and lower abundances, with no granular distribution, as shown in Fig. 4-11. Caudate putamen and cerebellum of Tg2576 are known to undergo amyloidogenesis, but at much reduced rates compared to hippocampal and cortical regions (Hsiao et al., 1996). Therefore, besides being presumably indicative of an on-going AD-related event, granules could also monitor inherent differences in sterol content between different regions, not necessarily associated with pathology. Hence, areas with increased granulation may monitor locally elevated Ch levels and/or even enhanced lipid redistribution due to neuronal reinnervation (Poirier et al., 1993), whereas regions with reduced or no granulation may be indicative of a physiologically normalized Ch content.

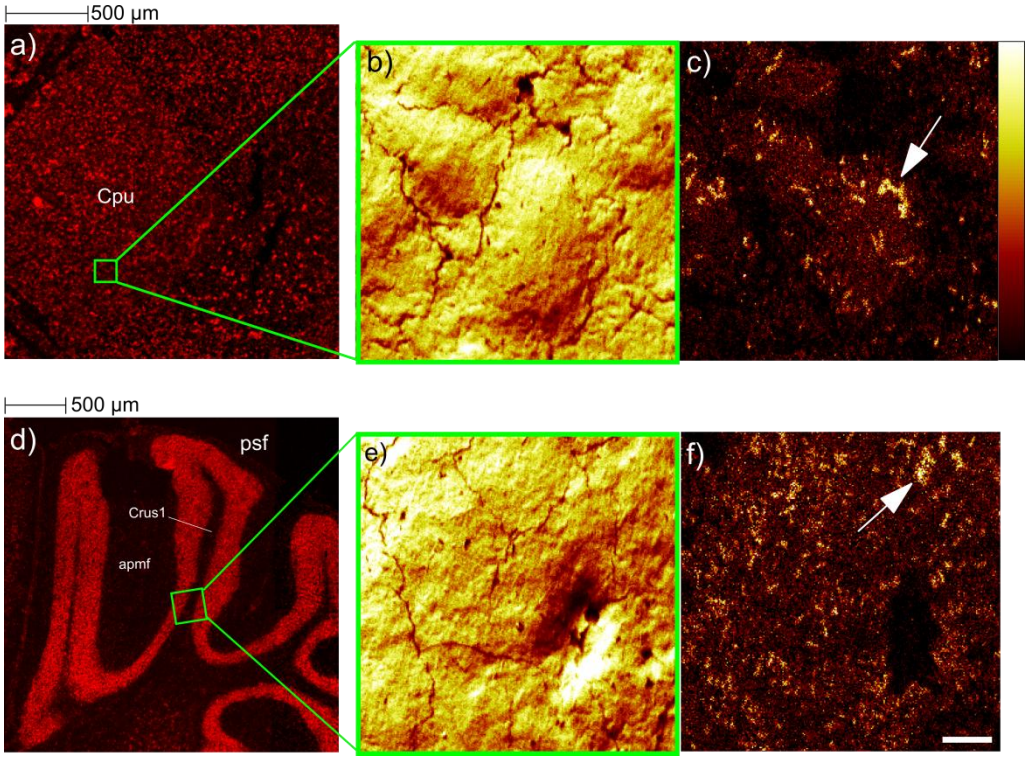


**Figure 4-11.** Study of the distribution of Ch in cerebellum and caudate putamen of Tg2576 mouse brain. **(a-c):** CLSM and ToF-SIMS images acquired from a region including caudate putamen display the (a) BOBO-1 (red) staining of the region, and the ToF-SIMS (b) TIM and (c) Ch distributions of the area delineated with a green square in (a). **(d-f):** similar analysis of a cerebellar region including ansiform lobule provided (d) CLSM images of the area stained with BOBO-1, and ToF-SIMS images displaying the (e) TIM and (f) Ch distribution of the scanned area. Both regions studied were devoid of mature senile plaques, as confirmed by subsequent p-FTAA staining (not shown). Note that Ch forms elongated deposits within regions of increased Ch background, as highlighted by white arrows. The images were acquired with ToF-SIMS optimized for maximum image resolution. White scale bar: 20 $\mu$m.

At the current stage, images acquired with ToF-SIMS are being evaluated visually by independent observers. Their task is to determine whether a particular region presents a granular or a homogeneous sterol distribution, and to classify it accordingly. However, visual assignment of images into categories is not trivial, and the inherent patchy characteristics of most Ch profiles recorded with ToF-SIMS make it difficult for an observer to be absolutely certain of the fact that a region indeed displays a purely homogeneous or a purely granular Ch profile. Therefore, we are now aiming at implementing automated quantification procedures such as those used in ImageJ or other specialized software. A first step will consist in defining the visual characteristics of the "cholesterol granule" in terms of number of pixels and intensity and to further quantify the images according to these criteria.

The Ch granules observed in regions undergoing plaque deposition resemble myelin fragments. Indeed, it is known that regions undergoing myelin degeneration display Ch ester crystals, as show in Fig. 4-12a (Miklossy and Van der Loos, 1987), and focal demyelination exclusively related to areas occupied by Aβ plaques has been observed in both human and Tg2576 brain (Mitew et al., 2010). Poirier et al. described the accumulation of phospholipids and Ch esters in the molecular layer of hippocampus following entorhinal cortex lesion in rats (Poirier et al., 1993). The molecular layer of

hippocampus, stained with Sudan Black, presented a granular pattern similar to that of most regions analyzed with ToF-SIMS. Furthermore, Wirths et al. described an age-dependent axonal degeneration in the APP/PS1 mouse model of AD that may be associated with intraneuronal oligomeric Aβ production. Interestingly, regions in spinal cord of APP/PS1 presented numerous white matter ovoids with diameters similar to the Ch deposits observed in ToF-SIMS images, as shown in Fig. 4-12b (Wirths et al., 2007). Besides, the inflammatory events and later neurodegenerative status of the AD brain leads to formation of myelin fragments in affected areas (Akiyama et al., 2000).

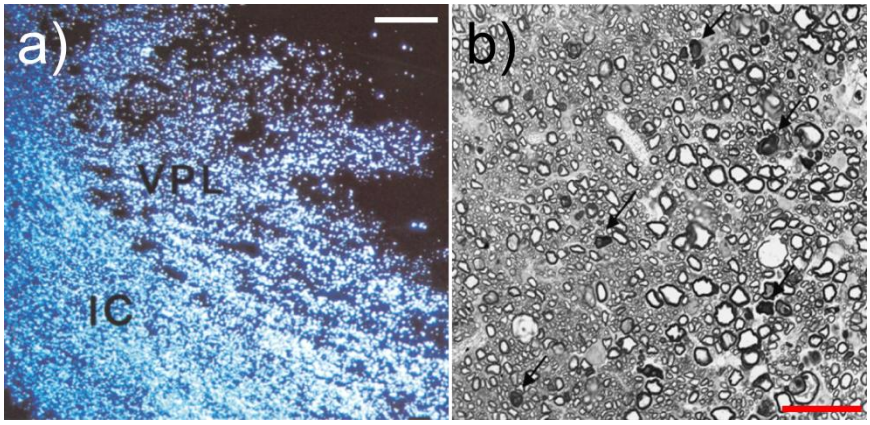


**Figure 4-12**. Brain regions undergoing myelin loss or neurodegeneration display specific staining features. **(a):** formalin-fixed human brain tissue section displays a region affected by infarction. Macrophages loaded with birefringent Ch ester crystals occupy the entire degenerated area. Abbreviations: VPL-ventral posterolateral nucleus of thalamus; IC-left internal capsule. Scale bar (white): 1mm. Reproduced from Miklossy et al. (1987) with permission of Elsevier. **(b):** Toluidine blue stained sections of the cervical spinal cord with numerous white matter ovoids in a 10-month-old APP/PS1ki mouse. Scale bar (red): 33$\mu$m. Reproduced from Wirths et al (2007) with permission of Elsevier.

According to the evidence, the Ch deposits observed in regions occupied by plaques could presumably monitor an on-going demyelination process (not necessarily associated with neuronal loss) that may be related to the amyloidogenic process itself. Late stages of AD are characterized by a pronounced neuronal cell loss accompanied by the resulting demyelination process. However, the question is whether myelin damage occurs also at very early stages of AD, and whether Aβ species (presumably oligomeric units) would be involved in the event. Interestingly, $A\beta_{1\text{-}42}$ fibrils have been identified intra-synaptically in the Tg19959 mouse model of AD at already 2 months of age (prior to plaque formation) causing degeneration of spines and neurites (Capetillo-Zarate et al., 2011).

The next step will be to determine the exact nature of the sterol accumulations observed in regions undergoing plaque deposition. Furthermore, ToF-SIMS study of brain regions affected by Aβ pathology in animal models, at early stages of AD, might provide valuable information regarding the presumably altered lipid status associated with AD pathogenesis.

## SENILE PLAQUES PER SE MAY NOT BE INVOLVED IN THE CHOLESTEROL GRANULATION PHENOMENON *(paper IV)*

A number of 3xTg-AD mouse brain sections analyzed with ToF-SIMS were subsequently studied using fluorescent techniques. At that stage, we decided to investigate the relationship between senile plaque structure and Ch granulation. In order to do so, we studied the structure and chemical composition of the extracellular Aβ deposits using the amyloidotropic dye p-FTAA, and correlated it to the Ch profile associated with each individual plaque, provided by ToF-SIMS. Those tissue sections previously analyzed with ToF-SIMS were subsequently stained with p-FTAA. However, given the fact that the p-FTAA protocol requires ethanol fixation, we could not perform an optimal GFAP staining on those sections. Therefore, the study of glial cell populations was carried out on sections adjacent to those subjected to ToF-SIMS analysis, and regions undergoing plaque deposition in both adjacent sections were overlaid. The study of glial populations and Ch profiles in overlaid brain regions will be discussed in the following section.

A number of early studies suggested that extracellular Aβ deposits were the main toxic units and key players in the development of AD (Dickson, 1997). However, later revision of the amyloidogenic cascade theory suggested that those toxic units may not be the senile plaques but the oligomeric Aβ units (Walsh et al., 2002; Haass and Selkoe, 2007; Selkoe, 2008). In order to investigate the involvement of Aβ in the observed Ch granulation phenomena, extracellular Aβ plaques in regions undergoing Ch granulation were stained with the amyloidotropic fluorescent dye p-FTAA and compared to plaques in regions with reduced or no granulation. Upon binding to Aβ, p-FTAA emits fluorescence at specific wavelengths (emission modes) that have their origin in the properties of the aggregated Aβ to which the dye binds; p-FTAA fluorescence emission from diffuse regions of the plaques is shifted towards longer wavelengths, whereas p-FTAA bound to more condensed regions emits towards shorter wavelengths (Åslund et al., 2009), as show in Figs. 4-13 and 4-14.

If senile plaques were to be involved in the Ch granulation process, their structure-related p-FTAA properties (associated with plaque density and chemical composition) should presumably differ depending on which Ch-type of area they are located. Indeed, it is known that some Aβ deposits with diffuse structure display increased cytotoxicity (Yoshiike et al., 2007) and may release oligomeric species more actively (Haass and Selkoe, 2007). Recently, a study showed that Aβ deposits in an animal model of AD carrying the human arctic mutation were enriched in $A\beta_{1\text{-}42}$ and displayed strong p-FTAA fluorescence shifted towards longer wavelengths (Lord et al., 2011). The increase in $A\beta_{1\text{-}42}$ formation enhances oligomer and protofibril formation, which causes progressive severe and permanent changes in synaptic function (Nilsberth et al., 2001).

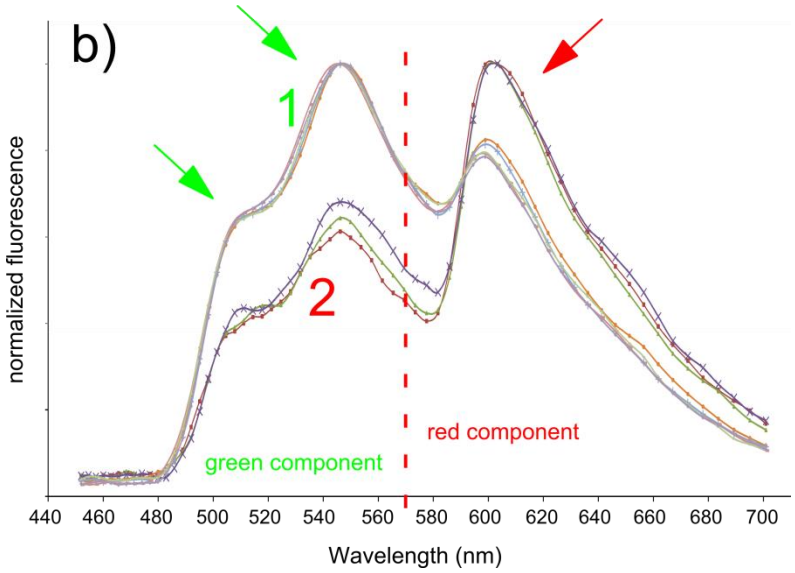


**Figure 4-13**. p-FTAA emission profile of plaques measured in hippocampus and cortex of Tg2576. The spectra are divided into two distinct regions, namely "green component" and "red component". Images of senile plaques stained with p-FTAA are usually composed of two channels, a channel, pseudo-colored green, integrating the fluorescence of the "green component" of the emission profile, and a channel, pseudo-colored red, integrating the fluorescence of the "red" component of the emission profile. The green component of the spectra presents two main emission modes (highlighted with green arrows) whereas the red component of the emission profile presents one main emission mode (highlighted with a red arrow). In the graphic, two groups of plaques stained with p-FTAA were measured and their emission profiles plotted in two groups, namely (1) with intense emission from the green component of the spectrum, and (2) with intense emission from the red component of the spectrum. These two distinct emission profiles are indicative of structural and chemical differences between the different plaques measured.

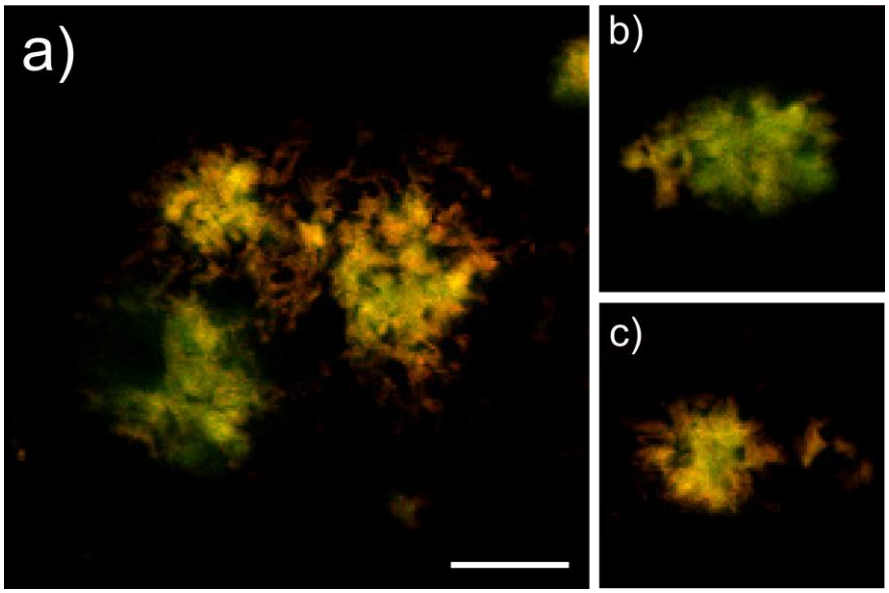


**Figure 4-14**. p-FTAA staining of senile plaques in Tg2576 mouse hippocampus. **(a):** images displaying a number of deposits stained with p-FTAA. Note that some deposits show distinct red and green emission profiles (integrating the red and green components of the p-FTAA fluorescence emission spectrum). **(b,c):** images presenting (b) a senile plaque with fluorescence emission shifted towards shorter wavelengths (green) and (c) a plaque with an emission profile shifted towards longer wavelengths. Note that the periphery of the Aβ deposit displayed in (c) presents intense emission mainly from the red component of the spectrum. Scale bar: 25 $\mu$m.

Senile plaques in regions analyzed with ToF-SIMS were subsequently stained with p-FTAA, and their fluorescence profiles measured. We compared the profiles of a number of hippocampal mature Aβ deposits present in regions with severe Ch granulation to that of mature deposits in regions with discrete or no Ch accumulation. However, analysis of profiles did not identify any characteristic structural p-FTAA-associated difference between plaques, suggesting that extracellular Aβ deposits may not be associated with the Ch granulation event. Assuming the fact that Ch deposits may presumably monitor an AD-related process (possibly an on-going myelin loss event), the fact that p-FTAA-related structural and chemical properties did not differ between plaques measured in areas with discrete or granulated Ch profile is consistent with the idea that mature senile plaques *per-se* may not be most toxic Aβ units.

## INCREASED ASTROCYTIC IMMUNOREACTIVITY ASSOCIATED WITH CHOLESTEROL GRANULATION *(paper IV)*

In an attempt to determine the involvement of glial cells in the Ch granulation event, sections adjacent to those analyzed with ToF-SIMS were processed with immunohistochemical methods and imaged using confocal microscopy. Antibodies against GFAP and Iba1 were used as markers of immunoreactive astrocytes and microglia, respectively. Sections were also stained with p-FTAA and BOBO-1 in order to visualize extracellular Aβ deposits and cell nuclei, respectively.

Since GFAP and Iba1 were mainly associated with senile plaques, we decided to quantify glial immunoreactivity within circular areas around individual Aβ deposits present in regions with severe Ch granulation, and to compare the measurements to those from other plaques located regions with discrete or no Ch accumulation. GFAP was quantified by measuring the intensity of the staining as integrated density, whereas microglia were quantified as the number of Iba1-positive cell nuclei recruited in a particular area being quantified. In order to help define and ensure consistency, glial immunoreactivity was only quantified for those Aβ deposits conserved between the sections subjected to ToF-SIMS analysis and the adjacent immunostained tissues. Consequently, only a limited number of senile plaques was measured.

Figure 4-15 displays a representative example of a region occupied by senile plaques undergoing severe Ch granulation. Figures 4-15a and 4-15b display a section analyzed with ToF-SIMS and the corresponding immunostained adjacent section, respectively, stained with BOBO-1 (red/green) and p-FTAA (yellow). The regions delineated with white squares include plaques that were conserved between sections, and were therefore quantified for GFAP and Iba1 immunoreactivity. Figure 4-15c to 4-15e display ToF-SIMS Ch images acquired from the regions delineated with white squares in Fig. 4-15a; the common color arrows in Figs. 4-15b and Figs. 4-15c/d/e indicate those plaques spatially matched between adjacent sections. Note that Ch presents a granulated distribution in all regions analyzed with ToF-SIMS (Figs. 4-15c/d/e). The immunolabeling of the region (in the immunostained adjacent section) displays intense

GFAP immunoreactivity in regions with intense Ch granulation (identified in the section subjected to ToF-SIMS analysis). Areas with a more homogeneous Ch distribution displayed reduced GFAP immunoreactivity (for more details, the reader is asked to consult paper IV).

Quantification of glial immunostaining revealed increased GFAP but not increased Iba1 immunoreactivity for plaques measured in regions with severe Ch granulation, as compared to deposits quantified in regions with a more homogeneous sterol distribution. Regions devoid of Aβ, also quantified for glial immunostaining, displayed very low glial immunoreactivity, even those areas occasionally found to display severe granular Ch distribution. A limited number of areas immunostained in WT mouse brain sections, also adjacent to those WT brain sections subjected to ToF-SIMS analysis, displayed similar glial immunoreactivity as those regions devoid of Aβ in 3xTg-AD. The images acquired for the immunostained WT brain sections are still being quantified using ImageJ.

The significance of the results, however, must be regarded cautiously. First, due to the predefined stringent conditions described above, only a limited number of senile plaques were quantified in regions with severe Ch granulation (n=12) or homogeneous sterol distribution (n=7). Secondly, those plaques that presented both reduced Ch granulation and reduced GFAP immunoreactivity were observed in two regions located in a single brain section only. However, since all tissue sections were processed simultaneously in a consistent way, and since GFAP immunostaining of Aβ regions is generally intense, the possibility that the observation could be due to a staining artifact is thus improbable.

Nevertheless, with these caveats in mind, the results offer multiple interpretations. As discussed previously, it is known that regions undergoing neuronal loss and/or synaptic degeneration display accumulation of lipids and Ch, most likely due to a concomitant demyelination event. Astrocytes have been shown to internalize Ch and lipid debris in brain areas undergoing neuronal damage (Shobab et al., 2005) and to provide lipids and Ch to regions undergoing reinnervation (Poirier et al., 1993). In fact, regions presenting synaptic degeneration may undergo massive Ch granulation, which in turn may lead to astrocytic recruitment in the affected areas. Indeed, astrocytes, have the capacity to accumulate large amounts of lipids, and may simultaneously attempt to recycle lipid remnants derived from myelin damage and set the conditions for initiating a reinnervation event. Astrocytes are activated during stroke and CNS trauma (Pekny and Nilsson, 2005). However, it is not known whether astrocytic recycling of Ch and other lipid debris *per se* results in increased astrocytic reactivity.

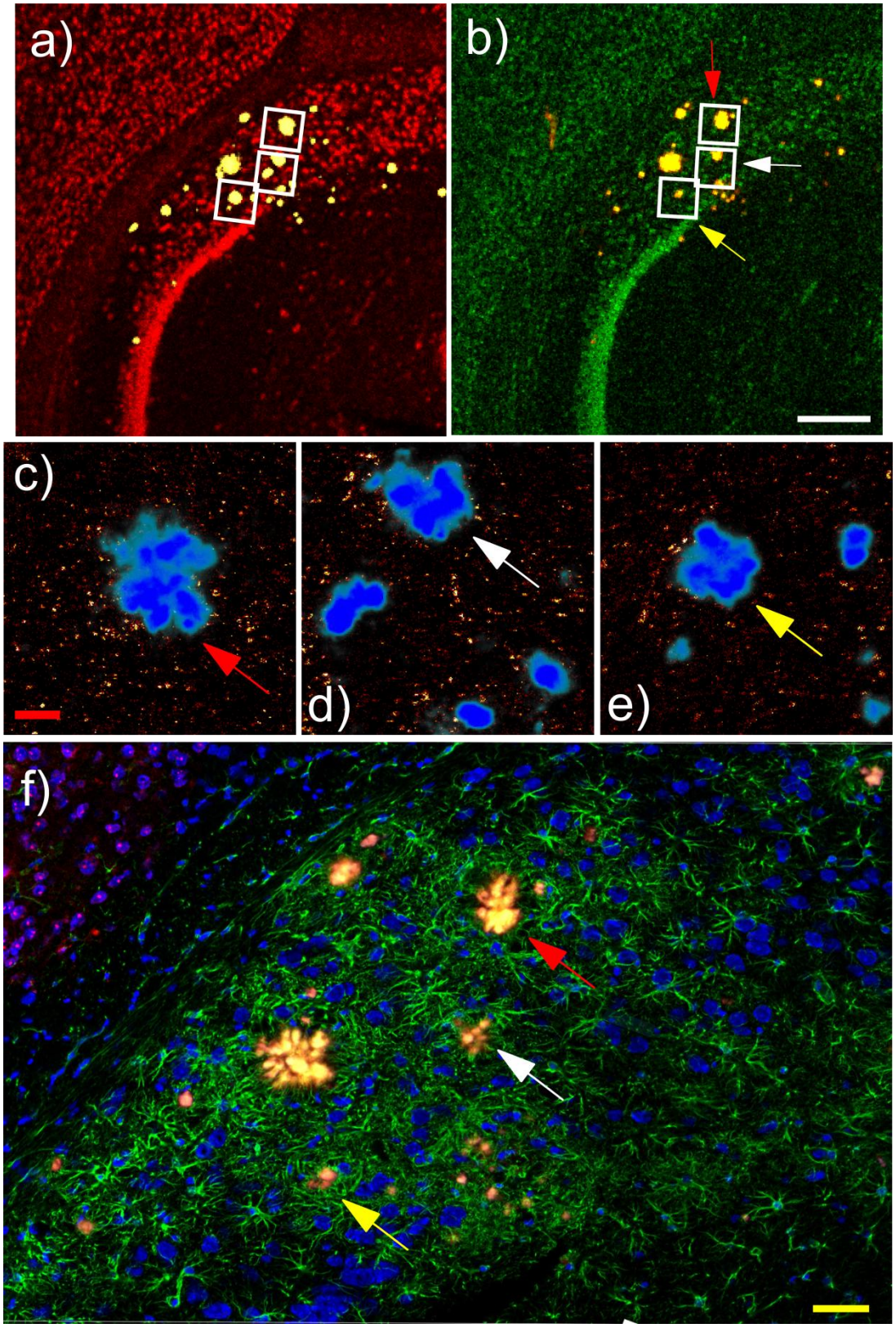


**Figure 4-15.** A 3xTg-AD hippocampal region presenting elevated GFAP immunoreactivity and severe Ch granulation. **(a,b):** CLSM images displaying the BOBO-1 (red/green) and p-FTAA (yellow) staining of (a) a section previously analyzed with ToF-SIMS and (b) the adjacent immunostained section. The white squares highlight common regions occupied with senile plaques. **(c-e):** ToF-SIMS images displaying the distribution of Ch in the regions delineated with white squares in (a). The arrows highlight those plaques that were specifically conserved between the two sections. Note that Ch presents a punctate distribution widespread over the entire areas analyzed. **(f):** CLSM image displaying the GFAP immunostaining of the region displayed in (b), which is adjacent to (a). Color arrows highlight those plaques that turn up in the adjacent immunostained region, matching the deposits studied in the section subjected to ToF-SIMS analysis. Note that the GFAP immunostaining is intense and extensive to the entire region displayed. Scale bars: white: 500 $\mu$m; red: 20 $\mu$m; yellow: 50 $\mu$m.

In contrast, the number of Iba1-positive cell nuclei recruited did not differ between plaques in regions undergoing Ch granulation and areas with reduced sterol accumulation. Reactive microglia are known to contribute directly to myelin damage through several mechanisms (Akiyama et al., 2000; Minagar et al., 2002), but it is not clear whether they are able to release or internalize Ch in significant amounts (Gilardi et al., 2009). However, unlike astrocytes, the lipid transport and/or storage capacity of microglia may be limited by their reduced cytosolic capacity. In addition, astrocytes outnumber microglia (and neurons), thus suggesting their preferential suitability in terms of lipid supply, transport and storage.

## STUDY OF SULFATIDES IN WHITE MATTER STRUCTURES *(paper III-IV)*

Besides Ch, other lipid species can be imaged with ToF-SIMS. Previously, several ST species have been detected in mouse brain tissue, namely ST 22:0, h24:1, 24:1, h24:0, 24:0 and h22:0 (Sjövall et al., 2004); the first digit denotes the number of carbon atoms and the second the number of double bonds of the variable fatty-acid chain, whereas h indicates the presence of a hydroxyl moiety attached to the structure. The various ST species have very similar spatial distributions in all regions analyzed and their signal intensities have therefore been added and are used as an index of the ST content.

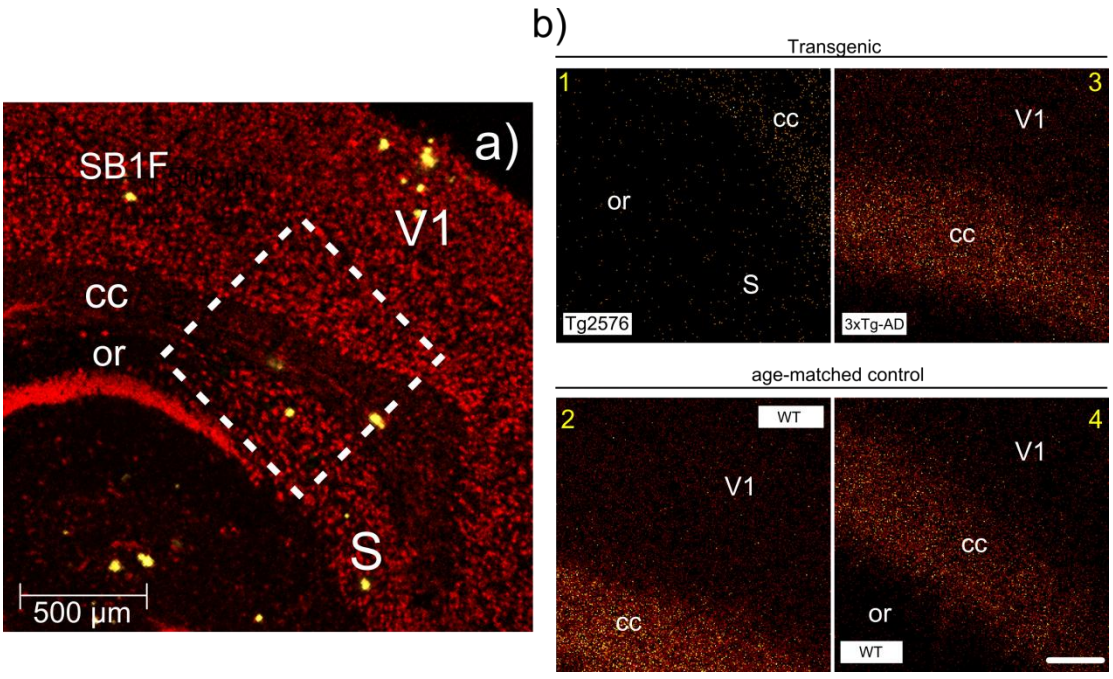


**Figure 4-16**. ToF-SIMS analysis of a region including corpus callosum for Tg and WT mouse brains. **(a):** CLSM image of a Tg2576 brain section analyzed with ToF-SIMS and subsequently stained with BOBO-1 (red) and p-FTAA (yellow). The dashed square indicates the approximate structures analyzed with ToF-SIMS for Tg2576 but also for 3xTg-AD and respective WT (for which the area assignment is therefore approximate). **(b):** ToF-SIMS images displaying the distribution of ST for (b1) Tg2576, (b2) WT control (matched to Tg2576), (b3) 3xTg-AD and (b4) WT control (matched to 3xTg-AD). Note that the ST content is much lower in corpus callosum of Tg2576 as compared to WT, whereas 3xTg-AD and matched WT do not seem to exhibit significantly gross differences in ST signal. White scale bar: 100 $\mu$m

A number of white matter structures from Tg2576, 3xTg-AD and age-matched control mice were analyzed using ToF-SIMS in order to investigate possible differences in ST content between Tg and WT. We did not acquire high resolution images in the regions studied, as we were not aiming at studying the exact distribution of the analytes. Instead, we were aiming in identyfing gross differences in ST signal and, for that purpose, acquisition of large 500x500 $\mu$m images using the high spectral resolution mode (bunched mode) seemed more appropriate.

Figure 4-16 displays a representative example of the ToF-SIMS analysis carried out in Tg2576 and 3xTg-AD white matter structures. Figure 4-16a displays a Tg2576 section analyzed with ToF-SIMS and subsequently stained with BOBO-1 (red) and p-FTAA (yellow). The dashed square highlights the regions analyzed for Tg2576, 3xTg-AD and matched controls, which all include corpus callosum. Figure 4-16b displays ToF-SIMS ST images scanned within the region highlighted with a square in 4-16a; Tg2576 (image b1) displays weak ST signal in the corpus callosum, whereas age-matched control (image b3) shows much higher signal. Interestingly, 3xTg-AD (image b2) displays similar ST ion signal as compared to WT (image b4). Only a limited number of regions were analyzed for Tg2576 (in one brain section only), and therefore the results obtained for the strain must be regarded as indicative only. However, most white matter regions analyzed for 3xTg-AD (including corpus callosum and fimbria of hippocampus) did not display significant differences in ST levels compared to WT.

For the animals studied, Tg2576 displayed increased Aβ load in cortical and hippocampal regions compared to 3xTg-AD. It is to mention that the Tg2576 mouse included in the study was 24 month old when sacrificed, whereas the 3xTg-AD was 18 month old. These animals display increased Aβ production upon aging, which may partially account for the differences in ST load observed between Tg genotypes. Nevertheless, Han and collaborators reported a decrease in ST levels in cortical structures of $APP_{swe}$ likely to be mediated by apoE (Cheng et al., 2008). In these animals, the onset of cortical ST depletion matched to that of cortical Aβ pathology. ST may be involved in the clearance of Aβ in brain regions (Han, 2010), which is consistent with the increased Aβ levels observed in regions undergoing ST depletion. However, in our studies, no significant plaque deposition was observed in white matter structures.

We have observed low ST levels in grey matter structures for all mouse strains analyzed (including WT) as compared to white matter regions, which is *a priori* expected. Interestingly, grey matter areas, which are poorly myelinated as compared to white matter structures, seem to be more prone to undergo ST depletion (Han, 2010). Therefore, it will be necessary to undertake a detailed imaging study of ST distribution in Tg2576 and 3xTg-AD, also including grey matter structures, in order to determine whether cortical and other regions affected by Aβ pathology undergo ST depletion.

## STUDY OF HUMAN TISSUE USING TOF-SIMS *(paper III)*

Human brain affected by AD was also studied using ToF-SIMS and CLSM. Figure 4-17 displays a temporal lobe region analyzed with ToF-SIMS and subsequently stained with p-FTAA; Fig. 4-17a presents the TIM of a region analyzed, showing abundant protrusion-like structures spread over the entire area. Fig. 4-17b displays the distribution of Ch in the region, which was correlated with the distribution of NFT in the Ch/p-FTAA staining shown in Figure 4-17c –note that p-FTAA has also been shown to stain tau deposits (Åslund et al., 2009).

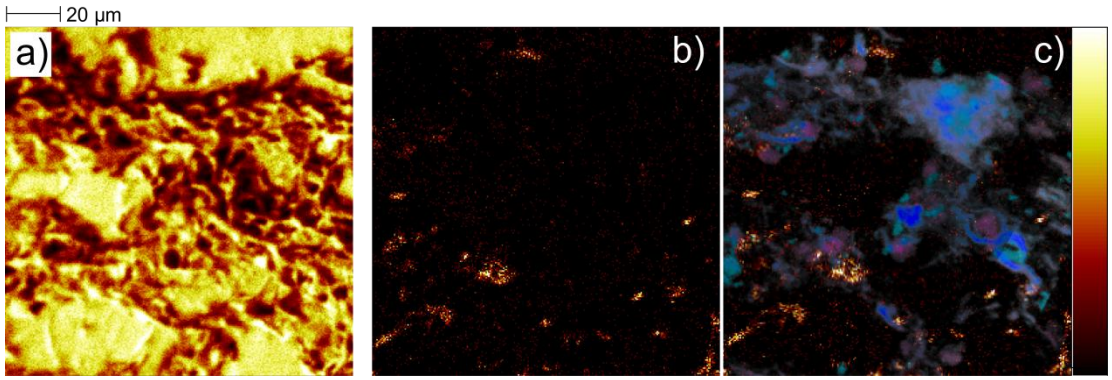


**Figure 4-17**. ToF-SIMS analysis of human brain tissue affected by AD pathology. ToF-SIMS analysis of a temporal lobe brain section provided the (a) TIM and (b) Ch images of the area scanned. Subsequent p-FTAA staining of the region revealed abundant NFT, as shown in the (c) overlay between Ch shown in (b) and p-FTAA (pseudo-colored blue-red).

The human AD tissues analyzed displayed abundant Ch accumulations that did not correlate with the presence of NFTs. In addition, regions devoid of NFT in AD and age-matched non-demented control brain displayed similar Ch accumulations (data not shown), suggesting that other factors besides an AD-related event may drive Ch deposition in the tissue studied. The size of the Ch accumulations observed in human brain ranged 3-19 µm, whereas most Ch granules observed in hippocampal regions of Tg2576 and 3xTg-AD mice ranged 2-9 µm. Hence, the Ch accumulation observed in both types of tissue may be reflecting different biological or pathological processes.

Nevertheless, the observed Ch deposits resemble myelin fragments, which is consistent with the already known demyelination process that occurs during the course of pathology-related neuronal loss (Miklossy and Van der Loos, 1987; Akiyama et al., 2000; Minagar et al., 2002; Mitew et al., 2010) and normal aging (Teipel et al., 1998; Bartzokis, 2004). However, since only one human AD brain section (and the respective age-matched control) have been analyzed, the results presented herein must be regarded as indicative only. At the current stage, the identity of these Ch deposits remains elusive, and more experiments are needed in order to determine the nature of the accumulations as well as any existing link between Ch accumulation and amyloidogenesis.

# CONCLUSIONS

I. The ToF-SIMS study of mouse adipose tissue revealed alterations in the distribution of surface lipids upon staining with osmium tetroxide. Furthermore, the study of 3xTg-AD brain tissue revealed considerable variation in the distribution of surface cholesterol upon changes in temperature, which is consistent with previous publications dealing with the variation of lipid ion signal as a function of sample temperature.

II. ToF-SIMS analysis of opioid and amyloid peptide preparations and further study of the spectra revealed specific spectral fingerprints related to structural features and demonstrated that SIMS of short length peptides induces a fragmentation pattern similar to that of collision induced dissociation. However, contrary to expected, the analysis of extracellular amyloid-beta deposits in biological tissue affected by Alzheimer's disease did not reveal any specific spectral fingerprints compared to synthetic amyloid peptides, most likely due to low secondary ion production associated with the senile plaques.

III. ToF-SIMS imaging was successfully combined with fluorescence techniques; This multiplexed imaging approach enabled us to simultaneously observe lipid and glial cell distributions in regions undergoing senile plaque deposition with great lateral (<500 nm) resolution, thus establishing the possibility to study the spatial correlation between lipid species and the enzymes/cell types responsible for their synthesis and processing.

IV. The study of mouse brain tissue areas affected by Alzheimer's disease pathology using the developed methodology revealed Ch granulation in regions undergoing senile plaque deposition that correlated with astrocytic activation but that neither correlated with microglial activation nor with senile plaque structure.

# FUTURE PERSPECTIVES

ToF-SIMS has been proven capable of providing valuable information of the content and distribution of lipids and lipid precursors in pathological and non-pathological tissue. Remarkably, specimens analyzed with ToF-SIMS can be subsequently studied using complementary techniques, thus offering the possibility to investigate the role of multiple biological components (such as lipids, cells and proteins) in a given biochemical problem, which would otherwise be virtually impossible with the only use of a single, isolated technique.

ToF-SIMS is the central actor of the combined methodology reported in the present work, which allowed for the simultaneous spatial study of lipids, lipid precursors, misfolded proteins and glial cell populations. In the near future, the method might enormously facilitate the understanding of the involvement and interaction of these components in neuropathology. Obvious future steps to be given are the study of brain tissue from mouse models of Alzheimer's disease at early stages of disease progression (1 to 6 months) in order to determine whether the observed cholesterol granulation event occurs prior to plaque formation; the detailed investigation of ST profiles, also at early stages of the disease, in order to clarify the relationship between plaque deposition and ST depletion, and the use of ToF-SIMS combined with fluorescence techniques in the study of other disease-related biological tissue samples. Furthermore, the combination of ToF-SIMS with other imaging techniques such as *in-situ* hybridization may provide new insights on the relationship between lipids and lipid precursors and regiospecific gene expression.

It is to note that, mainly due to technical limitations associated with the manipulation of biological tissue samples, excessive time-consuming data analysis procedures and slow data acquisition protocols, the technique has not yet found a broad use for solving biochemical problems in medicine and cell biology. In order to give an extended use to the methodology, it will be necessary to improve the existing operating protocols in order to facilitate data acquisition in a more automated way. In addition, it is of vital importance to make the methodology available to the medical research field, in order to receive feedback from biology-oriented research staff and being able to optimize the instrument for the study of complex biological and medical paradigms.

# ACKNOWLEDGEMENTS

Many things have changed since I came to Stockholm and started my PhD training at Karolinska Institutet, and many special people accompanied me in the journey. I would like to express my gratitude to:

My main supervisor Björn Johansson, for teaching me science, for supporting me unconditionally and for believing in my work, probably even more than I do. You are a genuinely good hearted person.

My supervisor Peter Sjövall, for your critical eye and your passion for things being well done. It has been a true pleasure to work with you, even though sometimes we may not have agreed upon some aspects of our collaboration. Your excellence and sharp style have helped me to build a critical view on my work and to enjoy science even more.

To my supervisor Lars Terenius, for always, always having time for discussing science.

To my supervisors Catharina Lavebratt and Martin Schalling, for providing a nice working environment and for being there when problems turn up. Thanks to Xinghua Zhou too, for being calm and kind. Wherever you may roam, I wish you the best.

To my "almost" 7th supervisor Vladana Vukojević, for teaching me confocal microscopy, for helping me with the writing and for being positive and friendly.

To Jeanette Johansen, for always having time for "Jeanette do you have 5 minutes? I have a problem". Thanks for helping me during the entire process leading to the Defence, for being practical, honest and straight forward.

To all members of our VR project, Fredrik, Anders, Louise and Tomas, for a wonderful research approach and for the nice meetings.

I'd like to thank all members of the Neurogenetics Unit; Anna, Lollo, Ida, Karin, Phille, Anna-Lee, Catharina G, Charlotte, Dzana, Annika, Louise, Carina, Yabin Wei, Ulrika, and former members Dalila (aaaaah-it's-a-good!) Tina, Rifat, and Sachin, for the nice moments together.

Those people who accompanied me in my every day's life at CMM; special thanks to:

Agneta Gunnar, for being such a kind person and not minding me infecting the cell cultures. To Mattias, for helping me with cell cultures and for staying calm each time I ask for cell media + plastic bottles + antibiotic + serum + more cell media. Thanks Sandra too. Many thanks to Meta for caring about the cell lab and for the nice coffees (during my lunch time).

To Chus & Chus, la pareja de moda, for being so natural and spontaneous and for opening the doors of their home. You have amazing children! What a tocayo!

To Yu Ming, for your vitality.

To Selim, for giving me little particles that allow me to reach the sky. You're N.1, and don't let anyone tell you contrary.

To Lennart Helleday, for helping me with computer stuff and…oh I just love the music you used to play in your office! Thanks to Britt-Marie Witasp too, for truly helping me with the finances and forms, and for caring.

To Elin K, for your kind smile and for being always patient, calm and nice.

To Martin E, for the chatting and gossiping and for such nice ski trips to Sälen. How was that, in our room, let met remember…"oh, we just figured it out long time ago"

I'd like to thank especially Hongya Han, for helping me so much in the cell lab and burning my tongue with his wonderful Chinese delicatessen. To Theresse, Valentina and Joelle, for sharing with me amazing Barça-Inter moments. By the way, Valentina listen to me, you are not listening to me… Milito's 3rd goal was offside, and you know that. Don't live in denial.

And special thanks to Sivonne Arvidsson and Siw Frebelius, for helping me crossing troubled waters and showing concern.

Among all those folks I have had the pleasure to meet in Stockholm, some have left a true print in me. I'd like to thank some very special ones:

Alina, thank you for being patient, for standing my bad mood and for caring as you do. I could not have done it without your help during these last days. I wish I could be only half the good friend you are for me. Thank you so much.

Thanks to Ruani Fernando for her priceless assistance fixing paper III and IV, for always having time for me, for such amazing science discussions about image quantification. You are one of the kindest persons I have met in Stockholm.

To Ebba, for standing my bad mood too, for the excursions to Stockholm Skärgård and the hiking to the islands, for the beers and coffees and discussions about heating and fatal electrostatic interactions, which are indeed inevitable in the science universe. For caring.

To Masako, for being just easy and relax, for making me feel comfortable in most situations and for sharing time with me. During these last weeks, having met you feels like a drop of rain in the desert.

To Roberto and Paola! Dubbelt indeed! I had great moments with you, skiing (perhaps not Paola though, I remember you saying something like "ti odio"). I really hope to meet more often once I have delivered.

To Souzanoula Mou, for being a true friend, and for preparing the best rakomelo ever. Kala?

To Maria Rogdaki, for being so honest and natural, and for sharing your time and making me feel like at home. I hope you will continue having a great time in UK.

To Petradaki Bro and Ntoumpas, for building barricades with home's furniture and blocking my room's door at 3 am. For receiving me with open arms each time I visit Greece, and for being my friends and accepting me the way I am. Many special thanks to Voltron and all friends from Lappis, for the wonderful moments we spent together during the first year in Stockholm.

To Zvoni, my friend and brother, for all the nice moments we have had in Croatia and Berlin, which I won't forget. It's hard to find people like you.

And last but not least, to Anna Aullón. Per la xispa!

To each one of you, thanks a lot, from the bottom of my heart.

*Després d'una temporada a Estocolm, i que consti que ha valgut la pena, crec que em calen vacances. I vacances llargues, de debò. És difícil estar tant lluny de vosaltres; m'hi he acostumat (lleugerament), però el pas del temps fa que us recordi amb més intensitat i nostàlgia.*

*En primer lloc, voldria agrair a en Joan i els seus pares l'ajuda que em van prestar durant els primers mesos que vaig passar a Barcelona, abans de marxar cap a Estocolm. Mai he tingut l'oportunitat d'agrair-vos l'acollida que em vau donar i els bons moments que vam passar junts. Gràcies!*

*Penya de l'espardenya que passa! En Santi torna a casa (o no). Us he trobat a faltar, moltíssim, sobretot per barraques de Girona i als estius. Cada vegada que em trobo amb vosaltres em sento com si encara m'hagués de llevar el dia següent per anar a classe d'orgànica. Moltes gràcies a tots i a totes per mantindre el contacte i fer que res canviés entre nosaltres, a pesar del temps. A l'Anna Díaz, per cuidar-me i apreciar-me només com un amic de debò sap fer.*

*Família Comalada i nous Comaladas, moltes gràcies per ser com sou. M'he adonat, durant aquests anys, que sou realment especials. El que us fa únics és la naturalitat amb la qual us relacioneu els uns amb els altres; quan vinc a Girona i em trobo amb vosaltres, és com si res no hagués canviat. Em sento a gust, a taula, amb en Chornet a mà dreta i mon pare a l'esquerra queixant-se en to desafiant "esta tot corromput!". No us podeu imaginar com ho he trobat a faltar...*

*A l'avi i a la iaia, que allà on siguin no es barallin gaire i es cuidin l'un a l'altre. Us trobo a faltar.*

*Moltes gràcies Tauler i Maura (i les respectives xicotes, que si no se m'enfaden) per ser collonuts i rebre'm amb els braços oberts a casa vostra. Per les excursions amb en Bruc i en Truc, i pels caps d'any i les nits d'insomni.*

*I finalment, el meu més sincer i profund agraïment als meus pares, Salvador i Dolors, per ajudar-me i estimar-me tal i com sóc. Sou les persones en qui més confio, i desitjo arribar a ser tan bon pare com vosaltres heu estat amb mi. Us estimo, de tot cor.*

# REFERENCES

(2002) MRC/BHF Heart Protection Study of cholesterol lowering with simvastatin in 20,536 high-risk individuals: a randomised placebo-controlled trial. Lancet 360:7-22.

Abildayeva K, Jansen PJ, Hirsch-Reinshagen V, Bloks VW, Bakker AH, Ramaekers FC, de Vente J, Groen AK, Wellington CL, Kuipers F, Mulder M (2006) 24(S)-hydroxycholesterol participates in a liver X receptor-controlled pathway in astrocytes that regulates apolipoprotein E-mediated cholesterol efflux. J Biol Chem 281:12799-12808.

Acton S, Rigotti A, Landschulz KT, Xu S, Hobbs HH, Krieger M (1996) Identification of scavenger receptor SR-BI as a high density lipoprotein receptor. Science 271:518-520.

Adams CM, Reitz J, De Brabander JK, Feramisco JD, Li L, Brown MS, Goldstein JL (2004) Cholesterol and 25-hydroxycholesterol inhibit activation of SREBPs by different mechanisms, both involving SCAP and Insigs. J Biol Chem 279:52772-52780.

Akiyama H, Barger S, Barnum S, Bradt B, Bauer J, Cole GM, Cooper NR, Eikelenboom P, Emmerling M, Fiebich BL, Finch CE, Frautschy S, Griffin WST, Hampel H, Hull M, Landreth G, Lue LF, Mrak R, Mackenzie IR, McGeer PL, O'Banion MK, Pachter J, Pasinetti G, Plata-Salaman C, Rogers J, Rydel R, Shen Y, Streit W, Strohmeyer R, Tooyoma I, Van Muiswinkel FL, Veerhuis R, Walker D, Webster S, Wegrzyniak B, Wenk G, Wyss-Coray T, Neuroinflammation Working G (2000) Inflammation and Alzheimer's disease. Neurobiology of Aging 21:383-421.

Argmann CA, Edwards JY, Sawyez CG, O'Neil CH, Hegele RA, Pickering JG, Huff MW (2005) Regulation of macrophage cholesterol efflux through hydroxymethylglutaryl-CoA reductase inhibition: a role for RhoA in ABCA1-mediated cholesterol efflux. J Biol Chem 280:22212-22221.

Ariga T, McDonald MP, Yu RK (2008) Role of ganglioside metabolism in the pathogenesis of Alzheimer's disease--a review. J Lipid Res 49:1157-1175.

Åslund A, Sigurdson CJ, Klingstedt T, Grathwohl S, Bolmont T, Dickstein DL, Glimsdal E, Prokop S, Lindgren M, Konradsson P, Holtzman DM, Hof PR, Heppner FL, Gandy S, Jucker M, Aguzzi A, Hammarstrom P, Nilsson KP (2009) Novel pentameric thiophene derivatives for in vitro and in vivo optical imaging of a plethora of protein aggregates in cerebral amyloidoses. ACS Chem Biol 4:673-684.

Bach D, Wachtel E (2003) Phospholipid/cholesterol model membranes: formation of cholesterol crystallites. Biochimica Et Biophysica Acta-Biomembranes 1610:187-197.

Balducci C, Forloni G (2011) APP Transgenic Mice: Their Use and Limitations. Neuromolecular Med 13:117-137.

Ballatore C, Lee VMY, Trojanowski JQ (2007) Tau-mediated neurodegeneration in Alzheimer's disease and related disorders. Nature Reviews Neuroscience 8:663-672.

Bartzokis G (2004) Age-related myelin breakdown: a developmental model of cognitive decline and Alzheimer's disease. Neurobiol Aging 25:5-18; author reply 49-62.

Bazan NG, Colangelo V, Lukiw WJ (2002) Prostaglandins and other lipid mediators in Alzheimer's disease. Prostaglandins & Other Lipid Mediators 68-9:197-210.

Bélazi D, Solé-Domènech S, Johansson B, Schalling M, Sjövall P (2009) Chemical analysis of osmium tetroxide staining in adipose tissue using imaging ToF-SIMS. Histochem Cell Biol 132:105-115.

Benninghoven A (1975) Developments in Secondary Ion Mass Spectroscopy and applications to surface studies. Surf Sci 53:596-625.

Benninghoven A (1994) Surface analysis by secondary ion mass spectrometry (SIMS). Surf Sci 299:246-260.

Benninghoven A, Sichtermann WK (1978) Detection, identification and structural investigation of biologically important compounds by secondary ion mass spectrometry. Anal Chem 50:1180-1184.

Benninghoven A, Jaspers D, Sichtermann W (1976) Secondary ion emission of amino acids. Appl Phys 11:35-39.

Björkhem I, Meaney S (2004) Brain cholesterol: Long secret life behind a barrier. Arteriosclerosis Thrombosis and Vascular Biology 24:806-815.

Björkhem I, Diczfalusy U, Lutjohann D (1999) Removal of cholesterol from extrahepatic sources by oxidative mechanisms. Current Opinion in Lipidology 10:161-165.

Blomqvist M, Gieselmann V, Mansson JE (2011) Accumulation of lysosulfatide in the brain of arylsulfatase A-deficient mice. Lipids in Health and Disease 10.

Bosio A, Binczek E, Stoffel W (1996) Functional breakdown of the lipid bilayer of the myelin membrane in central and peripheral nervous system by disrupted galactocerebroside synthesis. Proceedings of the National Academy of Sciences of the United States of America 93:13280-13285.

Braak H, Braak E (1991) Neuropathological stageing of Alzheimer-related changes. Acta Neuropathol 82:239-259.

Brulet M, Seyer A, Edelman A, Brunelle A, Fritsch J, Ollero M, Laprevote O (2010) Lipid mapping of colonic mucosa by cluster TOF-SIMS imaging and

multivariate analysis in cftr knockout mice. Journal of Lipid Research 51:3034-3045.

Brunelle A, Touboul D, Laprevote O (2005) Biological tissue imaging with time-of-flight secondary ion mass spectrometry and cluster ion sources. Journal of Mass Spectrometry 40:985-999.

Bu GJ, Maksymovitch EA, Nerbonne JM, Schwartz AL (1994) Expression and function of the low-density-lipoprotein receptor-related protein (LRP) in mammalian central neurons. Journal of Biological Chemistry 269:18521-18528.

Busciglio J, Lorenzo A, Yeh J, Yankner BA (1995) Beta-amyloid fibrils induce tau phosphorylation and loss of microtubule binding. Neuron 14:879-888.

Capetillo-Zarate E, Gracia L, Yu FM, Banfelder JR, Lin MT, Tampellini D, Gouras GK (2011) High-Resolution 3D Reconstruction Reveals Intra-Synaptic Amyloid Fibrils. American Journal of Pathology 179:2551-2558.

Casserly I, Topol E (2004) Convergence of atherosclerosis and Alzheimer's disease: inflammation, cholesterol, and misfolded proteins. Lancet 363:1139-1146.

Chait BT, Standing KG (1981) A time-of-flight mass spectrometer for measurement of secondary ion mass spectra. International Journal of Mass Spectrometry and Ion Processes 40:185-193.

Cheng H, Xu J, McKeel DW, Jr., Han X (2003) Specificity and potential mechanism of sulfatide deficiency in Alzheimer's disease: an electrospray ionization mass spectrometric study. Cell Mol Biol (Noisy-le-grand) 49:809-818.

Cheng H, Zhou Y, Holtzman DM, Han X (2008) Apolipoprotein E mediates sulfatide depletion in animal models of Alzheimer's disease. Neurobiol Aging.

Christopher K. Mathews KEvH (1990) Biochemistry. Redwood City: Benjamin/Cummings.

Chung H, Brazil MI, Soe TT, Maxfield FR (1999) Uptake, degradation, and release of fibrillar and soluble forms of Alzheimer's amyloid beta-peptide by microglial cells. J Biol Chem 274:32301-32308.

Coetzee T, Fujita N, Dupree J, Shi R, Blight A, Suzuki K, Popko B (1996) Myelination in the absence of galactocerebroside and sulfatide: Normal structure with abnormal function and regional instability. Cell 86:209-219.

Curatolo W (1987) Glycolipid function. Biochimica Et Biophysica Acta 906:137-160.

Debois D, Bralet MP, Le Naour F, Brunelle A, Laprevote O (2009) In Situ Lipidomic Analysis of Nonalcoholic Fatty Liver by Cluster TOF-SIMS Imaging. Analytical Chemistry 81:2823-2831.

Dehouck B, Fenart L, Dehouck MP, Pierce A, Torpier G, Cecchelli R (1997) A new function for the LDL receptor: transcytosis of LDL across the blood-brain barrier. J Cell Biol 138:877-889.

Dickson DW (1997) The pathogenesis of senile plaques. Journal of Neuropathology and Experimental Neurology 56:321-339.

Dietschy JM (2009) Central nervous system: cholesterol turnover, brain development and neurodegeneration. Biological Chemistry 390:287-293.

Dietschy JM, Turley SD (2001) Cholesterol metabolism in the brain. Current Opinion in Lipidology 12:105-112.

Dietschy JM, Turley SD (2004) Thematic review series: brain Lipids. Cholesterol metabolism in the central nervous system during early development and in the mature animal. J Lipid Res 45:1375-1397.

Ehehalt R, Keller P, Haass C, Thiele C, Simons K (2003) Amyloidogenic processing of the Alzheimer beta-amyloid precursor protein depends on lipid rafts. J Cell Biol 160:113-123.

Ehnholm C, Lukka M, Kuusi T, Nikkila E, Utermann G (1986) Apolipoprotein E polymorphism in the finnish population: gene frequencies and relation to lipoprotein concentrations. Journal of Lipid Research 27:227-235.

Elliott DA, Halliday GM, Garner B (2010) Apolipoprotein-E forms dimers in human frontal cortex and hippocampus. Bmc Neuroscience 11.

Farooqui AA, Ong WY, Horrocks LA (2004) Biochemical aspects of neurodegeneration in human brain: Involvement of neural membrane phospholipids and Phospholipases A(2). Neurochemical Research 29:1961-1977.

Gasic GP (1994) Basic-helix-loop-helix transcription factor and sterol sensor in a single membrane-bound molecule. Cell 77:17-19.

Gilardi F, Viviani B, Galmozzi A, Boraso M, Bartesaghi S, Torri A, Caruso D, Crestani M, Marinovich M, de Fabiani E (2009) Expression of sterol 27-hydroxylase in glial cells and its regulation by liver X receptor signaling. Neuroscience 164:530-540.

Gimenez-Llort L, Blazquez G, Canete T, Johansson B, Oddo S, Tobena A, LaFerla FM, Fernandez-Teruel A (2007) Modeling behavioral and neuronal symptoms of Alzheimer's disease in mice: a role for intraneuronal amyloid. Neurosci Biobehav Rev 31:125-147.

Gong JS, Kobayashi M, Hayashi H, Zou K, Sawamura N, Fujita SC, Yanagisawa K, Michikawa M (2002) Apolipoprotein E (ApoE) isoform-dependent lipid release from astrocytes prepared from human ApoE3 and ApoE4 knock-in mice. J Biol Chem 277:29919-29926.

Haass C, De Strooper B (1999) Review: Neurobiology - The presenilins in Alzheimer's disease - Proteolysis holds the key. Science 286:916-919.

Haass C, Selkoe DJ (2007) Soluble protein oligomers in neurodegeneration: lessons from the Alzheimer's amyloid beta-peptide. Nat Rev Mol Cell Biol 8:101-112.

Haass C, Schlossmacher MG, Hung AY, Vigopelfrey C, Mellon A, Ostaszewski BL, Lieberburg I, Koo EH, Schenk D, Teplow DB, Selkoe DJ (1992) Amyloid-beta peptide is produced by cultured cells during normal metabolism. Nature 359:322-325.

Hakomori SI (1990) Bifunctional role of glycosphingolipids: modulators for transmembrane signaling and mediators for cellular interactions. Journal of Biological Chemistry 265:18713-18716.

Han X (2010) The Pathogenic Implication of Abnormal Interaction Between Apolipoprotein E Isoforms, Amyloid-beta Peptides, and Sulfatides in Alzheimer's Disease. Mol Neurobiol.

Han X, Gross RW (2005) Shotgun lipidomics: electrospray ionization mass spectrometric analysis and quantitation of cellular lipidomes directly from crude extracts of biological samples. Mass Spectrom Rev 24:367-412.

Han X, Cheng H, Fryer JD, Fagan AM, Holtzman DM (2003a) Novel role for apolipoprotein E in the central nervous system. Modulation of sulfatide content. J Biol Chem 278:8043-8051.

Han X, Fagan AM, Cheng H, Morris JC, Xiong C, Holtzman DM (2003b) Cerebrospinal fluid sulfatide is decreased in subjects with incipient dementia. Ann Neurol 54:115-119.

Han XL, Holtzman DM, McKeel DW, Kelley J, Morris JC (2002) Substantial sulfatide deficiency and ceramide elevation in very early Alzheimer's disease: potential role in disease pathogenesis. Journal of Neurochemistry 82:809-818.

Hardy J (1997) Amyloid, the presenilins and Alzheimer's disease. Trends Neurosci 20:154-159.

Hartmann T, Kuchenbecker J, Grimm MOW (2006) Alzheimer's disease: the lipid connection. In: 2nd ISN Special Neurochemistry Conference, pp 159-170. Antigua & Barbu.

Hayashi H, Campenot RB, Vance DE, Vance JE (2004) Glial lipoproteins stimulate axon growth of central nervous system neurons in compartmented cultures. J Biol Chem 279:14009-14015.

Herz J, Beffert U (2000) Apolipoprotein E receptors: Linking brain development and Alzheimer's disease. Nature Reviews Neuroscience 1:51-58.

Hirsch-Reinshagen V, Burgess BL, Wellington CL (2009) Why lipids are important for Alzheimer disease? Mol Cell Biochem 326:121-129.

Hooijmans CR, Kiliaan AJ (2007) Fatty acids, lipid metabolism and Alzheimer pathology. In: Spring Meeting of the European Journal of Pharmacology, pp 176-196. Netherlands.

Hoshino T, Nakaya T, Homan T, Tanaka K, Sugimoto Y, Araki W, Narita M, Narumiya S, Suzuki T, Mizushima T (2007) Involvement of prostaglandin E2 in production of amyloid-beta peptides both in vitro and in vivo. J Biol Chem 282:32676-32688.

Hsiao K, Chapman P, Nilsen S, Eckman C, Harigaya Y, Younkin S, Yang F, Cole G (1996) Correlative memory deficits, Abeta elevation, and amyloid plaques in transgenic mice. Science 274:99-102.

Hu R, Li G, Kamijo Y, Aoyama T, Nakajima T, Inoue T, Node K, Kannagi R, Kyogashima M, Hara A (2007) Serum sulfatides as a novel biomarker for cardiovascular disease in patients with end-stage renal failure. Glycoconj J 24:565-571.

Irizarry MC (2003) A turn of the sulfatide in Alzheimer's disease. Ann Neurol 54:7-8.

Iwatsubo T, Odaka A, Suzuki N, Mizusawa H, Nukina N, Ihara Y (1994) Visualization of Aβ42(43) and Aβ40 in senile plaques with end-specific Aβ monoclonals: evidence that an initially deposited species is Aβ42(43). Neuron 13:45-53.

Jabs HU, Assmann G, Greifendorf D, Benninghoven A (1986) High performance liquid chromatography and time-of-flight secondary ion mass spectrometry: a new dimension in structural analysis of apolipoproteins. J Lipid Res 27:613-621.

Jick H, Zornberg GL, Jick SS, Seshadri S, Drachman DA (2000) Statins and the risk of dementia. Lancet 356:1627-1631.

Jordan BD, Relkin NR, Ravdin LD, Jacobs AR, Bennett A, Gandy S (1997) Apolipoprotein E epsilon4 associated with chronic traumatic brain injury in boxing. JAMA 278:136-140.

Joseph SB, McKilligin E, Pei L, Watson MA, Collins AR, Laffitte BA, Chen M, Noh G, Goodman J, Hagger GN, Tran J, Tippin TK, Wang X, Lusis AJ, Hsueh WA, Law RE, Collins JL, Willson TM, Tontonoz P (2002) Synthetic LXR ligand inhibits the development of atherosclerosis in mice. Proc Natl Acad Sci U S A 99:7604-7609.

Kandel ER. (2000) Principles of Neural Science. McGraw-Hill.

Kandutsch AA, Chen HW (1974) Inhibition of sterol synthesis in cultured mouse cells by cholesterol derivatives oxygenated in the side chain. J Biol Chem 249:6057-6061.

Karten B, Hayashi H, Francis GA, Campenot RB, Vance DE, Vance JE (2005) Generation and function of astroglial lipoproteins from Niemann-Pick type C1-deficient mice. Biochem J 387:779-788.

Katsel P, Li C, Haroutunian V (2007) Gene expression alterations in the sphingolipid metabolism pathways during progression of dementia and Alzheimer's disease: a shift toward ceramide accumulation at the earliest recognizable stages of Alzheimer's disease? Neurochem Res 32:845-856.

Knebl J, DeFazio P, Clearfield MB, Little L, McConathy WJ, McPherson R, Lacko AG (1994) Plasma lipids and cholesterol esterification in Alzheimer's disease. Mech Ageing Dev 73:69-77.

Knowles TPJ, Buehler MJ (2011) Nanomechanics of functional and pathological amyloid materials. Nature Nanotechnology 6:469-479.

Kollmer F (2004) Cluster primary ion bombardment of organic materials. Appl Surf Sci 203:153-158.

Kuo YM, Emmerling MR, Bisgaier CL, Essenburg AD, Lampert HC, Drumm D, Roher AE (1998) Elevated low-density lipoprotein in Alzheimer's disease correlates with brain A beta 1-42 levels. Biochemical and Biophysical Research Communications 252:711-715.

LaDu MJ, Falduto MT, Manelli AM, Reardon CA, Getz GS, Frail DE (1994) Isoform-specific binding of apolipoprotein E to beta-amyloid. J Biol Chem 269:23403-23406.

Lebouvier T, Perruchini C, Panchal M, Potier MC, Duyckaerts C (2009) Cholesterol in the senile plaque: often mentioned, never seen. Acta Neuropathologica 117:31-34.

Ledesma MD, Dotti CG (2006) Amyloid excess in Alzheimer's disease: what is cholesterol to be blamed for? FEBS Lett 580:5525-5532.

Lee JLS, Gilmore IS, Seah MP, Fletcher IW (2011) Topography and Field Effects in Secondary Ion Mass Spectrometry - Part I: Conducting Samples. Journal of the American Society for Mass Spectrometry 22:1718-1728.

Liu Q, Zerbinatti CV, Zhang J, Hoe HS, Wang B, Cole SL, Herz J, Muglia L, Bu GJ (2007) Amyloid precursor protein regulates brain apolipoprotein e and cholesterol metabolism through lipoprotein receptor LRP1. Neuron 56:66-78.

Lord A, Philipson O, Klingstedt T, Westermark G, Hammarstrom P, Nilsson KP, Nilsson LN (2011) Observations in APP bitransgenic mice suggest that diffuse and compact plaques form via independent processes in Alzheimer's disease. Am J Pathol 178:2286-2298.

Lucin KM, Wyss-Coray T (2009) Immune Activation in Brain Aging and Neurodegeneration: Too Much or Too Little? Neuron 64:110-122.

Lund EG, Guileyardo JM, Russell DW (1999) cDNA cloning of cholesterol 24-hydroxylase, a mediator of cholesterol homeostasis in the brain. Proc Natl Acad Sci U S A 96:7238-7243.

Malm J, Giannaras D, Riehle MO, Gadegaard N, Sjövall P (2009) Fixation and Drying Protocols for the Preparation of Cell Samples for Time-of-Flight Secondary Ion Mass Spectrometry Analysis. Analytical Chemistry 81:7197-7205.

Marcus J, Popko B (2002) Galactolipids are molecular determinants of myelin development and axo-glial organization. Biochimica Et Biophysica Acta-General Subjects 1573:406-413.

Marcus J, Dupree JL, Popko B (2000) Effects of galactolipid elimination on oligodendrocyte development and myelination. Glia 30:319-328.

Martins IC, Kuperstein I, Wilkinson H, Maes E, Vanbrabant M, Jonckheere W, Van Gelder P, Hartmann D, D'Hooge R, De Strooper B, Schymkowitz J, Rousseau F (2008) Lipids revert inert Abeta amyloid fibrils to neurotoxic protofibrils that affect learning in mice. EMBO J 27:224-233.

Masliah E, Mallory M, Ge N, Alford M, Veinbergs I, Roses AD (1995) Neurodegeneration in the central nervous system of apoE-deficient mice. Exp Neurol 136:107-122.

Mattson MP (2004) Pathways towards and away from Alzheimer's disease. Nature 430:631-639.

Michikawa M, Fan QW, Isobe I, Yanagisawa K (2000) Apolipoprotein E exhibits isoform-specific promotion of lipid efflux from astrocytes and neurons in culture. J Neurochem 74:1008-1016.

Miklossy J, Van der Loos H (1987) Cholesterol ester crystals in polarized light show pathways in the human brain. Brain Res 426:377-380.

Minagar A, Shapshak P, Fujimura R, Ownby R, Heyes M, Eisdorfer C (2002) The role of macrophage/microglia and astrocytes in the pathogenesis of three neurologic disorders: HIV-associated dementia, Alzheimer disease, and multiple sclerosis. Journal of the Neurological Sciences 202:13-23.

Mitew S, Kirkcaldie MTK, Halliday GM, Shepherd CE, Vickers JC, Dickson TC (2010) Focal demyelination in Alzheimer's disease and transgenic mouse models. Acta Neuropathologica 119:567-577.

Molander-Melin M, Blennow K, Bogdanović N, Dellheden B, Mansson JE, Fredman P (2005) Structural membrane alterations in Alzheimer brains found to be associated with regional disease development; increased density of gangliosides GM1 and GM2 and loss of cholesterol in detergent-resistant membrane domains. Journal of Neurochemistry 92:171-182.

Morichika H, Hamanaka Y, Tai T, Ishizuka I (1996) Sulfatides as a predictive factor of lymph node metastasis in patients with colorectal adenocarcinoma. Cancer 78:43-47.

Mutoh T, Hirabayashi Y, Mihara T, Ueda M, Koga H, Ueda A, Kokura T, Yamamoto H (2006) Role of glycosphingolipids and therapeutic perspectives on Alzheimer's disease. CNS Neurol Disord Drug Targets 5:375-380.

Näslund J, Thyberg J, Tjernberg LO, Wernstedt C, Karlstrom AR, Bogdanović N, Gandy SE, Lannfelt L, Terenius L, Nordstedt C (1995) Characterization of stable complexes involving apolipoprotein E and the amyloid beta peptide in Alzheimer's disease brain. Neuron 15:219-228.

Nilsberth C, Westlind-Danielsson A, Eckman CB, Condron MM, Axelman K, Forsell C, Stenh C, Luthman J, Teplow DB, Younkin SG, Näslund J, Lannfelt L (2001) The 'Arctic' APP mutation (E693G) causes Alzheimer's disease by enhanced A beta protofibril formation. Nature Neuroscience 4:887-893.

Nimmerjahn A, Kirchhoff F, Helmchen F (2005) Resting microglial cells are highly dynamic surveillants of brain parenchyma in vivo. Science 308:1314-1318.

Oddo S, Caccamo A, Shepherd JD, Murphy MP, Golde TE, Kayed R, Metherate R, Mattson MP, Akbari Y, LaFerla FM (2003) Triple-transgenic model of Alzheimer's disease with plaques and tangles: intracellular Abeta and synaptic dysfunction. Neuron 39:409-421.

Ostrowski SG, Van Bell CT, Winograd N, Ewing AG (2004) Mass spectrometric imaging of highly curved membranes during Tetrahymena mating. Science 305:71-73.

Ostrowski SG, Kurczy ME, Roddy TP, Winograd N, Ewing AG (2007) Secondary ion MS imaging to relatively quantify cholesterol in the membranes of individual cells from differentially treated populations. Analytical Chemistry 79:3554-3560.

Pai AS, Rubinstein I, Onyuksel H (2006) Modulation of beta-amyloid fibrillogenesis and neurotoxicity by phospholipids: Potential implications for Alzheimer's disease. In: 25th CINP Congress, pp S216-S216. Chicago, IL.

Papassotiropoulos A, Lutjohann D, Bagli M, Locatelli S, Jessen F, Buschfort R, Ptok U, Björkhem I, von Bergmann K, Heun R (2002) 24S-hydroxycholesterol in cerebrospinal fluid is elevated in early stages of dementia. Journal of Psychiatric Research 36:27-32.

Passarelli MK, Winograd N (2011) Lipid imaging with time-of-flight secondary ion mass spectrometry (ToF-SIMS). Biochimica Et Biophysica Acta-Molecular and Cell Biology of Lipids 1811:976-990.

Pekny M, Nilsson M (2005) Astrocyte activation and reactive gliosis. Glia 50:427-434.

Pettegrew JW, Panchalingam K, Hamilton RL, McClure RJ (2001) Brain membrane phospholipid alterations in Alzheimer's disease. Neurochem Res 26:771-782.

Pfrieger FW (2003) Cholesterol homeostasis and function in neurons of the central nervous system. Cellular and Molecular Life Sciences 60:1158-1171.

Pike CJ, Walencewicz AJ, Glabe CG, Cotman CW (1991) In-vitro aging of beta-amyloid protein causes peptide aggregation and neurotoxicity. Brain Research 563:311-314.

Pitas RE, Boyles JK, Lee SH, Hui D, Weisgraber KH (1987) Lipoproteins and their receptors in the central nervous-system: characterization of the lipoproteins in cerebrospinal fluid and identification of apolipoprotein B, E (LDL) receptors in the brain. Journal of Biological Chemistry 262:14352-14360.

Piwowar AM, Lockyer NP, Vickerman JC (2009) Salt Effects on Ion Formation in Desorption Mass Spectrometry: An Investigation into the Role of Alkali Chlorides on Peak Suppression in Time-of-Flight-Secondary Ion Mass Spectrometry. Anal Chem.

Poeppel P, Habetha M, Marcao A, Bussow H, Berna L, Gieselmann V (2005) Missense mutations as a cause of metachromatic leukodystrophy. Degradation of arylsulfatase A in the endoplasmic reticulum. FEBS J 272:1179-1188.

Poirier J, Hess M, May PC, Finch CE (1991) Astrocytic apolipoprotein E messenger RNA and GFAP messenger RNA in hippocampus after entorhinal cortex lesioning Molecular Brain Research 11:97-106.

Poirier J, Baccichet A, Dea D, Gauthier S (1993) Cholesterol synthesis and lipoprotein reuptake during synaptic remodeling in hippocampus in adult rats. Neuroscience 55:81-90.

Puglielli L, Tanzi RE, Kovacs DM (2003) Alzheimer's disease: the cholesterol connection. Nat Neurosci 6:345-351.

Puglielli L, Konopka G, Pack-Chung E, Ingano LA, Berezovska O, Hyman BT, Chang TY, Tanzi RE, Kovacs DM (2001) Acyl-coenzyme A: cholesterol acyltransferase modulates the generation of the amyloid beta-peptide. Nat Cell Biol 3:905-912.

Puglielli L, Friedlich AL, Setchell KD, Nagano S, Opazo C, Cherny RA, Barnham KJ, Wade JD, Melov S, Kovacs DM, Bush AI (2005) Alzheimer disease beta-amyloid activity mimics cholesterol oxidase. J Clin Invest 115:2556-2563.

Rahman A, Akterin S, Flores-Morales A, Crisby M, Kivipelto M, Schultzberg M, Cedazo-Minguez A (2005) High cholesterol diet induces tau hyperphosphorylation in apolipoprotein E deficient mice. FEBS Lett 579:6411-6416.

Ranscht B, Clapshaw PA, Price J, Noble M, Seifert W (1982) Development of oligodendrocytes and Schwann cells studies with a monoclonal antibody against galactocerebroside. Proceedings of the National Academy of Sciences of the United States of America-Biological Sciences 79:2709-2713.

Reid PC, Sakashita N, Sugii S, Ohno-Iwashita Y, Shimada Y, Hickey WF, Chang TY (2004) A novel cholesterol stain reveals early neuronal cholesterol accumulation in the Niemann-Pick type C1 mouse brain. J Lipid Res 45:582-591.

Repa JJ, Li H, Frank-Cannon TC, Valasek MA, Turley SD, Tansey MG, Dietschy JM (2007) Liver X receptor activation enhances cholesterol loss from the brain, decreases neuroinflammation, and increases survival of the NPC1 mouse. J Neurosci 27:14470-14480.

Russell DW, Halford RW, Ramirez DMO, Shah R, Kotti T (2009) Cholesterol 24-Hydroxylase: An Enzyme of Cholesterol Turnover in the Brain. Annual Review of Biochemistry 78:1017-1040.

Sambamurti K, Granholm AC, Kindy MS, Bhat NR, Greig NH, Lahiri DK, Mintzer JE (2004) Cholesterol and Alzheimer's disease: clinical and experimental models suggest interactions of different genetic, dietary and environmental risk factors. Curr Drug Targets 5:517-528.

Seedorf U, Fobker M, Voss R, Meyer K, Kannenberg F, Meschede D, Ullrich K, Horst J, Benninghoven A, Assmann G (1995) Smith-Lemli-Opitz syndrome diagnosed by using time-of-flight secondary ion mass spectrometry. Clin Chem 41:548-552.

Selkoe DJ (1994) Cell biology of the amyloid beta protein precursor and the mechanism of Alzheimer's disease. Annual Review of Cell Biology 10:373-403.

Selkoe DJ (2008) Soluble oligomers of the amyloid beta-protein impair synaptic plasticity and behavior. Behav Brain Res 192:106-113.

Selkoe DJ (2011) Alzheimer's Disease. Cold Spring Harbor Perspectives in Biology 3.

Shepherd J, Blauw GJ, Murphy MB, Bollen EL, Buckley BM, Cobbe SM, Ford I, Gaw A, Hyland M, Jukema JW, Kamper AM, Macfarlane PW, Meinders AE, Norrie J, Packard CJ, Perry IJ, Stott DJ, Sweeney BJ, Twomey C, Westendorp RG (2002) Pravastatin in elderly individuals at risk of vascular disease (PROSPER): a randomised controlled trial. Lancet 360:1623-1630.

Shobab LA, Hsiung GYR, Feldman HH (2005) Cholesterol in Alzheimer's disease. Lancet Neurology 4:841-852.

Sjövall P, Lausmaa J, Johansson B (2004) Mass spectrometric imaging of lipids in brain tissue. Anal Chem 76:4271-4278.

Sjövall P, Johansson B, Lausmaa J (2006) Localization of lipids in freeze-dried mouse brain sections by imaging TOF-SIMS. Applied Surface Science 252:6966-6974.

Sparks DL, Liu H, Gross DR, Scheff SW (1995) Increased density of cortical apolipoprotein E immunoreactive neurons in rabbit brain after dietary administration of cholesterol. Neurosci Lett 187:142-144.

Studer D, Humbel BM, Chiquet M (2008) Electron microscopy of high pressure frozen samples: bridging the gap between cellular ultrastructure and atomic resolution. Histochemistry and Cell Biology 130:877-889.

Svennerholm L, Gottfries CG (1994) Membrane lipids, selectively diminished in Alzheimer brains, suggest synapse loss as a primary event in early-onset form (type I) and demyelination in late-onset form (type II). J Neurochem 62:1039-1047.

Tampellini D, Rahman N, Lin MT, Capetillo-Zarate E, Gouras GK (2011) Impaired beta-Amyloid Secretion in Alzheimer's Disease Pathogenesis. Journal of Neuroscience 31:15384-15390.

Tanzi RE, Bertram L (2001) New frontiers in Alzheimer's disease genetics. Neuron 32:181-184.

Teipel SJ, Hampel H, Alexander GE, Schapiro MB, Horwitz B, Teichberg D, Daley E, Hippius H, Moller HJ, Rapoport SI (1998) Dissociation between corpus callosum atrophy and white matter pathology in Alzheimer's disease. Neurology 51:1381-1385.

Tontonoz P, Mangelsdorf DJ (2003) Liver X receptor signaling pathways in cardiovascular disease. Mol Endocrinol 17:985-993.

Touboul D, Laprevote O, Brunelle A (2011) Micrometric molecular histology of lipids by mass spectrometry imaging. Current Opinion in Chemical Biology 15:725-732.

Touboul D, Brunelle A, Halgand F, De La Porte S, Laprevote O (2005) Lipid imaging by gold cluster time-of-flight secondary ion mass spectrometry: application to Duchenne muscular dystrophy. Journal of Lipid Research 46:1388-1395.

Touboul D, Halgand F, Brunelle A, Kersting R, Tallarek E, Hagenhoff B, Laprevote O (2004) Tissue molecular ion imaging by gold cluster ion bombardment. Analytical Chemistry 76:1550-1559.

Tseng BP, Kitazawa M, LaFerla FM (2004) Amyloid beta-peptide: the inside story. Curr Alzheimer Res 1:231-239.

Tseng BP, Green KN, Chan JL, Blurton-Jones M, LaFerla FM (2008) Abeta inhibits the proteasome and enhances amyloid and tau accumulation. Neurobiol Aging 29:1607-1618.

Wahrle SE, Jiang H, Parsadanian M, Legleiter J, Han X, Fryer JD, Kowalewski T, Holtzman DM (2004) ABCA1 is required for normal central nervous system ApoE levels and for lipidation of astrocyte-secreted apoE. J Biol Chem 279:40987-40993.

Walker AV (2008) Why is SIMS underused in chemical and biological analysis? Challenges and opportunities. Anal Chem 80:8865-8870.

Walsh DM, Selkoe DJ (2007) A beta oligomers - a decade of discovery. J Neurochem 101:1172-1184.

Walsh DM, Lomakin A, Benedek GB, Condron MM, Teplow DB (1997) Amyloid beta-protein fibrillogenesis - Detection of a protofibrillar intermediate. Journal of Biological Chemistry 272:22364-22372.

Walsh DM, Tseng BP, Rydel RE, Podlisny MB, Selkoe DJ (2000) The oligomerization of amyloid beta-protein begins intracellularly in cells derived from human brain. Biochemistry 39:10831-10839.

Walsh DM, Klyubin I, Fadeeva JV, Cullen WK, Anwyl R, Wolfe MS, Rowan MJ, Selkoe DJ (2002) Naturally secreted oligomers of amyloid beta protein potently inhibit hippocampal long-term potentiation in vivo. Nature 416:535-539.

Vance JE, Hayashi H, Karten B (2005) Cholesterol homeostasis in neurons and glial cells. Seminars in Cell & Developmental Biology 16:193-212.

Wang HY, Li WW, Benedetti NJ, Lee DHS (2003) alpha(7) nicotinic acetylcholine receptors mediate beta-amyloid peptide-induced tau protein phosphorylation. Journal of Biological Chemistry 278:31547-31553.

Wang L, Schuster GU, Hultenby K, Zhang Q, Andersson S, Gustafsson JA (2002) Liver X receptors in the central nervous system: from lipid homeostasis to neuronal degeneration. Proc Natl Acad Sci U S A 99:13878-13883.

Wang W, Shinto L, Connor WE, Quinn JF (2008) Nutritional biomarkers in Alzheimer's disease: the association between carotenoids, n-3 fatty acids, and dementia severity. J Alzheimers Dis 13:31-38.

Wang X, Sato R, Brown MS, Hua X, Goldstein JL (1994) SREBP-1, a membrane-bound transcription factor released by sterol-regulated proteolysis. Cell 77:53-62.

Vega GL, Weiner MF, Lipton AM, Von Bergmann K, Lutjohann D, Moore C, Svetlik D (2003) Reduction in levels of 24S-hydroxycholesterol by statin treatment in patients with Alzheimer disease. Arch Neurol 60:510-515.

Wenk GL (2003) Neuropathologic changes in Alzheimer's disease. J Clin Psychiatry 64 Suppl 9:7-10.

Whitfield GB, Brock TD, Ammann A, Gottlieb D, Carter HE (1955) Filipin, an antifungal antibiotic: isolation and properties. Journal of the American Chemical Society 77:4799-4801.

Whitney KD, Watson MA, Collins JL, Benson WG, Stone TM, Numerick MJ, Tippin TK, Wilson JG, Winegar DA, Kliewer SA (2002) Regulation of cholesterol homeostasis by the liver X receptors in the central nervous system. Mol Endocrinol 16:1378-1385.

Wirths O, Weis J, Kayed R, Saido TC, Bayer TA (2007) Age-dependent axonal degeneration in an Alzheimer mouse model. Neurobiology of Aging 28:1689-1699.

Wolozin B (2004) Cholesterol, statins and dementia. Curr Opin Lipidol 15:667-672.

Wolozin B, Kellman W, Ruosseau P, Celesia GG, Siegel G (2000) Decreased prevalence of Alzheimer disease associated with 3-hydroxy-3-methyglutaryl coenzyme A reductase inhibitors. Arch Neurol 57:1439-1443.

Voneckardstein A, Funke H, Henke A, Altland K, Benninghoven A, Assmann G (1989) Apolipoprotein A-I variants: naturally ocurring substitutions of proline residues affect plasma concentration of apolipoprotein A-I. J Clin Invest 84:1722-1730.

Voneckardstein A, Funke H, Walter M, Altland K, Benninghoven A, Assmann G (1990) Structural analysis of human apolipoprotein A-I variants: amino acid substitutions are non-randomly distributed throughout the apolipoprotein A-I primary structure. J Biol Chem 265:8610-8617.

Vos JP, Lopescardozo M, Gadella BM (1994) Metabolic and functional aspects of sulfogalactolipids. Biochimica Et Biophysica Acta-Lipids and Lipid Metabolism 1211:125-149.

Xie C, Richardson JA, Turley SD, Dietschy JM (2006) Cholesterol substrate pools and steroid hormone levels are normal in the face of mutational inactivation of NPC1 protein. J Lipid Res 47:953-963.

Yoshiike Y, Akagi T, Takashima A (2007) Surface structure of amyloid-beta fibrils contributes to cytotoxicity. Biochemistry 46:9805-9812.

Yu L, York J, von Bergmann K, Lutjohann D, Cohen JC, Hobbs HH (2003) Stimulation of cholesterol excretion by the liver X receptor agonist requires ATP-binding cassette transporters G5 and G8. J Biol Chem 278:15565-15570.

Zagol-Ikapitte I, Masterson TS, Amarnath V, Montine TJ, Andreasson KI, Boutaud O, Oates JA (2005) Prostaglandin H(2)-derived adducts of proteins correlate with Alzheimer's disease severity. J Neurochem 94:1140-1145.

Zamaria N (2004) Alteration of polyunsaturated fatty acid status and metabolism in health and disease. Reprod Nutr Dev 44:273-282.

Zeng YC, Han X (2008) Sulfatides facilitate apolipoprotein E-mediated amyloid-beta peptide clearance through an endocytotic pathway. Journal of Neurochemistry 106:1275-1286.